INEEL/EXT-04-02492

Fluidized Bed Steam Reforming of Hanford LAW Using THOR^{sm} Mineralizing Technology

Arlin L. Olson
Nicholas R. Soelberg
Douglas W. Marshall
Gary L. Anderson

November 2004

Idaho National Engineering and Environmental Laboratory
Bechtel BWXT Idaho, LLC

INEEL/EXT-04-02492

Fluidized Bed Steam Reforming of Hanford LAW Using THOR^{sm} Mineralizing Technology

Arlin L. Olson
Nicholas R. Soelberg
Douglas W. Marshall
Gary L. Anderson

November 2004

Idaho National Engineering and Environmental Laboratory
Environmental R&D Laboratory
Idaho Falls, Idaho 83415

Prepared for the
U.S. Department of Energy
Assistant Secretary for Environmental Management
Under DOE Idaho Operations Office
Contract DE-AC07-99ID13727

ABSTRACT

The U.S. Department of Energy (DOE) documented, in 2002, a plan for accelerating cleanup of the Hanford Site, located in southeastern Washington State, by at least 35 years. A key element of the plan was acceleration of the tank waste program and completion of "tank waste treatment by 2028 by increasing the capacity of the planned Waste Treatment Plant (WTP) and using supplemental technologies for waste treatment and immobilization." The plan identified steam reforming technology as a candidate for supplemental treatment of as much as 70% of the low-activity waste (LAW).

Mineralizing steam reforming technology, offered by THOR Treatment Technologies, LLC would produce a denitrated, granular mineral waste form using a high-temperature fluidized bed process. A pilot scale demonstration of the technology was completed in a 15-cm-diameter reactor vessel. The pilot scale facility was equipped with a cyclone separator and heated sintered metal filters for particulate removal, a thermal oxidizer for reduced gas species and NO_x destruction, and a packed activated carbon bed for residual volatile species capture. The pilot scale equipment is owned by the DOE, but located at the Science and Technology Applications Research (STAR) Center in Idaho Falls, ID. Pilot scale testing was performed August 2–5, 2004. Flowsheet chemistry and operational parameters were defined through a collaborative effort involving Idaho National Engineering and Environmental Laboratory, Savannah River National Laboratory (SRNL), and THOR Treatment Technologies personnel. Science Application International Corporation, owners of the STAR Center, personnel performed actual pilot scale operation.

The pilot scale test achieved a total of 68.4 hrs of cumulative/continuous processing operation before termination in response to a bed de-fluidization condition. 178 kg of LAW surrogate were processed that resulted in 148 kg of solid product, a mass reduction of about 17%. The process achieved essentially complete bed turnover within approximately 40 hours. Samples of mineralized solid product materials were analyzed for chemical/physical properties. SRNL will report separately the results of product performance testing that were accomplished.

EXECUTIVE SUMMARY

The US Department of Energy (DOE) desired further experimental data, with regard to fluidized bed steam reforming (FBSR) technology, to make informed decisions concerning the selection of supplemental treatment technology for Hanford low-activity waste (LAW) and to support a 2006 decision date. Radioactive experimental data were desired to provide the most beneficial information to DOE. It was recognized that there was not an experimental fluidized bed test system/facility available to generate experimental radioactive data in the desired time frame. Therefore, a collaboration involving laboratory work at Savannah River National Laboratory (SRNL) and pilot scale work at the Idaho National Engineering and Environmental Laboratory (INEEL) was initiated to provide the information in the required time frame.

The INEEL's pilot scale fluidized bed processing test system at the Science Applications International Corporation's (SAIC) Science and Technology Applications Research (STAR) facility was successfully operated during the first week of August 2004 to conduct a continuous processing test of THOR^{SM} Treatment Technology's (TTT) mineralized FBSR process technology with simulated waste materials representative of Hanford LAW. This report documents the experiments performed with Hanford LAW simulants, performance of the fluidized bed system, physical characteristics of the mineralized products, and mass balances. Assessment of the product performance with regard to leach resistance and durability (e.g., the Product Consistency Test) are to be reported by SRNL separately.

The pilot scale test generated a large amount of process/system conditions data real time and process materials sampling data. The data has been compiled and has undergone considerable analysis leading to the test results presented herein. Considerable further analyses are possible, however, to generate increased understanding of the technology and response to changes in key process parameters and hardware design.

The pilot scale test achieved a total of 68.4 hrs of cumulative/continuous processing operation, and resulting mineralized products, before termination in response to a bed de-fluidization condition. The process achieved essentially complete bed turnover within approximately 40 hrs (greater than 98% replacement of the starting bed with mineralized product solids) and operated for the remaining hours essentially under relatively steady bed product and process conditions. This did not meet the desired test objective of operating for >80 hours at a feed rate of ~ 4 kg/hour, but effectively satisfied an underlying objective of 100% bed turnover.

The pilot scale test produced a significant quantity of representative FBSR mineralized solid product materials, samples of which have been analyzed for chemical/physical properties, and can be used to compare/validate equivalency with small lab-scale batch equilibrium mineralizing chemistry studies/tests by SRNL. The total amount of simulated LAW feed and additives processed was approximately 364 kg and the total solid products mass was approximately 145 kg indicating a total mass reduction within the process of 219 kg, or about 60%. The total input of solids includes 43.9 kg of carbon and about 142 kg clay. Therefore, about 178 kg of LAW surrogate resulted in about 145 kg of solid product, a mass reduction of about 19%. The net solid waste product material mass and volume are of course of interest for any subsequent processing or direct handling and disposal activities. The bed product to fines collected mass ratio was about 1 to 1. This value did not achieve the desired value of 3.5 to 1 as stated in the test objectives, and further optimization and/or development is needed to achieve this objective.

The mineralized steam reforming process is intended to immobilize the metal-nitrates in the LAW liquid waste feed solution into a stable product solid consisting largely of sodium/potassium-alumina-silicate target mineral phases of various structures. The mineral phases are formed as a result of the clay

(aluminosilicate) additive and are intended to capture and retain (stabilize) the alkali metals (Na, K), target radionuclides (Tc) and other toxic metals and anions. Test results show that nitrates and nitrites in the liquid waste feed were essentially destroyed and that the bed and fines products largely consisted of desired target mineral phases. The major phase found in the bed product was carnegieite, with lesser amounts of nepheline and minor amounts of nosean. The fines consisted of the major phase carnegieite, with lesser amounts of nepheline and TiO_2.

Elemental analysis of the products indicate that aluminum and chromium partitioned somewhat preferentially to the bed product; calcium, phosphorous, and chlorine distributed evenly between the bed product and elutriated fines captured by a high temperature filter. Rhenium, sodium, and potassium appear to partition somewhat to the fines rather than to the bed product, but not as significantly as do silicon and sulfur. Cesium clearly partitions preferentially to the filter fines.

The majority (estimated >95 wt%) of the total mass of mineralized product solids was of a form expected during stable, steady mineralized process operations. These consisted of small (typically 0.2 – 0.3 mm), generally granular solids in the bed product or much smaller granular solids in the fines product (typical diameter .01 mm). Elutriated fines that were captured in a cyclone (upstream of the heated filter) and were recycled to the fluidized bed averaged about 0.04 mm in diameter. Only a small amount of the total product in the bed was undesirable larger solid pieces, either from nozzle deposit/accretion break-off (typical diameters from 6 to 12 mm) or the very large defluidized bed agglomerates (diameters greater than 70 mm) that occurred rapidly near the end of the test.

NO_x was satisfactorily destroyed throughout the process run. NO_x destruction in the steam reforming process (upstream of the thermal oxidizer) averaged 92% and was near 96% much of the time, effectively meeting the test objective of greater than 80% destruction. Response of NO_x generation/destruction in the steam reforming process was as expected, being directly proportional to carbon feed rate/inventory changes which drive the attendant proportional production of H_2 and CO that are thought to participate in NO_x reduction reactions.

ACKNOWLEDGEMENTS

Personnel from several organizations contributed to the performance of this technology demonstration activity. Overall direction was provided by the Department of Energy (Joel Case and Bill Owca).

The collaborative technical team consisted of THOR Treatment Technologies, LLC (Brad Mason, Kevin Ryan, and Brad Eldredge), Savannah River National Laboratory (Jim Marra and Carol Jantzen), and the authors from the Idaho National Engineering and Environmental Laboratory (INEEL).

Science Applications International Corporation (SAIC) modified and operated the DOE-owned fluidized bed test facility at the Science and Technology Research (STAR) Center under direction from the INEEL. The SAIC team was led by Tim Hertzler. This demonstrational activity could not have been accomplished without the intensity and diligence with which SAIC personnel performed their work, the innovation they used to solve problems and issues, and the overall quality of the tasks performed.

Significant changes were also made to the process logic controller interfaces, software, and data acquisition/data archive system. A team led by Curtis St Michel with the support of Havlovick Engineering (John Yadon) performed this activity.

The authors wish to acknowledge and thank all those involved.

CONTENTS

FIGURES

TABLES

ACRONYMS

ASTM	American Society for Testing and Materials
CAI	California Analytical Instruments
CEMS	continuous emissions monitoring system
COT	continuous operating time
DOE	Department of Energy
FBSR	fluidized bed steam reforming
GUI	graphical user interface
HMPD	harmonic mean particle diameter
HMI	human machine interface
HWC	hazardous waste combustor
LAW	low activity waste
MACT	maximum achievable control technology
MMPD	mass-mean particle diameter
MTEC	maximum theoretical emission concentration
NAR	nozzle atomizing ratio
NAS	alkali aluminosilicate minerals
NDIR	nondispersive infrared
NSNCR	non-selective, non-catalytic reduction
PDF	Powder Diffraction File
PE	polyethylene
P/F	product to fines ratio
PCT	Product Consistency Test
PLC	process logic controller
PNNL	Pacific Northwest National Laboratory
PSD	particle size distribution
PUF	pressurized unsaturated flow
SAIC	Science Applications International Corporation
SBW	Sodium Bearing Waste
SEM	scanning electron micrograph
SPFT	single pass flow through test
SRNL	Savannah River National Laboratory
STAR	Science and Technology Applications Research
TCLP	Toxicity Characteristic Leach Procedure
TTT	THOR^{sm} Treatment Technologies
UTB	uniaxial-tube Bernoulli-effect nozzle
WTP	Waste Treatment Plant

Fluidized Bed Steam Reforming of Hanford LAW Using THOR^{sm} Mineralizing Technology

1. INTRODUCTION

The U.S. Department of Energy (DOE) documented, in 2002, a plan for accelerating cleanup of the Hanford Site, located in southeastern Washington State, by at least 35 years. A key element of the plan was acceleration of the tank waste program and completion of "tank waste treatment by 2028 by increasing the capacity of the planned Waste Treatment Plant (WTP) and using supplemental technologies for waste treatment and immobilization." The plan identified specific technologies to be evaluated for supplemental treatment of as much as 70% of the low-activity waste (LAW). In concert with this acceleration plan, DOE, the U.S. Environmental Protection Agency (EPA), and the Washington State Department of Ecology proposed to accelerate – from 2014 to 2006 – the Hanford Federal Facility Agreement and Consent Order milestone (M-62-11) associated with a final decision on the balance of tank waste that is beyond the capacity of the WTP.

The DOE Office of River Protection tank farm contractor, CH2M HILL Hanford Group, Inc. (CH2M HILL), was tasked with testing and evaluating selected supplemental technologies to support final decisions on tank waste treatment. Three technologies and corresponding vendors were selected to support an initial technology selection in 2003. The three technologies were containerized grout called cast stone (Fluor Federal Services); bulk vitrification (AMEC Earth and Environmental, Inc.); and steam reforming (THOR Treatment Technologies, LLC.). Steam reforming produces a denitrated, granular mineral waste form using a high-temperature fluidized bed process.

DOE identified the need in January 2004 for further experimental data, with regard to steam reforming technology, to make informed decisions concerning selection of supplemental treatment technology and to support the 2006 decision date. Radioactive experimental data were desired to provide the most beneficial information to DOE. It was recognized that there was not an experimental fluidized bed test system/facility available to generate experimental radioactive data in the desired time frame. Therefore, a plan was conceived that would provide the information in the required time frame.

The basis for the plan was that a correlation between laboratory and pilot scale results existed and would need to be validated such that radioactive laboratory experiments performed in hot cells would provide the desired information. A collaboration involving laboratory work at Savannah River National Laboratory (SRNL) and pilot scale work at INEEL was initiated to validate the correlation. This report documents the results of the pilot scale experiments performed with Hanford LAW simulants.

1.1 Background

Several demonstrations of fluidized bed steam reforming (FBSR) technology as applied to simulated radioactive liquid waste streams have been performed in the last two years. Three tests that are specifically related to the work reported here were performed earlier. The first, conducted at the Hazen Research facility in Colorado, pertained to generating a sodium aluminosilicate (mineralized) product from Hanford low-activity waste (LAW). The results of this experiment were considered promising and characteristics of the product have been published [Jantzen, 2002].

The second demonstration, performed at the Science Applications International Corporation (SAIC) Science and Technology Applications Research (STAR) Center, located in Idaho Falls, ID, under the oversight of Idaho National Engineering and Environmental Laboratory (INEEL) personnel, generated a sodium aluminosilicate product from INEEL's simulated sodium-bearing waste (SBW). The results of this experimental demonstration were also considered promising and have been published [Soelberg, et. al., 2004b].

A third demonstration was recently performed during the period July 8-16, 2004 at the STAR Center. This activity was based on selected additive materials, enhanced equipment configuration, and was performed with simulated SBW. Sufficient product was generated for characterization, but the results are yet to be documented and published.

Other FBSR demonstrations have been performed forming alkali carbonate or alkali silicate solids that are potentially disposable at the Waste Isolation Pilot Plant and/or for recycle to a melter for vitrification. These products, which can be considered for the alternate applications given above, were not the aluminosilicate mineralized waste form examined in the current study. As stated previously, an initial correlation between laboratory and pilot scale work has been shown [Soelberg, et. al., 2003 and Jantzen 2003] for the carbonate and silicate FBSR products. The Savannah River Site desired to make space in the SRS Tank farm by removing/processing the Tank 48H waste. Tank 48H waste consists of nitrates, nitrites, and sodium tetraphenyl borate (NaTPB) and destroying/removing these in order to reduce impacts of these species before it was vitrified at the DWPF was desired. Fluidized bed steam reforming was considered as a candidate technology for destroying the nitrates and the NaTPB prior to melting. The INEEL was tasked to perform a proof-of-concept steam reforming test to evaluate the technical feasibility for pretreating the Tank 48H waste. The crucible (bench scale) tests conducted at the SRNL were initiated to optimize and augment the parameters subsequently tested at the pilot scale at INEEL. These activities provided the basis for correlating laboratory and pilot scale experiments.

1.2 Scope

The scope of the collaborative work performed by the SRNL and INEEL includes:

- Performing laboratory scale simulated FBSR experiments at SRNL that would optimize steam reforming raw materials selection and mineralization chemistry.
- Performing pilot scale FBSR experiments at INEEL with simulants that produce a mineralized product to which the products of the laboratory scale tests could be compared.
- Characterize products via chemical assays, x-ray diffraction, and scanning electron microscopy.
- Product durability will be measured via Toxic Characteristic Leach Procedure (TCLP), and Product Consistency Test (PCT) measurements; performance will be measured by the single pass flow through (SPFT) testing and pressurized unsaturated flow (PUF) testing.
- Determine, based on comparisons to the products of the pilot-scale tests, if the laboratory tests produce steam reforming conditions and mineralized products that are representative of actual fluidized bed steam reforming.

This report documents the mineralized steam reforming tests conducted in the INEEL pilot scale fluidized bed steam reformer. Results from the test operations, physical characteristics of the mineralized LAW products, and process mass balances are provided. Assessment of the product performance with regard to leach resistance and durability are to be reported by SRNL separately.

2. THEORY/APPROACH

Mineralizing steam reforming technology is being considered by the Department of Energy as a treatment and immobilization method for liquid radioactive wastes being managed by the Department. In addition to being radioactive, these liquid wastes also contain large quantities of alkali metals and nitrates, and lesser quantities of hazardous metals and other anions such as fluoride, chloride, and sulphate. Classical steam reforming is a versatile process that decomposes organic materials through reaction with steam. Steam reforming has been used on a large scale by the petrochemical industry to produce hydrogen for at least 65 years. If the material being reformed contains halogens, phosphorus, or sulfur, mineral acids are also formed (e.g., hydrochloric acid, phosphorous acid, phosphoric acid, and hydrogen sulfide) unless inorganic materials capable of scavenging these species are present in the waste or additives [Nimlos, 1990, 1992]. Organic nitrogen is converted to N_2 and organic oxygen is converted to CO or CO_2.

It is desired to immobilize radioactive components of the waste into a form that is quite durable (i.e., leach resistant) for hundreds or thousands of years. More recently, steam reforming has been proposed, along with the use of mineralizing additives, to immobilize liquid radioactive wastes into forms that meet durability criteria required at a wide variety of disposal sites.

2.1 Mineral Waste Forms

Previous development work has shown that alkali aluminosilicate (NAS) minerals provide host phases to accommodate radionuclide species. Waste forms of aluminosilicate based crystalline assemblages of mutually compatible, refractory, and leach-resistant solid solution phases have been proposed for the incorporation of radionuclide species of concern [Rusin, 1979]. An assemblage of silicate mineral phases (supercalcine ceramics) such as apatite (host for lanthanides), pollucite (host for Cs), and other oxide host phases for Sr, Ba, U, Zr, etc. seem appropriate [McCarthy, 1976 and Rusin 1979]. If the waste contains considerable Na and Si, then phases such as nepheline may form while wastes enriched in Al may form high temperature phases such as Al_2O_3 and magnetoplumbite aluminate species [Morgan, 1981 and Jantzen 1982]. The feldspathoid, sodalite, is a mineral phase found to incorporate Cs and Sr and Mo into the cage-like structure, e.g. Mo as $(NaAlSiO_4)_6(NaMoO_4)$ [Brookins, 1984] A more detailed discussion of this subject can be found in Jantzen, 2002.

The sodium aluminosilicate (NAS) mineral phase assemblage(s) are anhydrous feldspathoid phases such as sodalite that are unique because they have cage-like structures formed of aluminosilicate tetrahedra (Figure 2.1-1). The remaining feldspathoid minerals, such as nepheline, have a silica “stuffed derivative” ring type structure. The cage structures are typical of sodalite and/or nosean phases where the cavities in the cage structure retain anions and/or radionuclides that are ionically bonded to the aluminosilicate tetrahdra and to sodium. The cage structured feldspathoid system of minerals has the basic structural framework formula $Na_6[Al_6Si_6O_{24}]$. The alumina:silica ratio of the cage structure is 1:1.

The nomenclature of the feldspathoid series of mineral species is governed by the species that occupy the cavities in the aluminosilicate framework and whether or not the resulting crystals have cubic or hexagonal crystal structures. Sodalite has the formula $Na_8[Al_6Si_6O_{24}](Cl_2)$. The cage is occupied by two sodium and two chlorine ions in natural sodalites [Deer, 1963]. The formula can also be written as $Na_6[Al_6Si_6O_{24}]\bullet(2NaCl)$ to indicate that two NaCl molecules are chemically bonded in the cavities of the cage structure while the remaining Na:Si:Al have a 1:1:1 stoichiometry [Deer, 1963]. When the sodium chloride molecules are replaced by Na_2SO_4, Na_2CO_3, $2NaNO_3$, and/or 2NaOH, the mineral and/or chemical names are as given in Table 2.1-1.

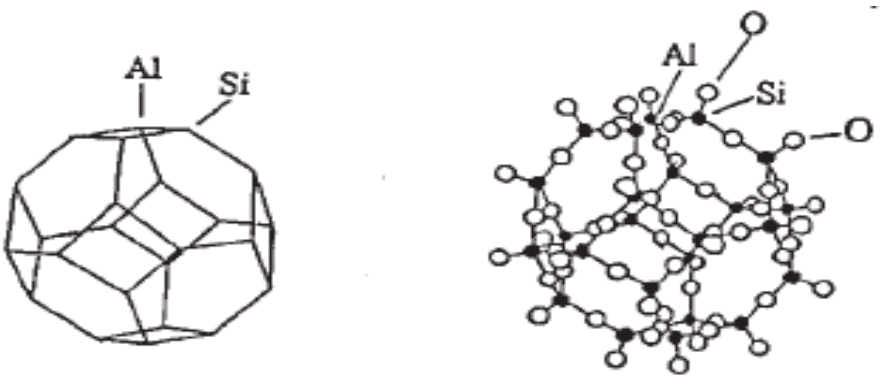

Figure 2.1-1. Part of the aluminosilicate framework in the structure of the feldspathoid sodalite [Deer, 1963].

One of the feldspathoid cage structured minerals is nosean, $Na_6[Al_6Si_6O_{24}](Na_2SO_4)$). Nosean has Na_2SO_4 bonded in the sodalite cage like structure. Since the Cl^-, $SO_4^=$, and/or S_2 are bonded inside the sodalite cage structure, these species do not readily leach out of the respective waste form mineral phases. A second feldspathoid mineral is nepheline ($NaAlSiO_4$) [Berry, 1959]. Nepheline is a hexagonal structured feldspathoid mineral. The ring structured aluminosilicate framework of nepheline forms cavities within the framework. There are eight large (nine-fold oxygen) coordination sites and six smaller (8-fold oxygen) coordination sites [Deer, 1963]. The larger nine-fold sites can hold large cations such as Cs, K, and Ca while the smaller sites accommodate the Na. The K analogue is known as leucite ($KAlSi_2O_6$). In nature, the nepheline structure is known to accommodate Fe, Ti and Mg as well.

A sodium rich cubic structured nepheline derivative $(Na_2O)_{0.33}Na[AlSiO_4]$ (PDF#39-0101) is also known to form. This nepheline derivative structure has large (twelve-fold oxygen) cage like voids in the structure [Klingenberg, 1986]. This cage-structured nepheline is not known to occur in nature but the large cage-like voids should be capable of retaining large radionuclides, especially monovalent radionuclides such as Cs.

The objective of this work has been to create the types of minerals that would provide leach resistant (durable) waste forms for the immobilization of Hanford's low-activity waste (LAW). This has been approached by selecting a kaolin clay type with the appropriate Al:Si mole ratio that would suitably react with the Na and anions in the LAW. A ternary phase diagram (Figure 2.1-2) shows the target region of compositions that are thought to be most favorable for producing the desired mineral products. The most favorable atomic ratios that would produce the desired nepheline and sodalite products are thought to be M/Si = 1-1.33, M/Al = 1-1.33, Al/Si ≥ 1, and M/(Al+Si) = 0.5-0.67, where M represents an alkali metal, mostly Na in this case [Jantzen, 2004]. The LAW is ~100% Na_2O on a calcine basis. The acceptable composition region is not necessarily as small as indicated by the shaded region in Figure 2.1-2, it be could anywhere in the valley that points to the nepheline melting region. The atomic ratios provide guidelines because there may be significant substitution of different alkali and alkaline earths, and some Fe for Al, in these feldspathoid minerals.

Table 2.1-1. Structurally related zeolite and feldspathoid (sodalite and cancrinite) group mineral phases [Jantzen, 2002].

Substitution In Cage Structure	Chemical Formula	Common Mineral Name	Density (g/cm3)	Crystal Type	Ref.
Precursor					
NONE	$Na_{12}[Al_{12}Si_{12}O_{48}] \cdot 27H_2O$	Zeolite-A	1.99‡	Cubic	Kirk-Othmer, 1995
Sodalite Group (Anhydrous)					
2NaCl	$Na_6[Al_6Si_6O_{24}](2NaCl)$	Sodalite	2.31*	Cubic*	Deer, 1963
2NaOH	$Na_6[Al_6Si_6O_{24}](2NaOH) \cdot 1.5H_2O$	Basic Sodalite or Hydroxysodalite	2.215**	Cubic**	Barrer, 1959
$2NaNO_3$	$Na_6[Al_6Si_6O_{24}](2NaNO_3)$	Nitrated Sodalite	2.342	Cubic	PDF#50-0248
Na_2SO_4	$Na_6[Al_6Si_6O_{24}] (Na_2SO_4)$	Nosean	2.21tt	Cubictt	Dana, 1932
1-2(Ca,Na)SO_4	$(Na)_6[Al_6Si_6O_{24}] ((Ca,Na)(S,SO_4)_{1-2})^t$	Hauyne	2.4t	Cubict	Deer, 1963
x(Ca,Na)(S,SO_4 ,Cl)	$(Ca,Na)_6[Al_6Si_6O_{24}]((Ca,Na)S,SO_4,Cl)_X^t$	Lazurite	2.43	Cubic	PDF #17-749
Cancrinite Group (Anhydrous)					
$2NaNO_3$	$Na_6[Al_6Si_6O_{24}](2NaNO_3) \cdot 4H_2O$	Nitrated Cancrinite	2.51	Hexagonal	PDF #38-513
$(Na,Ca,K)_2CO_3$	$(Na,Ca,K)_6 [Al_6Si_6O_{24}]$ $((Na,Ca,K)_2CO_3)_{1.6} \cdot 2.1H_2O$	Cancrinite	2.60	Hexagonal	PDF #25-776
2(Na, K)Cl	$(Na,Ca,K)_6[Al_6Si_6O_{24}] (2(Na,K)Cl)_{2-3}$	Microsommite	2.34	Hexagonal	PDF #20-743
2(Na, K)Cl	$(Na,Ca,K)_6[Al_6Si_6O_{24}]$ $((Na,K)2SO_4,Cl)_3$	Davyne	2.46	Hexagonal	PDF #20-379
Na_2CO_3	$Na_6[Al_6Si_6O_{24}] (Na_2CO_3)$	Natrodavyne	Not given	Hexagonal	PDF #15-794

[t] PDF #20-1087 * PDF # 20-495 ‡ PDF #11-0590 and #38-241
[tt] PDF #17-538 ** PDF #11-401 PDF – Powder Diffraction File

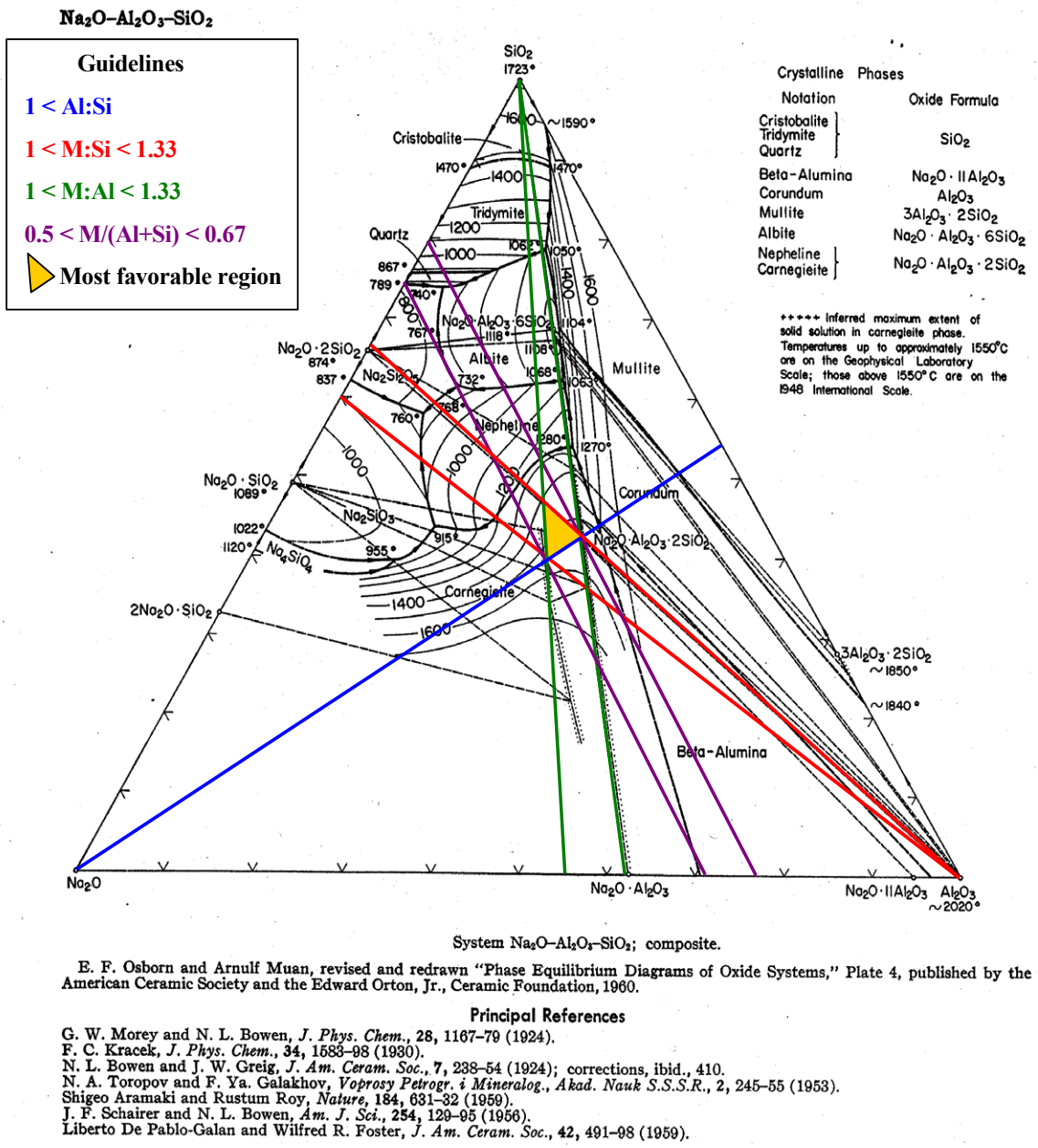

System Na_2O–Al_2O_3–SiO_2; composite.

E. F. Osborn and Arnulf Muan, revised and redrawn "Phase Equilibrium Diagrams of Oxide Systems," Plate 4, published by the American Ceramic Society and the Edward Orton, Jr., Ceramic Foundation, 1960.

Principal References

G. W. Morey and N. L. Bowen, *J. Phys. Chem.*, **28**, 1167–79 (1924).
F. C. Kracek, *J. Phys. Chem.*, **34**, 1583–98 (1930).
N. L. Bowen and J. W. Greig, *J. Am. Ceram. Soc.*, **7**, 238–54 (1924); corrections, ibid., 410.
N. A. Toropov and F. Ya. Galakhov, *Voprosy Petrogr. i Mineralog., Akad. Nauk S.S.S.R.*, **2**, 245–55 (1953).
Shigeo Aramaki and Rustum Roy, *Nature*, **184**, 631–32 (1959).
J. F. Schairer and N. L. Bowen, *Am. J. Sci.*, **254**, 129–95 (1956).
Liberto De Pablo-Galan and Wilfred R. Foster, *J. Am. Ceram. Soc.*, **42**, 491–98 (1959).

Figure 2.1-2. Most favorable composition region on the Na_2O – Al_2O_3 – SiO_2 ternary phase diagram.

2.2 Steam Reforming Chemistry

Fluidized bed steam reforming (FBSR) for treating liquid radioactive wastes involves (a) a bed of particles fluidized by an upward flowing gas (steam in the THOR^{sm} steam reforming process) into which the liquid waste is sprayed, and (b) a reductant that is reformed by reactions with steam to produce reformed products and intermediate products that create a reactive, reducing environment to destroy nitrates and nitrites in the feed to produce environmentally benign N_2, H_2O, and CO_2. A reductant, such as carbon, is steam reformed at elevated temperatures, exemplified by the following simple reaction:

$$C + H_2O \rightarrow CO + H_2 \qquad (1)$$

CO reacts further with both steam and H_2:

$$CO + H_2O \rightarrow CO_2 + H_2 \qquad (2)$$

$$CO + 3\ H_2 \rightarrow CH_4 + H_2O \qquad (3)$$

Consumption of CO and H_2 (such as through reactions with NO_x in a steam reformer, in addition to reactions (2) and (3) drives reaction (1) to produce more CO and H_2. Reaction (1) is endothermic, so added heat is required to enable this reaction to proceed. If air or oxygen is included in the reaction mixture, the process can be autothermal. That is, exothermic reactions of carbon and the reduced gas species H_2 and CH_4 with oxygen, to produce more oxidized species CO and CO_2. Heat from the exothermic oxidation reactions provides the heat needed for the steam reforming reactions. A tendency for steam reforming reactions to form more complex hydrocarbon species is suppressed by operating with a moderate excess of steam.

In principle, all organic compounds can be steam-reformed. The process has been demonstrated on a number of organic liquids (e.g., simple hydrocarbons, alcohols, ketones, and chlorocarbons), a variety of polymeric organic materials (paint residues, caulks, shredded paper, plastics, and wood products; organics adsorbed on soils, debris, activated carbon and ash), and even coal [Elliott, 1981] and cellulosic wastes [Antal, 1979].

Nitrate salts will thermally decompose, even in the absence of reducing agents, at elevated temperatures (see below). The complete thermal decomposition of $NaNO_3$ is not well understood. Rapid heating to very high temperatures (2,200 °C) results primarily in the formation of N_2 and O_2, which are thermodynamically and kinetically favored over NO_x gas species at such high temperatures. However, at more moderate temperatures, in the absence of a reductant that participates in the thermal decomposition process to tie up oxygen, the decomposition of nitrate salts favors NO_x as the primary product [Meile, 1984].

There is general agreement in the literature that at lower temperatures the first reaction in the thermal decomposition of $NaNO_3$ is the loss of oxygen to form $NaNO_2$.

$$2\ NaNO_3 \rightarrow 2\ NaNO_2 + O_2$$

In fact, at typical steam reforming temperatures (600-750 °C), the equilibrium between $NaNO_3$, $NaNO_2$, and O_2 (without the presence of a reductant) has been studied and quantified [Freeman, 1956]. Following the initial decomposition of $NaNO_3$ to $NaNO_2$ and O_2, the mechanism of interest is the decomposition of $NaNO_2$. The decomposition of $NaNO_2$ has been reported as probably first producing NO_x [Addison, 1964].

$2\ NaNO_2 \rightarrow Na_2O + N_2O_3$

$N_2O_3 \rightarrow NO_2 + NO$

Many other reactions, some involving the direct conversion of $NaNO_3$ to products other than $NaNO_2$, have been postulated in the literature [Kramer, 1983]. N_2O has also occasionally been reported as being a product of nitrate decomposition [Bartos, 1956, Brown, 1975]. Although reaction mechanisms were not reported, N_2O can be produced from NO_x, especially in the presence of a catalyst or a reducing agent such as SO_2 [Hayhurst, 1992]. Additional products encountered include both NH_3 and HCN in prior tests [Soelberg, 2003].

The reactions above illustrate one possible route for $NaNO_3$ decomposition. In reality, it is likely that many of the above reactions occur in parallel with others such as the decomposition of nitrogen dioxide to nitric oxide and oxygen.

$2\ NO_2 \leftrightarrow 2\ NO + O_2$

Ultimately, the final mix of gaseous products from the thermal decomposition of nitrate, i.e., the ratio of NO_x to N_2 in the product stream, depends on a number of chemical and physical factors, such as catalyzing metals, residence times, reductant:oxidant stoichiometry, temperature, and flow patterns in the reaction vessel.

Reacting nitrates with reducing agents is a more direct and efficient route to producing N_2 rather than NO_x as a final decomposition product. A large number of chemical reducing agents have been examined for the denitrification of aqueous solutions. These chemicals include iron metal, Fe^{2+}, N_2H_2, glucose, CO, formaldehyde [Gunderloy, 1968, 1970], formic acid [Bradley, 1972], sugar [Bray, 1963], glycolic acid [Seymour, 1995], starch [Ryan, 1995], and urea [Cox, 1994]. Nitrate ions can be reduced to ammonia (and sometimes N_2) with aluminum [Murphy, 1991; Mattus, 1993] or iron [Cheng, 1997] powder, depending on the pH of the solution. Thermochemical reduction has also been applied to dry nitrate wastes. Ammonia and ammonium compounds have been reported to reduce nitrates directly to N_2 at temperatures of 300-600 °C [Dotson, 1975]. Coke (carbon) has also been successfully used to directly reduce nitrates to N_2 although higher temperatures were required [Meile, 1984]. The reaction of sodium nitrate and coke is representative of the thermochemical processes.

$2\ NaNO_3 + 4\ C \rightarrow Na_2CO_3 + N_2 + 3\ CO$

Carbonaceous reductants fed to the reformer provide chemically reducing conditions in the reformer via the types of steam reforming reactions described above. The higher the reducing conditions of the reformer, the more effectively nitrates in the feed are chemically reduced to N_2.

A summary of potential reaction mechanisms (not all inclusive) is given in Table 2.2-1.

Table 2.2-1. Various potential chemical reactions under steam reforming conditions.

Process Step	General Reaction Examples	Comments
Solution evaporation/particles drying	Waste sol'n (liquid) → H_2O (gas) + $NaNO_3$, $Al(NO_3)_3$, etc.	Commences in liquid droplet, continues in particle film, except at high temperatures/high heating rates when evaporation occurs above the solid-gas boundary layer. Rapid evaporation of spray droplets results in sub-micron-size particles.
Solid salt thermal dissociation/ decomposition	$2\ Al(NO_3)_3$ (s) → Al_2O_3 (s) + $6\ NO_2$ (g) + $1½\ O_2$ (g) $2NaNO_3$ (s) → Na_2O (s) + $2\ NO_2$ (g) + $½\ O_2$ (g) Na_2CO_3 (s) ↔ Na_2O (s) + CO_2 (g) Na_2CO_3 (s) + H_2O (g) ↔ 2 NaOH (l) + CO_2 (g)	Transition metal nitrates typically rapidly dissociate below 400°C. Alkali metal nitrates typically denitrate slowly and can persist to temperatures up to 600°C. Molten alkali hydroxides can lead to dissolution of other salts and bed agglomeration, which is not desirable in a fluidized bed.
Organic compound depolymerization/ devolatilization/ char formation	C_mH_n (s) → char (s) + tars/oils, C_xH_y (g) $C_lH_mO_n$ → char (s) + tars/oils, C_xH_y (g) + H_2, OH^-, H_2O (g) $C_{12}H_{22}O_{11}$ (s) → 12 C (s) + $11H_2O$ (g)	Organic evolution rates and speciation depends on hydrocarbon functional groups, particle heating rates, reactor temperature, and particle residence time. Light gases and tars evolve competitively.
Solid state organic REDOX reactions	$2\ NaNO_3$ (s) + C(s) or carbon source (s) → Na_2CO_3 (s) + N_2 (g) @ solid waste–char or carbon particle boundary [or] @ solid waste–organic compound/char in dehydrated droplets or solid layer on an existing particle.	Nitrate-organic reduction occurs spontaneously at 250–350°C and the reaction zone rapidly propagates through the remaining unreacted solid reactant mixture.
Solid state inorganic reactions	$2\ NaNO_3$ (s) + Al_2O_3 (s) → $2\ NaAlO_2$ (s) + $2\ NO_2$ (g) + $1½\ O_2$ (g) Na_2O (s) + Al_2O_3 (s) → $2\ NaAlO_2$ (s) Na_2O (s) + SiO_2 (s) → Na_2SiO_3 (l) Na_2O (s) + $Al_2Si_2O_7 \cdot 2H_2O$ (s) → $2\ NaAlSiO_4$ (s) + $2\ H_2O$ (g)	Silica is present as a contaminant in the makeup water and in the simulated heel solids. Aluminum nitrate is present in the LAW and decomposes to Al_2O_3. Alkali silicates may be molten at process temperatures. Kaolin can be added to the simulant to form alkali aluminosilicates.
Heterogeneous carbon gasification reactions	H_2O (g) + C (s) → CO (g) + H_2 (g) CO_2 (g) + C (s) → 2 CO (g) O_2 (g) + 2 C (s) → 2 CO (g) NO_2 (g) + C (s) → CO (g) + NO (g)	Gasification to CO is typically endothermic. Equation 3 is negligible under fuel-rich, steam reforming conditions unless oxygen is intentionally introduced. Equation 4 is slower than Equations 1 and 2 and may not be significant. Oxides and carbonates in the solids can catalyze char reactions.
Heterogeneous inorganic reactions	Na_2O (s) + NO_2 (g) + NO (g) ↔ $2\ NaNO_3$ (s) Na_2O (s) + CO_2 (g) → Na_2CO_3 (s) Na_2O (s) + H_2O (g) → 2 NaOH (l) Na_2O (s) + 2 HCl (g) → 2 NaCl (s) + H_2O (g) CaO (s) + 2 HCl (g) → $CaCl_2$ (s) + H_2O (g) 2 NaOH (l) + Al_2O_3 (s) → $2\ NaAlO_2$ (s) + H_2O (g) 2 NaOH (l) + SiO_2 (s) → Na_2SiO_3 (l) + H_2O (g) 2 NaOH (l) + $Al_2Si_2O_7 \cdot 2H_2O$ (s) → $2\ NaAlSiO_4$ (s) + $3\ H_2O$ (g)	Product nitration, carbonate formation, and hydration are all possible. Nitration occurs at T< 400°C. Carbonate formation occurs at T< 800°C. Hydration produces a molten phase of alkali metals capable of dissolving other product solids and causing agglomerations. Formation of alkali silicates is undesirable due to molten phases that can cause agglomeration. Kaolin can be added to form alkali aluminosilicates, which are insoluble and do not melt at process temperatures.

Table 2.2-1. Various potential chemical reactions under steam reforming conditions (continued).

Process Step	General Reaction Examples	Comments
Gaseous hydrocarbon chemistry	$CO + H_2O \leftrightarrow CO_2 + H_2$ $CO + 3\ H_2 \leftrightarrow CH_4 + H_2O$ $H_2O \leftrightarrow H\cdot + OH\cdot$ $CO + OH\cdot \rightarrow CO_2 + H\cdot$ $H_2 \leftrightarrow 2H\cdot$ $H\cdot + H_2O \leftrightarrow H_2 + OH\cdot$ $CO_2 \leftrightarrow CO + ½\ O_2$ $CH_3\cdot + H\cdot \leftrightarrow CH_4$ $2\ CH_3\cdot + H2 \rightarrow 2\ CH_4$	1. Water-gas shift reaction, significant at T>600-625°C. 2. Methanation is generally low. Hydrogen and carbon give rise to highly reactive hydrogen, hydroxide, peroxide, and oxygen radicals through the fuel-rich zone. Such reactions promote ring opening, chain breaking, hydrogen extraction/substitution reaction, etc. These reactions are very fast for T>600-650°C and lead to chain propagation. Below 600°C, many radicals terminate and continued reaction is driven by OH· radical (e.g., Reaction 4).
Gaseous nitrogen chemistry	$CH_4 + 4\ NO_2 \rightarrow 4\ NO + CO_2 + 2\ H_2O$ $CH_3\cdot + NO \rightarrow HCN + H2O$ $CH_3\cdot + NO_2 \rightarrow CH_3O\cdot + NO$ $CH_2\cdot + NO \rightarrow HCN + OH\cdot$ $CH\cdot + NO \rightarrow HCN + O\cdot$ $HCN + OH\cdot \rightarrow HNCO + H\cdot$ $HCNO + H\cdot \rightarrow \ldots NH_{i=1,2,3}$ $NH_2 + NO \rightarrow N_2 + H_2O$ $2\ CO + 2\ NO \rightarrow N_2 + 2\ CO_2$ $NO + H_2 \rightarrow NH\cdot + OH\cdot$ $NH_{i=0,1,2} + H\cdot \rightarrow NH_{j=1,2,3}$ $2\ NO_2 \leftrightarrow 2\ NO + O_2$	Nitrogen oxides are reduced to cyanides, ammonia, and nitrogen in the reducing atmosphere. Upward of 100 significant elementary-step reactions may be important. The reactions between the methyl radical and NO_x species are thought to be important mechanisms for NO_x destruction under these reforming conditions, especially for NO_2, based on prior tests conducted by the INEEL.
Overall C-NO_3 REDOX Reactions	$5\ C + 4\ MNO_3 \rightarrow 2\ M2CO_3 + 2\ N_2 + 3\ CO_2$ $5\ C + 4\ MNO_3 + 2\ Al_2Si_2O_7{\cdot}2H_2O \rightarrow 4\ MAlSiO_4 + 2\ N_2 + 5\ CO_2 + 4\ H_2O$ $3C + 4\ MNO_2 \rightarrow 2M_2CO_3 + 2N_2 + CO_2$ $3C + 4\ MNO_2 \rightarrow 2M_2O + 2N_2 + 3CO_2$	The most efficient C: MNO_3 and C:MNO_2 REDOX reactions produce N_2 and no CO, H_2, or C char. The most efficient C:NO_3 mole ratio is 1.25 to 1. The most efficient C:NO_2 mole ratio is 0.75 to 1. Numerous REDOX reactions can be written that produce various proportions of reduced or incompletely oxidized products including NO, N_2O, HCN, NH_3, H_2, CO, or C. These are all less efficient or summed with water-gas reactions. All of these reaction equations have a C:NO_3 mole ratio of 1.25 to 1.

2.3 Fluidized Bed Dynamics

2.3.1 Particle Dynamics [Boardman, 2004]

Stable fluidized bed particle dynamics requires a balance between the production of fines and control of particle growth in the fluidized bed. Excessive particle growth can lead to defluidizing agglomerations. The production of particles small enough to be elutriated with the upward moving gases must be minimized while producing a sufficient amount of small "seed" particles to provide nuclei for particle growth. Uniform feed deposition on the particles requires a uniform nozzle spray pattern and thorough mixing of the bed while the product is continually drawn from the bed to maintain a constant bed height. Buildup of particle agglomerates (caking) in the bed, on the vessel walls, on the vessel appurtenances, or on the feed nozzles must be avoided. The combined processes that affect the particle size distribution are illustrated in Figure 2.3-1. In order to maintain steady bed particle fluidization and dynamics, a target mean particle diameter must be achieved while the bed is withdrawn at the same rate as it is generated. This requires a balance between building the bed (increasing the particle diameters) and generating seed particles. If an excessive amount of fines are generated, or if the diameters of the fines are too small, then the fines will be elutriated from the bed, causing excessive loading on the off-gas cleanup equipment and possibly resulting in a product that is difficult to pneumatically transport. It is desired to maintain bed media particle sizes within the area marked "size interval" in Figure 2.3-1.

Fines generation is accomplished by two mechanisms: particle attrition and flash vaporization. The product to fines ratio (P/F) is a measure of the mass ratio of the product and fines generated during a test.

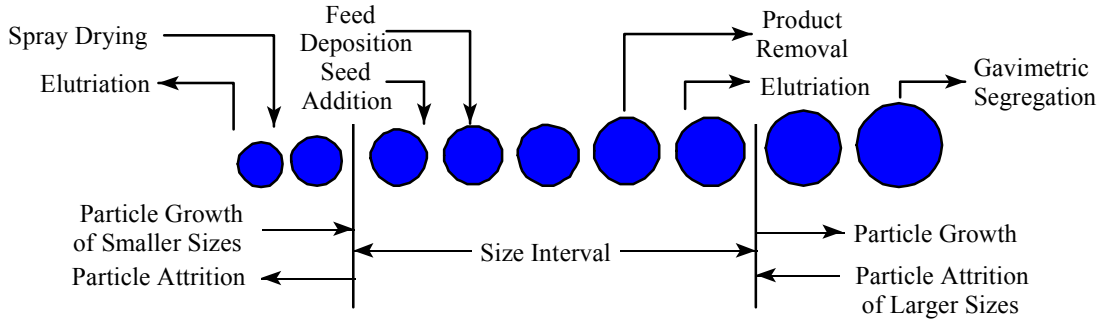

Figure 2.3-1. Processes that affect the particle size distribution during fluidized bed operation.

The mass of product includes bed that was built (or lost) during the test; therefore, the P/F can be determined by the following equation:

$$P/F = (P + FB - (SB - COT\ 0\ P\&F))/F$$

where

P/F	=	product-to-fines ratio
P	=	mass of product collected during the test (excluding COT 0)
FB	=	mass of the final bed
SB	=	mass of the starting bed

COT 0 P&F = mass of product and fines collected at COT 0 hr

F = mass of fines collected during the test (excluding COT 0).

Several operating parameters could affect particle size in the mineralizing FBSR process. These include (a) amounts and properties of slurried clay particles, (b) FBSR operating temperature, (c) atomizing gas flow rate and nozzle atomizing ratio (NAR, the ratio of the volumetric flow rates of the atomizing gas and the atomized slurry), and (d) properties such as resistance to attrition of the product particles.

The atomizing gas can affect the particle size through jet grinding and controlling the atomized feed droplet size. Increasing the velocity of the atomizing air, up to the point where sonic velocity is reached, increases the momentum of the feed spray. This increases the intensity of the particle-particle collisions in the vicinity of the feed nozzle. The collisions result in particle fracturing (attrition). The fluidizing air circulates the bed and causes particle collisions, but the fraction of fines attributed to the fluidizing air is considered minor compared to the feed nozzle atomizing gas. A separate jet grinder is sometimes used to control particle growth in order to conserve feed conditions and to prevent feed nozzle wear.

Particle elutriation is affected by the fluidizing air velocity at the top of the bed and by bubble eruption at the bed surface. As the air bubbles burst at the surface, both large and small particles are ejected up into the particle disengaging section. The fines that are entrained in the gas stream can be carried into the off-gas system unless they lose momentum and disengage from the off-gas in the freeboard section above the calciner bed. Most of the larger particles fall back to the bed; however, some of the fines remain entrained and are carried over into the off-gas cleanup train. Only those particles that have a terminal velocity that is lower than the velocity in the disengaging section ("freeboard") of the fluidized-bed will be carried out of the reactor. Particle collisions in the freeboard region also result in loss of momentum and particle disentrainment. It is therefore instructive to understand the relationship between bed fluidizing velocity and particle terminal velocity to bound operating conditions that will result in excess fines carryover.

Figures 2.3-2 and 2.3-3 illustrate the concept of (1) the minimum calculated bed fluidization velocity and terminal velocity as a function of particle diameter for various particle densities. Both charts indicate the fluidizing gas velocity of approximately 0.59 m/s at the bed "surface" (including vaporized feed water and atomizing gases). The corresponding terminal velocity plot indicates that all particles of diameter less than about 80 μm can be lost or elutriated from the bed, with all other considerations—such as particle-particle collisions, particle-wall collision, and gas velocity decrease with temperature and expansion in the freeboard section—not being taken into consideration.

The particle size distribution (PSD) is a good indicator as to whether agglomeration of the bed is occurring. In the context of this report, MMPD signifies the mass-mean particle diameter or the particle size within the particle distribution where half of the mass is attributed to particles of lesser diameters and the other half to particles of larger diameters. HMPD signifies the harmonic mass mean diameter, which is interpreted as the particle size within the distribution with the same surface-area to volume ratio as the average of the entire bed. The MMPD is readily skewed toward the larger particles because the mass of the particles is proportional to the cube of the particle diameter (assuming nearly spherical particles). The HMPD is more sensitive to the smaller particles because they have a higher surface-area to volume ratio. HMPD is used when calculating pressure drop through the bed (i.e., Ergun equation) and minimum fluidizing gas velocity. Close agreement between the MMPD and HMPD is indicative of a narrow particle size distribution. Poor agreement is indicative of a wide particle size distribution or the presence of extreme particle sizes (e.g., significant quantities of coarse agglomerates or fine "flour") that differ

from the particle sizes in the bulk media. Although the HMPD is used for calculating fluidizing gas velocity requirements, both numbers have value in monitoring dynamic changes in the bed particle size distribution.

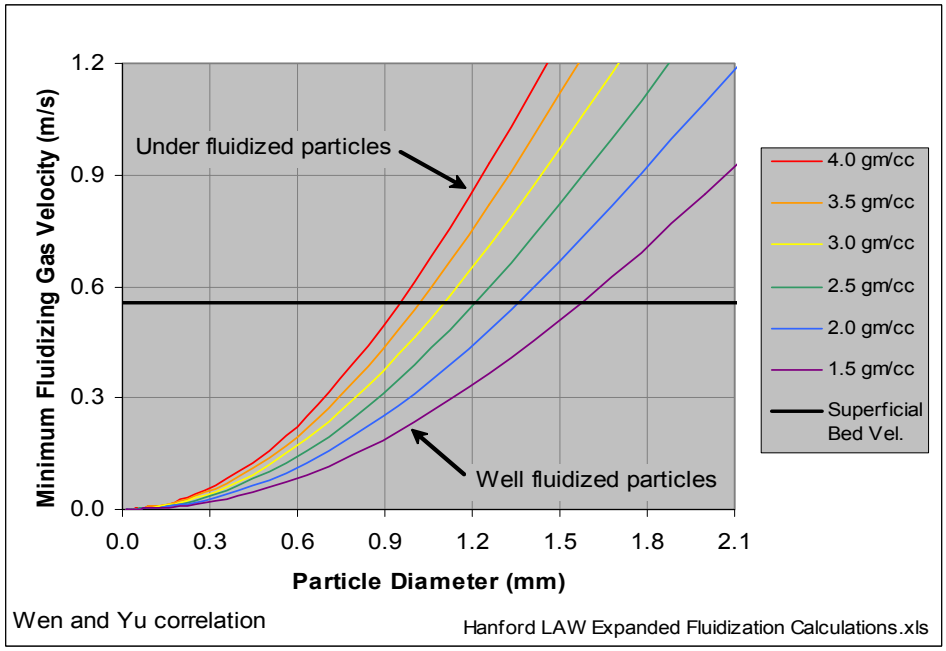

Figure 2.3-2. Minimum theoretical fluidization velocity as a function of particle diameter and density.

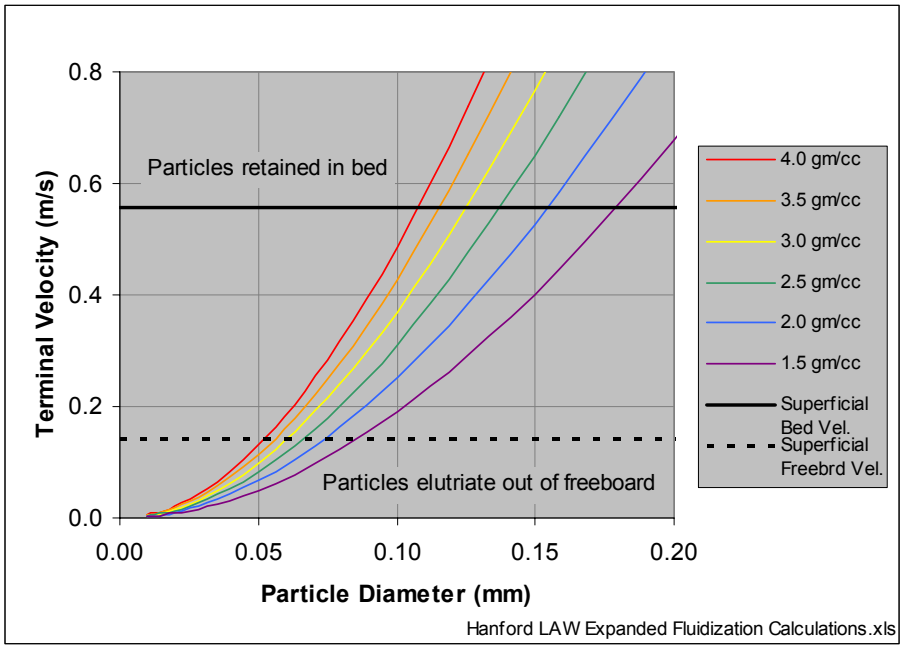

Figure 2.3-3. Theoretical particle terminal velocity as a function of particle diameter and density.

The PSD, if plotted as the cumulative percent less than the screened particle size as a function of the particle size, usually forms an s-shaped curve. A PSD with very little size variation, as is normally the case with the starting bed, is indicated by a very steep center section of the curve. A gradual slope in the center section indicates a wider variation in particle size. Departure from an s-shaped curve indicates two or more dominant chemical or physical mechanisms controlling particle growth. For example, bed agglomeration results in a bi-modal particle distribution with a particle accumulation at a high particle diameter channel. Severe bed attrition can result in small particle (fines) buildup. Ideally, particle growth will be balanced by particle attrition, resulting in a steady state MMPD and HMPD.

2.3.2 Feed Droplet Evaporation

Fine particles are generated by flash evaporation of the liquid droplets before and after adhering to the bed particles. The current feed nozzle design produces a finely divided mist in order to enhance uniform deposition on the bed particles. The atomized feed droplets, if they do not contact any solid surface including bed particles, evaporate according to the "d-squared" evaporation law [Kuo, 1986]:

$$d^2 = d_o^2 - [8 \frac{\rho_{air} D_{H_2O,gas}}{\rho_l} ln(1+B)]t$$

where B is the Spaulding transfer number calculated from the following relationship,

$$B = C_{p,l} \frac{(T_\infty - T_s)}{\Delta H_v}$$

(with standard convention for all other symbols). The longest possible droplet life, when droplets do not contact any bed particles, is thus a direct function of the properties of the gas, the temperature difference between the droplet surface and the surroundings, and, most importantly, the initial diameter of the feed droplets size. Hence, the feed droplet size can be increased to offset enhanced flash evaporation at elevated bed temperatures. However, droplets that are too large can impinge on the far wall of the fluidized bed if they do not first impinge on bed particles. This impingement can occur during slugs of fluidizing gas in a slugging fluidized bed. Larger droplets can also result in single particle quenching when they do hit a bed particle, which can give rise to possible particle-particle sticking (agglomeration) when the excessive liquid dries on the particle.

Figure 2.3-4 shows a plot of the theoretical extinction time for a droplet of water in a humid nitrogen gas stream at 600 and 700°C, respectively. The droplet life accounts for particle heating by conduction to the droplet, assuming that the velocity of the droplet is equivalent to the velocity of the surrounding gas. This assumption is a reasonable approximation for droplets that are atomized by the co-flowing atomizing gas. *These calculations assume that the atomizing gas is already at the bed temperature*. In reality, the atomizing gas must first be heated to the bed temperature; hence, the actual time of flight in non-obstructed space exceeds the correlation shown in Figure 2.3-4. This chart reveals, for example, that a 0.050-mm (or 50-micron particle) will be flash dried in 0.018 s (or 18 milliseconds).

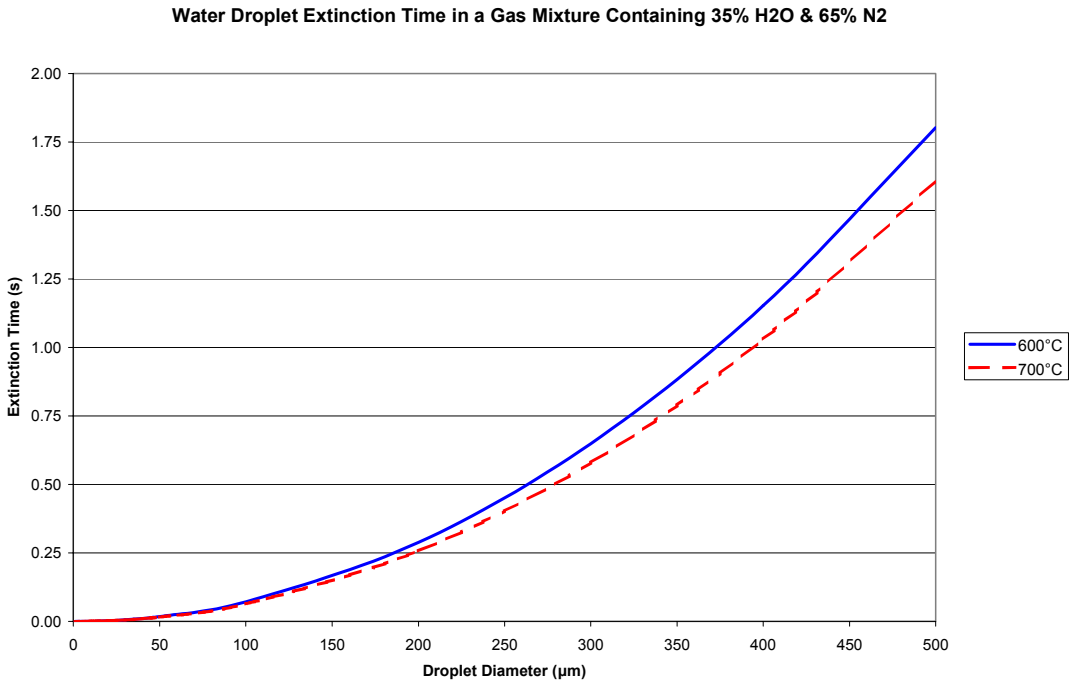

Figure 2.3-4. Comparison of droplet extinction time is a gas stream of 600 and 700°C (0 to 500 mm diameter particle size range).

Consider the following example:

Assumptions:

- *Spraying Systems nozzle*. 40/100 liquid cap, 120 air cap
- *Gas orifice surface area*. 2.2 mm^2
- *Liquid injection rate*. 6 $L \cdot hr^{-1}$
- *Nozzle atomizing air volumetric flow*. 3000 $L \cdot hr^{-1}$ (NAR = 500)
- *Gas temperature*. 600°C.

Then, using 2.3-4 and the gas velocity, the calculated extinction distance for a given water droplet is:

- *0.100 mm droplet*. 27 mm
- *0.200 mm droplet*. 80 mm
- *0.250 mm droplet*. 104 mm.

This example illustrates that a 0.250 mm particle leaving the nozzle at a spray angle of 35 degrees will impinge on the near side of a 150-mm diameter reactor (~91 mm actual distance to the wall) before it is fully evaporated, unless it impacts bed particles first. In order to minimize feed deposit on the wall, three conditions must be avoided; bed slugging (that periodically allows large gas bubbles to pass in front

of the feed nozzle, providing an open path for atomized spray to the wall at that instant), "cold" surfaces in the reformer, and coarse atomization of the feed (that allows the formation of larger spray droplets). Nozzle spray testing with water and simulant feeds should be performed to determine the minimum NAR necessary to fully nebulize the waste feeds. Nozzle plugging, however, may disrupt the spray pattern, resulting in large droplet formation that will likely exacerbate bed agglomeration and feed deposition on the wall or vessel appurtenances. Maintaining vessel wall and surface temperatures heated well above 400°C helps to prevent accretions from building on the surfaces because radiant heat transfer is sufficient to cause "film" boiling and the steam expelled from the droplets provide a protective gas barrier that prevents the droplets from physically contacting and wetting the surfaces.

The calculations also show that the affect of temperature increase from 600 to 700°C does not greatly affect particle evaporation times. Thus, spray drying of particles is more dependent on initial particle size.

Heat transfer from the bed particle to the liquid can enhance evaporation when the atomized feed droplets contact the hot bed particles. It can cause undesired over-cooling of the bed particles if the feed droplet is too large, which can lead to particle agglomeration. If the particles are hot enough, then evaporation by film boiling on the surface can result in the formation of small satellite particles that are easily ejected from the surface of the host particles. Film boiling results when the rate of heat transfer from the bed particles is high enough to cause rapid evaporation, which consequently prevents the droplets from wetting and adhering to a particle surface. Once the moisture is evaporated in the film layer above the particle, there may be insufficient adhesion of the residual solid to the surface of the particle.

Depending on the viscosity and surface tension of the feed and heat capacity of the solids, film boiling is observed at bed temperatures in excess of 600°C. Above 700°C, film boiling has been considered severe for some fluidized bed operations, and, in fact, resulted in quantitative conversion of liquid feed to fines (i.e., P/F ratio of 0.05–0.1 observed at 700°C in comparison to 0.5–0.75 at 625°C). This phenomenon thus limits the bed operating temperature when feed is being atomized and the objective is to minimize fines generation.

2.3.3 Bed Turnover

Bed turnover plays a significant role in determining the fluidized bed operating characteristics and product quality when initiating the activity with a starting bed of significantly different composition than the material to be fed to the bed. It is defined as the mass fraction of the bed that represents the feed composition as to the starting bed composition. A bed turnover of greater than 90% is generally needed to ensure that the feed and bed material are indicative of the new product versus the behavior and characteristics of the starting bed.

Bed turnover at a particular time for an experiment is defined as:

$$TO = (1 - e^{-[P/W]})*100$$

where:

$TO \equiv$ bed turnover percentage (%)

$P \equiv$ cumulative net product mass (kg) [$P = Mass_{out} - Mass_{in} + W$]

$Mass_{out}$ ≡ mass of bed material harvested from the process (excluding the cyclone sample and filter catch)

$Mass_{in}$ ≡ mass of bed material added to the reactor [$Mass_{in} = Mass_0 + Mass_{augmentation}$]

$Mass_0$ ≡ mass of the initial bed charge

$Mass_{augmentation}$ ≡ mass of seed particles, catalysts, and recycled bed media added to the bed.

W ≡ bed mass including the unfluidized heel (kg) [$W = Mass_{fluidized} * (Mass_0 \div Mass_{0,\,fluidized})$].

$Mass_{fluidized}$ ≡ mass of the fluidized bed as seen by the instrumentation

The cumulative mass of removed product is *not* equal to the cumulative net product mass (P). This is because the mass of bed is changing over time as the bed density changes. Instead, the net product must account for the change in bed mass as well as the amount of product.

The bed mass (W) used in this equation is the total bed mass and not just the fluidized bed mass. For example, some amount of the bed resides in the bottom receiver of the reactor vessel. Since this material is not fluidized, it does not show up in the bed mass as indicated by the bed pressure drop or density measurements. However, the mass of this material must be included in the total bed mass when calculating the bed turnover.

3. EXPERIMENTAL SETUP/APPROACH

Mineralizing, steam reforming process technology, offered by THOR^{SM} Treatment Technologies (TTT), LLC, under U.S. Patent No. 6280694, provided the basis for process materials and conditions utilized in this experimental program. The performing team consisted of personnel from INEEL, TTT, and SAIC. The mineralization steam reforming process technology tests were performed by the team in the INEEL's pilot scale fluidized bed processing test system located at the SAIC STAR Center in Idaho Falls. The test system/equipment is briefly described in Section 3.2. The test data collection system/methods for process monitoring/control and the process/product materials sample collection and analyses methods utilized are described in Section 3.3. The process specific input materials selected and utilized for the mineralizing steam reforming test are described in Section 3.4. Section 3.5 details the startup conditions and operational parameters that were planned.

3.1 Test Objectives

Within the overall objectives of the collaborative approach, discussed in section 1, the pilot-scale FBSR LAW tests objectives were to: 1) produce a representative FBSR mineralized product for use in validating and further developing correlations with product from stepwise laboratory scale simulated FBSR chemistry experiments, 2) generate data that validates the operability of fluidized bed steam reforming with the appropriate waste mineralizing chemistry, 3) provide fundamental understanding of the chemistry and mineralization of waste forms in containing and holding radionuclide surrogates and hazardous contaminants, and 4) provide information about the longer term performance/durability of the mineralized product.

The pilot-scale tests were configured to provide data to address the above objectives by addressing the more specific test objectives summarized, and prioritized in order of their perceived importance, in the following Table 3.1-1.

Table 3.1-1. Pilot scale mineralizing, steam reforming test objectives.

Objective Statement	Quantifiable Objective Target or Criteria	Measurable Parameters and Test Methods
Generate a product that incorporates sodium into the mineral forms of nepheline, sodalite, and nosean. Determine if product generated is leach resistant and durable. Determine the fate of radionuclide surrogates (I, Re) and hazardous metal components (Cr). [Note: For the most part, the product performance measurements will be performed by SRNL and PNNL, and reported by those entities.]	• <3 wt% soluble Na in bed product relative to product mass • <1 wt% soluble nitrate in bed product and fines particles. • <3 wt% carbonate in bed product • <1 wt% organic in bed product, exclusive of carbon added as reductant • Passes TCLP for hazardous metals • Results of PCT are comparable to LRM glass • Performance is comparable to LRM glass	• XRD/SEM analysis of product • Chemical analysis of product per sample analysis plan • Perform PCT and TCLP measurements for durability • Perform single pass flow through (SPFT) testing and pressurized unsaturated flow (PUF) testing to measure performance
Produce a non-agglomerating bed product and fines fraction. Determine product bulk and true density. Maximize product to fines ratio.	• <10 wt% particle agglomeration/clustering relative to bed mass • P/F mass ratio >3.5 desirable to maximize the density (minimize	• Bed and fines size particle distribution and density trends • Product to fines ratio as calculated from measurement of product and fines cumulative masses

Objective Statement	Quantifiable Objective Target or Criteria	Measurable Parameters and Test Methods
	the volume) of blended product	
Determine suitable fluidized-bed operating parameters for treating the simulated LAW that will minimize carryover of unreacted carbon and clay additives in the filter product	• 80 hrs continuous operation at a feed rate of >3 L/hr blended feed • Uniform temperature distribution in bed with no greater than ±10ºC axial temperature variation in the bed • Bed height, as measured by bed pressure drop and bed density, to be maintained between 25 -28 inches. • Approach a controllable steady-state bed particle size distribution	• System flow meters, temperature indicators and pressure transducers • Gravimetric measurement of 8-hr bed samples and fines samples • MMPD and HMPD of 4-hr bed and fines samples density, agglomeration, etc.
Demonstrate acceptable material balance closure for major and minor constituents	• Material balance closure of ±10% for simulant constituents (Al, Na, K, Cl, F, NO_3, Cr, Re, I, etc.).	• Chemical analysis and mass measurements of FBSR products • Off-gas analysis with the continuous emissions monitoring instrumentation (CO, CO_2, Cl, etc.)
Demonstrate destruction of organic components in the feed.	• Achieve >98% destruction of organic constituents relative to organics in the feed.	• CEM measurements upstream and downstream of the thermal oxidizer. Analysis of bed product and fines for organic carbon. Mass balance analysis.
Demonstrate decomposition of nitrates, nitrites, and NO_x	• Achieve >80% destruction of NO_x off-gas emissions relative to nitrates and nitrites in the feed.	• Measurement of residual nitrate and nitrite in the FBSR solid products, and CEM NO_x measurements.

3.2 Test System Equipment

This section provides a summary description of the INEEL's pilot scale Fluidized Bed Processing Test system (FBPT) in the steam reforming processing configuration utilized for the LAW mineralizing tests reported herein. An overview of the Fluidized Bed Steam Reforming (FBSR) test system is provided along with further description of selected key components/equipment of particular interest for this test.

The fluidized bed processing test system has been utilized to date to provide for a variety of fluidized bed steam reforming and calcination/oxidation process test conditions on various waste simulant materials for several potential liquid radioactive/mixed waste applications. The different tests have employed somewhat varied and evolving components and configurations appropriate to the particular process and waste application of interest, but most of the test system/components have remained the same.

3.2.1 FBSR Test System Overview

A simplified process flow and instrumentation diagram for the FBSR mineralizing process test system is shown in Figure 3.2-1. The fluidized bed section of the test system has a six-inch nominal inside diameter. Experience at the INEEL with pilot scale fluidized beds, ranging in diameters from as small as 3 inches up to 12 inches, has shown that a 6-inch diameter bed is typically the smallest size that still provides product bed particle attrition and growth dynamics that approach those of larger reactor beds. Even with a 6-inch bed diameter, the bed operates in an axial slugging mode for the fluidizing gas rates of interest, rather than the bubbling mode that would be more typical of larger-diameter, full-scale reactor beds. The axial slugging mode, however, provides the vigorous bed solids/gas mixing and large interface area for gas/solids contacting necessary for effective representation of the process thermal and chemical reaction conditions expected in a full scale fluidized bed reactor system. The 6-inch diameter bed is a reasonable compromise between a bed large enough to provide representative processing test data and a system small enough to control experimental parameters and minimize test permitting, operations, and waste disposal costs.

The FBSR test system/equipment consists of several primary subsystems including: 1) feed systems/equipment for gases, liquids/slurry, and small solids, 2) the fluidized bed reactor vessel consisting of the bed bottom receiver and fluidizing gas distributor section, the fluidized bed section, the upper larger diameter freeboard (bed particulate disengaging) section, and the vessel wall external heating system, 3) the process product/solids collection and management systems, 4) the off-gas treatment/emissions-control systems, and 5) the process monitoring and control system.

The FBSR test system occupies a space approximately 40 feet by 40 feet in area and 20 feet in height. All wetted components are constructed from corrosion resistant materials. Equipment and piping are fabricated from 300-series stainless steel except for the reformer vessel, which is fabricated from Inconel 800H. The system can be manually controlled or automatically controlled using a Process Logic Controller (PLC) system with multiple human-machine interface (HMI) stations. The STAR Center provides for all necessary test system utilities and support services including electrical power, water, compressed air, nitrogen, oxygen, various specialty calibration gases for continuous emissions monitoring systems, test system operations, permits, and materials/wastes management.

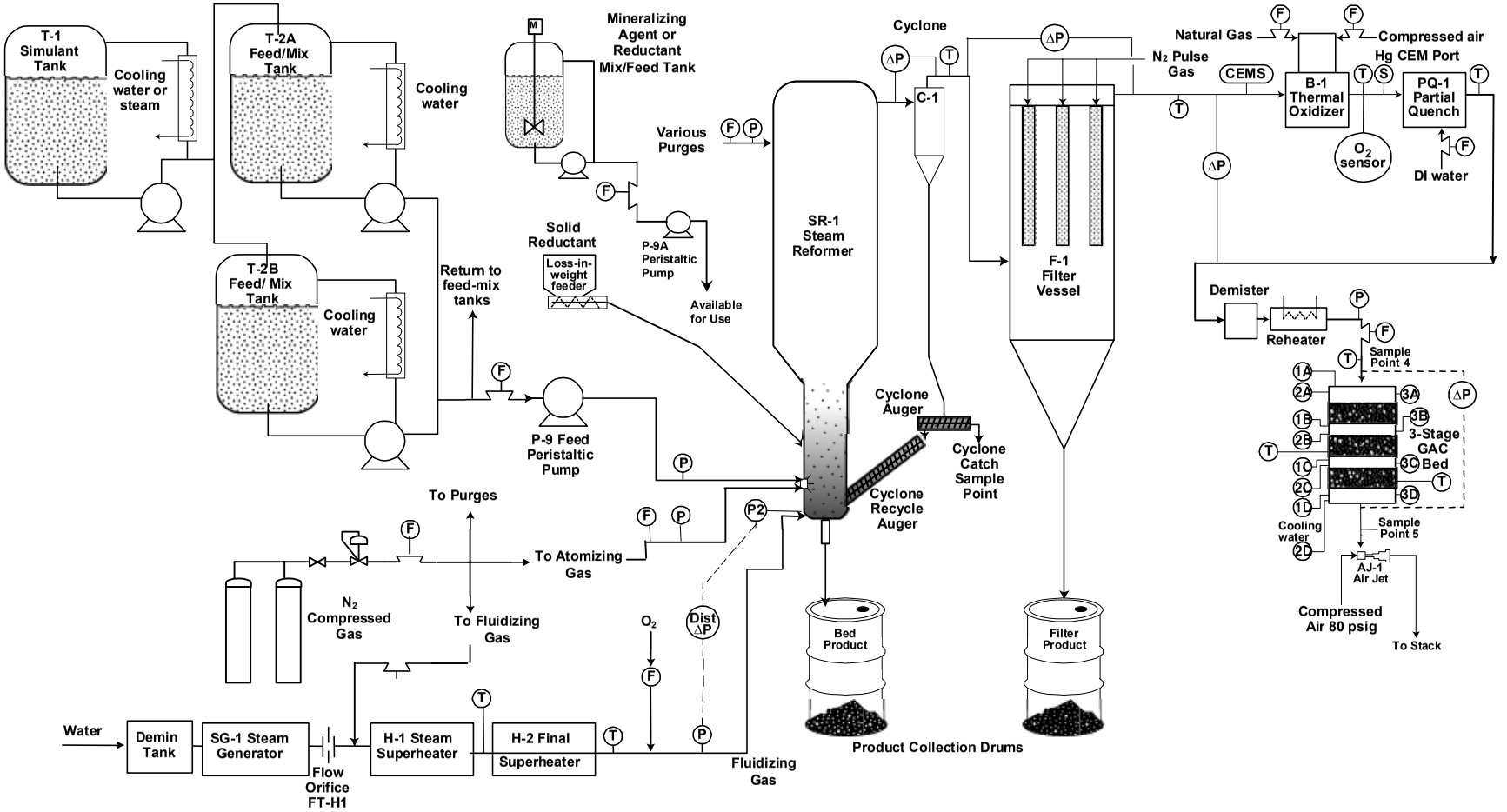

Figure 3.2-1. Process flow diagram for the fluidized bed mineralizing steam reforming demonstration.

3.2.2 Fluidized Bed Reactor Vessel

The fluidized-bed reactor vessel (shown in Figure 3.2-2) is made of Inconel 800H pipe to tolerate operating conditions, including temperatures that could reach 800°C, oxidizing or reducing conditions, and the presence of corrosive or hazardous materials. The main features of the fluidized bed vessel are the fluidized-bed section and the freeboard (particle disengaging) section. The stainless steel bottom bed receiver and fluidizing gas distributor section (shown in Figure 3.2-3) provides the reactor bottom vessel closure and entry/distribution for the bed fluidizing gas.

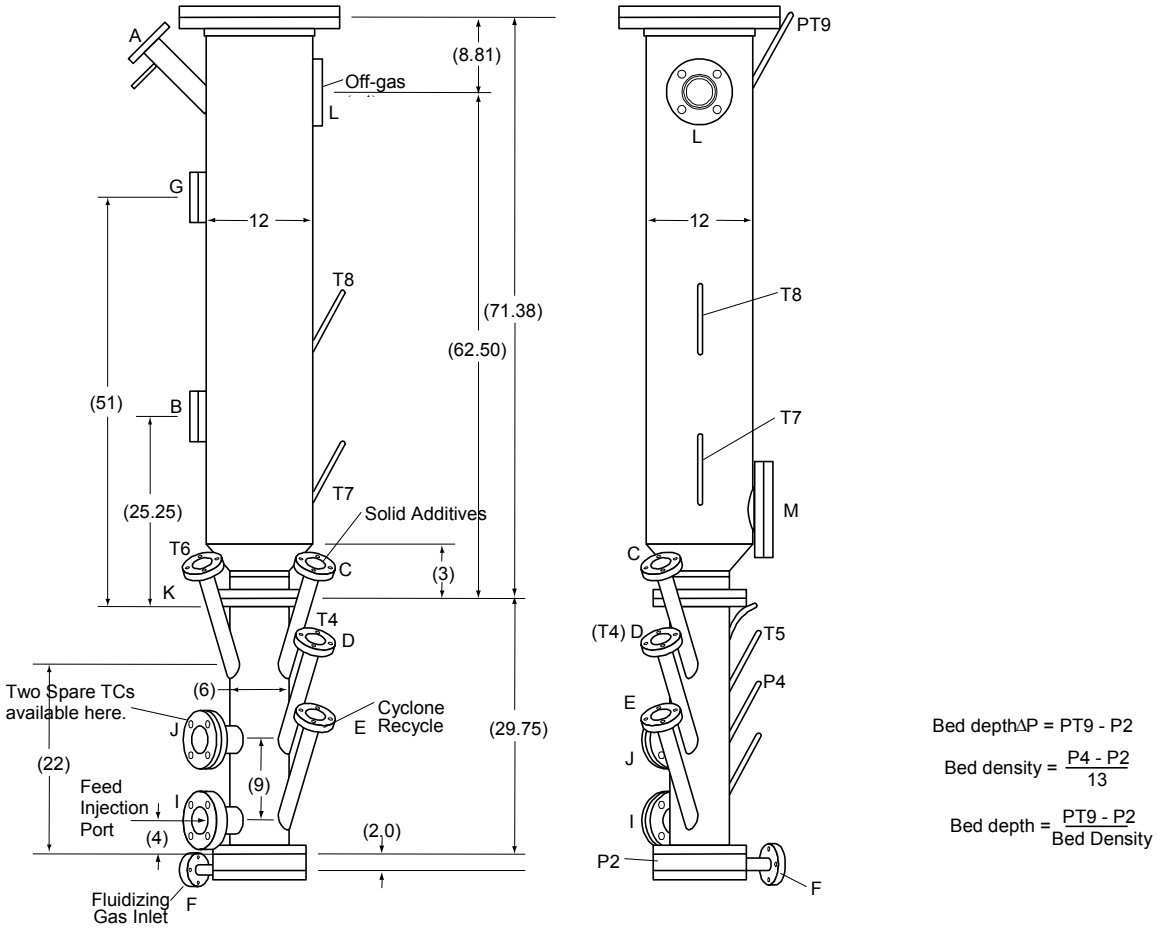

Figure 3.2-2. Fluidized bed reactor vessel.

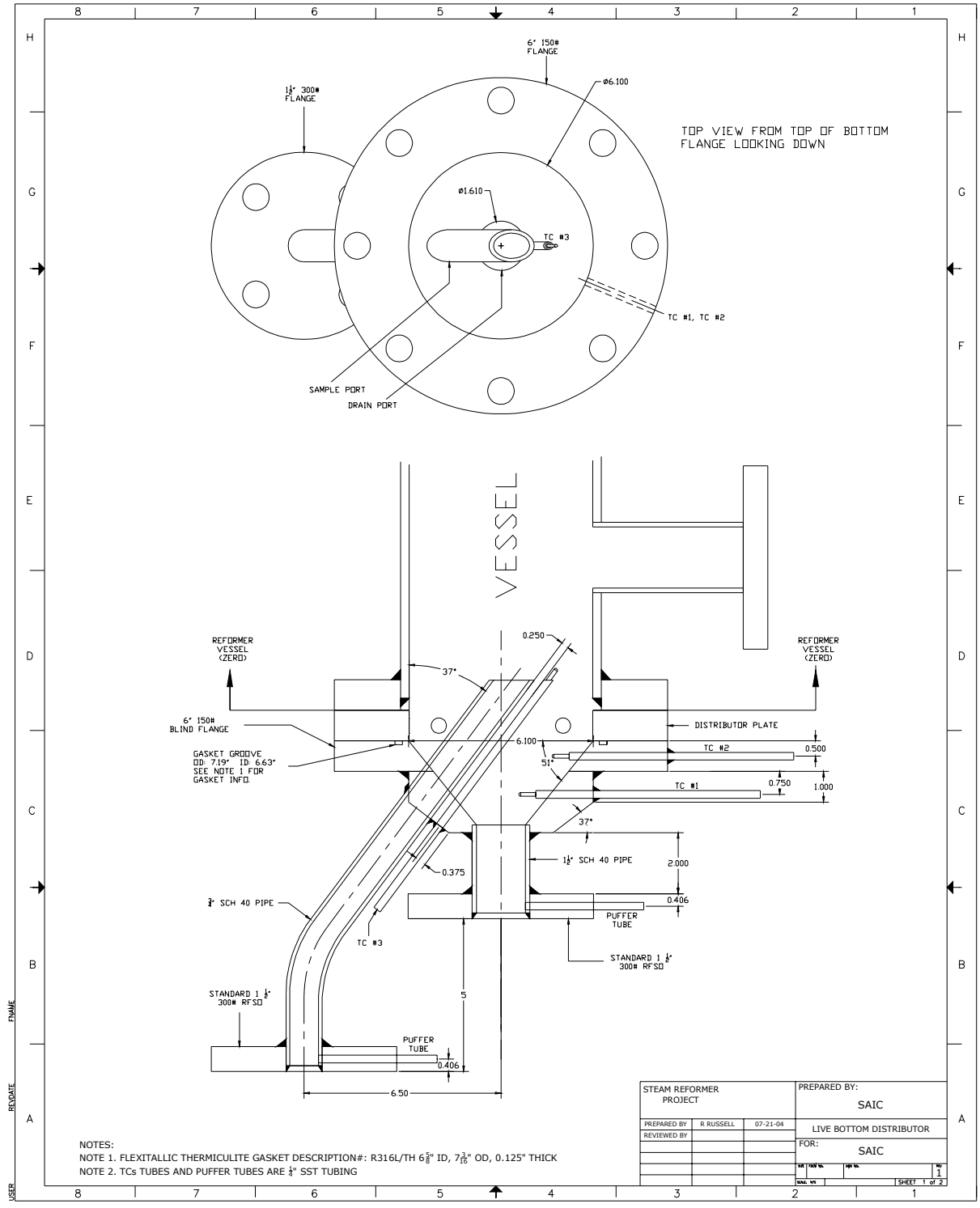

Figure 3.2-3. Reactor/reformer vessel bottom receiver.

The vessel bottom receiver consists of 6-inch, 150# flange and flat stock machined and welded to provide a conical type bottom that will collect static bed materials and facilitate the in-process removal/draining of product bed and agglomerates through a standard 1 ½ -inch drain pipe. The bottom receiver also provides for a ¾-inch sample tube/riser for fluid bed sample collection and three thermocouples for bottom bed region temperature measurement. One thermocouple (TC3) extends into the fluid bed along with the sample tube and the other two (TC1 and TC2) extend into the conical bottom bed region. Small purge/pulse gas ports are also provided both in the bed sample and drain port flanges/receivers to loosen, if necessary, collected/static product bed granules or larger agglomerates for in-process sampling/draining.

The fluidizing gas distributor bolts in between the reactor vessel flange and the bottom receiver flange. A pressure measurement port is provided through the side of the distributor flange for measuring local static pressure in the bed/vessel at the distributor elevation and for use in determining total bed height and bed density from differential pressures. The pressure drop of fluidizing gas flow across the distributor is designed to be sufficient ($\Delta P_{dist} \geq 14$"WC) for the range of bed fluidization gas flows/velocities needed to properly fluidize both the starting bed and later product bed materials, which can be of different particle density and size, and to prevent backflow of particulate into the distributor.

Various fluidizing gas distributor types are possible and several different designs have been utilized and described in earlier test reports. The fluidizing gas distributor utilized for this mineralizing steam reforming test was a THOR^{SM} Treatment Technologies, LLC proprietary design.

Direct observations of the fluidized bed flow convection cells and fluidization mode cannot be made in the 6-inch steam reformer reactor vessel during processing test operations. Prior to the mineralized steam reforming tests the FBSR vessel bed section was, therefore, modeled using a Plexiglas tube and suitable bed material, so that a visible representation of the likely bed fluidization/flow patterns could be obtained and photographically recorded in comparative nonthermal tests of the INEEL ring distributor [Soelberg, 2004b] and the THOR^{SM} distributor. The objective was to obtain a qualitative visual comparison of the fluidization of bed material and flow patterns resulting from the gas injection points and differing distributor geometries, rather than to evaluate distributor pressure drop. The distributors utilized were from existing available stock and selected to have similar pressure-drop values during operation. Hydraulic similitude was considered in establishing the cold flow test conditions. Appendix A provides details of hydraulic similarity experimental results.

These nonthermal hydraulic similarity tests showed that both the THOR^{SM} and INEEL distributor designs adequately fluidize the bed. The emulsion phase was observed to be in motion at all points in the bed and around the bottom flange at the elevation of the distributor. The bubbles emanating from the THOR^{SM} distributor were visible near the edge of the supporting flange, but not along the reactor wall orthogonal to the distributor. The ring distributor bubbles were seen at the reactor wall around most of the reactor circumference. By all appearances, the ring distributor seemed to distribute the gases more uniformly in the immediate vicinity of the distributor than the THOR^{SM} distributor. The movement of the emulsion phase appeared to be independent of the distributor type and configuration at the elevation of side port I in the reformer vessel (location of the liquid/slurry feed atomization nozzle).

3.2.3 Solids/Fines Collection

Solid and gaseous materials are produced during the fluidized bed reactor processing of simulated wastes and additive feed materials. The solid particles of sufficient mass remain fluidized within the bed and are sampled/drained into containers as appropriate through manually operated valves and piping beneath the sample and drain ports in the reactor bottom receiver. The gases and smaller entrained solids (fines) exit the fluidized bed reactor vessel freeboard section and flow through a 6-inch diameter cyclone

separator designed to remove 70% of 3-5 μm solid particles when operating at a pressure drop of 5 inches of w.c. The off-gas exiting the cyclone is subsequently further filtered for remaining very small entrained particulate in a "hot candle filter." This "hot filter" consists of a stainless vessel containing seven 2.5-inch-diameter, 24-inch-long, sintered-metal filters with a nominal pore size of 2 μm.

The solids collected in the cyclone (cyclone catch) during this steam reforming process are continuously drained and recycled to the fluidized bed through a series of two augers. The first auger can be operated in either a forward or reverse rotation. With the forward rotation, the cyclone catch is fed into the second auger, which pushes the product through port E (Fig 3.2-2) into the bottom of the fluidized bed section of the reactor vessel. When the first auger is operated in reverse, the cyclone catch is drained and subsequently collected in a sample container, which is located below two valves in the drainpipe in order to provide for process pressure isolation and minimize air in-leakage during sampling. With the exception of the cyclone solids collected during sampling events, the cyclone catch is continuously recycled to the fluidized bed.

The hot filter particulate catch is collected continuously and drained into a filter fines/product container located below the filter vessel. The product container is periodically emptied and weighed for material balance closure and to obtain samples for analyses.

3.2.4 Process Feed Systems

Various materials in the form of liquids, solids, and gases are provided through several feed subsystems in order to obtain desired process materials and conditions in the fluidized bed reactor. For the mineralizing steam reforming process the primary liquid feed is a slurry consisting of the liquid waste simulant solution mixed with selected amounts of an insoluble powdered solid (kaolin clay) as a mineralizing additive. The primary dry solid feed materials are granular carbon and initial starting bed media (alumina grit). Process feed gases consist of fluidizing gas (superheated steam), atomizing gas (nitrogen and oxygen), and minor purge gas (nitrogen).

3.2.4.1 Liquid Feed System

The liquid feed system consists of three tanks equipped with variable speed agitators and a recirculation/transfer pump to ensure that solutions are fully mixed and that insoluble solids remain suspended and uniformly blended (e.g., clay additive solids in the mineralizing process waste feed/slurry).

The liquid waste (LAW) simulant from the simulant solution tank is mixed with the powdered clay additive in the feed mixing tanks and is continually recirculated through the feed/mix tanks with recirculation pumps. The solution is pumped, via a slipstream, as a slurry to the fluidized bed by a peristaltic pump. A coriolis mass flow meter for measurement and control of the liquid/slurry flow is in this line to the fluidized bed. The liquid/slurry waste simulant feed enters the fluid bed as an atomized spray via an atomizing nozzle located in Port I of the reactor vessel (see Figure 3.2-2).

Several different nozzle types and sizes were evaluated prior to this Hanford LAW FBSR test. This evaluation was performed in an effort to improve longer-term atomization performance and minimize the chance of forming defluidizing agglomerations during FBSR operation due to nozzle accretions or other forms of nozzle anomalies. The nozzle types included: (a) SprayCo nozzles of different sizes, with and without the SprayCo antibearding configuration, that were designed for atomizing feed through the FBSR side wall, and (b) uniaxial-tube Bernoulli-effect (UTB) nozzles of different sizes and configurations. The UTB nozzle was modeled after the nozzle design used in previous THOR^{sm} experimental activities [Jantzen, 2002]. The UTB nozzle is designed to atomize feed co-axially with the flow of the atomizing gas. A variation of the SprayCo nozzle design, designated the

Marshall/Eldredge nozzle, was selected for use during this Hanford LAW demonstration. This nozzle was based on prior nozzle evaluation and testing activities. The Marshall/Eldredge nozzle was uniquely modified to prevent or minimize the formation of process solid deposits on the nozzle surfaces exposed to the fluidized bed.

The nozzle maintains the same liquid/slurry feed and annular atomizing gas orifice dimensions of the original SprayCo nozzle (0.100 inch ID and 0.150 inch OD liquid feed tube with a 0.180 inch ID air cap). Maintaining these dimensions was intended to preserve satisfactory liquid/slurry spray atomization performance (drop size distribution over desired flow ranges) previously obtained with the SprayCo nozzle when tested with sodium-bearing waste and Hanford LAW slurries.

The atomization performance of each nozzle type and size was tested by spraying feed slurries through the nozzles under selected atomizing conditions and observing the atomizing results. Appendix B summarizes the results of several nozzle atomization tests. A limited qualitative photographic record of the tests was made. Both UTB and SprayCo nozzle types were tested at various times prior to the Hanford LAW FBSR test. The UTB nozzle was not selected for use in the Hanford LAW test, because operational experience indicated that the nozzle type might have contributed to bed defluidizations during an SBW FBSR test in July (data to be published).

Liquid atomization depends on, among other factors, the liquid viscosity. In conjunction with the nozzle atomization tests, relative viscosity measurements were made for the Hanford LAW simulant and compared to measured viscosities for water and SBW simulant, with and without slurried clay. The viscosity measurements are also summarized in Appendix B.

Marshall/Eldredge nozzle atomization tests performed prior to this demonstration confirmed earlier nozzle atomization test results. The smallest average Hanford LAW simulant slurry droplet size was about 0.1 mm, even at NARs up to 750 and atomizing gas flow rates up to 3.4 kg/hr. This size is about ½ of the average bed particle size for the 70-grit alumina starting bed used in the Hanford LAW FBSR test. The minimum atomizing gas flow rate that still achieved average droplet sizes of about 0.1 mm was about 2.5 kg/hr. Smaller average droplet sizes, under 0.1 mm, may be achievable by extrapolating the range of measured data out to higher atomizing gas flow rates, perhaps to 4 kg/hr or higher. At atomizing gas flow rates less than about 2.5 kg/hr the average atomized droplet size and the droplet particle size distribution rapidly increased, even at lower slurry feed rates.

Analysis of the atomization test data showed that (a) the atomizing gas flow rate, rather than the nozzle atomizing ratio (NAR) dominated the slurry atomization, (b) the SprayCo nozzle atomized the slurry to a smaller particle size distribution than did the UTB nozzle at higher slurry feed rates of 7 kg/hr and higher atomizing gas flow rates, and (c) the UTB nozzle atomized the slurry to a smaller particle size distribution than did the SprayCo nozzle at lower slurry feed rates of 3.5 kg/hr and lower atomizing gas flow rates.

3.2.4.2 Solid Feed Systems

Solid carbon utilized as a reductant material in the steam reforming reaction process is metered into the process by a vibratory feeder. The hopper of the vibratory ramp feeder is manually charged with a batch of carbon that is then fed via a controlled vibratory ramp to a small weigh hopper/funnel mounted on a load cell. The weigh hopper records and discharges a small feed batch to a feed pipe lock hopper section bounded on the inlet and outlet by two ball valves that operate sequentially to form the lock hopper. Nitrogen gas purges in the lock hopper/pipe keep atmospheric air from entering the process with the carbon feed and provide minor motive force to loosen and inject the low density carbon granules into

the bed. This system is calibrated for the specific carbon that is used, and the PLC controls the carbon feed rate near the desired value.

Starting bed solid granular material (e.g. alumina grit) and any similar subsequent solid additions to the bed are made by simple manual batch feed and gravity drain through vessel port C (Figure 3.2-2). The two-valve lock hopper prevents process pressure disturbance and air in-leakage. Materials of sufficient density subside into the fluidized bed without further assistance. Other granular solid additions to the bed can also be made via the carbon feed/funnel system.

3.2.4.3. Gas Injection Systems

Process gases supplied to the fluidized bed include the reactor bed fluidizing gas and the atomizing nozzle gas. The fluidizing gas used for this steam reforming process was superheated steam, along with a small amount of oxygen. Nitrogen was used as the atomizing nozzle gas and also for a variety of small instrument and feed line purges, hot filter pulse gas, etc. Air is utilized as the oxidizing gas in the off-gas system thermal oxidizer.

Compressed air is utilized in various other portions of the system for functions external to the process, such as pilot valve operations and the facility gas eductor pump. The system is configured to provide compressed air from a diesel-powered compressor.

Small amounts of various bottled specialty gases are also utilized in periodic calibration of the off-gas monitoring instruments (CEMs), but do not enter the process flow.

The fluidizing steam is generated by the test system in a small steam generator/boiler and super-heated in electrical resistance Inconel tube heaters, which include customized 303 stainless steel mesh internals for improved heat transfer to the fluidizing gas at low flow rates. The superheater element (pipe) temperatures are maintained just below a maximum operating temperature limit of 1,100°C. The maximum fluidizing gas temperatures achievable at the super-heaters' exit may vary as a function of the fluidizing gas properties and mass flow rates, but is generally close to the operating bed temperature. Supply lines from the super-heaters to the vessel fluidizing gas distributor are insulated to maintain temperatures as much as possible.

3.2.5 Off-Gas Treatment System

The off-gas treatment system, down-stream of the cyclone and hot filters, consists of a natural gas-fired thermal oxidizer, partial quench vessel, demister, re-heater, and a three-stage granular activated carbon filter bed. The process gases exiting the hot filter are passed into the natural gas-fired thermal oxidizer (typically operated at 1,000°C), where they are combined with air to oxidize the hydrogen, carbon monoxide, methane, and other hydrocarbons resulting from the steam reforming process. The oxidized gases are then partially quenched with water spray to a temperature of 130°C. Although the partially quenched gases are not over quenched during normal operation, and remain above the dew-point temperature (no entrained mist), the off-gas is still passed through a demister and a re-heater to assure desired gas conditions entering the granular activated carbon filter/sorption column. The carbon captures trace concentrations of halogen gases, SO_2, NO_x, and trace hydrocarbons.

3.3 Test Data Collection and Sampling

Diagnostics performed during the FBSR tests included (a) continuous process measurements including key process flow rates, temperatures, and pressures, (b) continuous off-gas composition measurements, and (c) sample collection for laboratory analysis. These diagnostic activities provided data for controlling the process within test acceptance limits and for mass balance calculations to determine the fate of feed constituents.

3.3.1 Process Measurements

The fluidized bed test system data acquisition and control system (DACS) uses Allen Bradley programmable logic controllers (PLCs) for control and data acquisition. The PLC uses Rockwell hardware and software to monitor and control operation of the process from two or more human-machine interface (HMI) personal computer workstations, located in the vicinity of the process equipment. Additional workstations are available, one for use at the CEMS panels, and one for monitoring only (no control allowed) located in an office area for non-operating personnel.

The process control functions include automated control of valve and pump sequences for the feed system, automated control of all total gas flow rates, selectable input temperature control for the fluidized bed vessel, vacuum control of the system based on the pressure in the reformer, and limited control of the CEMS. The graphical user interface (GUI) for the system shows the status of the components, provides a control interface for the operator, and displays readings from all the instrumentation in numeric and graphical trend form.

The data acquisition system utilizes Rockwell software (RSSql) integrated Sequel databases for electronically archiving data as it is monitored. Each record in the database includes the tag name for the data-point, the description, the value, the units, and a time-stamp. Analog values from the system are archived once per second, and discrete values are archived on change of state. Table 3.3-1 lists key process data recorded during the LAW FBSR demonstration. Hundreds of other parameters and calculations, including the CEMS data, were logged automatically by the PLC, and other parameters such as purge gas flow rates, measured using rotameters, were logged manually.

The process monitoring workstation in the office area was equipped with a Web interface to the database for access to the archived data during the test. The Web interface provides data access from the database and averages at user-defined intervals in Microsoft Excel spreadsheets.

Process data that was not electronically logged by the PLC system was recorded manually on operator data sheets. Manual control of many process parameters was also done according to operator discretion, the test plan, and steam reformer system operating instructions. The measured data are provided in subsequent sections of this report.

Table 3.3-1. Key process data that was electronically or manually logged.

Parameter	Units	Instrument	PLC tag name	Manual log frequency	Comments
Simulant feed rate	kg/hr	Micro Motion CFM010M 0-15 kg/hr coriolus mass flow meter	SR1_F1A_VAL	1/hr	
	liters/hr		SR1_F1A_VFR	Not logged manually	Local readout
Simulant density	gm/ml		SR1_D1_VAL	1/hr	
Simulant composition	---	---	---	Each feed mix	Determined at time of simulant preparation from recipe, including any organic or inorganic additives; verified by post-test sample analysis

Parameter	Units	Instrument	PLC tag name	Manual log frequency	Comments
Composition of each simulant additive	---	---	---	Each additive	Use vendor-provided composition or sample analysis
Atomizing gas flow rate	kg/hr	Brooks SLA 5850 0-100 SLM mass flow meter	SR1_F1B_KGH	1/hr	
Solid reductant feed rate	kg/hr	Pioneer Feeder model 1.5 cu.ft.	LF2_FD_RATE	1/hr	Calibrated vibratory feeder with load cell for active feed rate control
Solid reductant cumulative mass fed	kg		LF2_TOTAL2	---	The cumulative mass fed is calculated by the PLC from the feed rate and the time fed
		Weigh scale	---	1/hr	The mass of carbon added to the feed hopper is weighed, totaled, and recorded manually
Solid reductant composition, density, and particle size	---	---	---	Each additive	Use vendor-provided composition or sample analysis
Starting bed media mass	kg	Weigh scale	---	At test start	
Starting bed media composition, density, and particle size	---	---	---	Each additive	Use vendor-provided composition or sample analysis
Fluidizing gas 1 (steam) flow rate	kg/hr	Rosemount 1195/3095 Pro-Plate Tri-Loop orifice plate	H1_F_PV	1/hr	
Fluidizing gas 2 (O_2) flow rate	kg/hr	Brooks SLA 5850 0-30 SLM mass flow controller	SR1_F2_KGH	1/hr	
Fluidizing gas composition	---	---	---	Each gas	Based on recommendation and gas mass flow
Fluidizing gas temperature (below distributor plate)	^oC	K-Type TC	H2_T_VAL	1/hr	Measured upstream of the steam distributor and upstream of where the fluidizing O_2 mixes with the steam
Fluidizing gas velocity ratio (U_{mf}, ratio to minimum velocity)	---	---	---	1/hr	Calculation from fluidizing gas flow rate and minimum velocity
Fluidizing gas velocity	m/s	---	FLUIDIZING_FV	1/hr	Calculation from fluidizing gas flow rate
Total N_2 flow rate	kg/hr	Kurz 504FT thermal meter	V1_F_VAL	1/hr	Total N_2 flow rate is the sum of the atomizing N_2 flow rate and purge N_2 flow rates
Fluidized bed lower wall temperature	^oC	K-Type TCs	SR1_T20_VAL	---	
Fluidized bed upper wall temperature			SR1_T19_VAL	1/hr	
Disengage section lower wall temperature			SR1_T13_VAL	---	
Disengage section upper wall temperature			SR1_T11_VAL	1/hr	
Parameter	Units	Instrument	PLC tag name	Manual log frequency	Comments
Distributor plate dP	inches water	Rosemount 0305RC5/2024D 0-100 in. H_2O	SR1_PD1_VAL	1/hr	
Fluidized bed lower 12 in. dP			SR1_PD2_Averaged	1/hr	
Fluidized bed dP			SR1_PD3_Averaged	1/hr	
Bed temperature 1 in. below distributor	^oC	K-type TCs	SR1_T2_VAL	1/hr	
Bed temperature 1 in. above distributor			SR1_T3_VAL	1/hr	
Bed temperature 11 in. above distributor			SR1_T4_VAL	1/hr	
Bed temperature 17 in. above distributor			SR1_T5_VAL	1/hr	
Bed temperature 21 in. above distributor			SR1_T6_VAL	1/hr	

Parameter	Units	Instrument	PLC tag name	Manual log frequency	Comments
Disengage section lower off-gas temperature			SR1_T7_VAL	1/hr	
Disengage section mid off-gas temperature			SR1_T8_VAL	1/hr	
Disengage section upper off-gas temperature			SR1_T9_VAL	1/hr	
Cyclone dP	inches water	Rosemount 2024D 0-100 in. H_2O	C1_PD_VAL	1/hr	
Cyclone exit off-gas temperature	°C	K-type TC	C1_T3_VAL	---	
Filter dP	inches water	Rosemount 2024D 0-100 in. H_2O	F1_PD_VAL	1/hr	
Filter exit off-gas temperature	°C	K-type TC	F1_T2_VAL	1/hr	
Filter outlet off-gas flow rate	kg/hr	---	TOTAL_KGH_BEFORE_OXI	1/hr	Calculated from the input flow rates, gas generation in the FBSR, and gas mole weight
Oxidizer gas temperatures, stages 1, 2, and 3	°C	K-type TCs	B1_T1_VAL B1_T1_VAL B1_T1_VAL	1/hr --- ---	
Partial quench off-gas temperature	°C	K-type TC	PQ1_T1_VAL	1/hr	
Reheater outlet (carbon bed inlet) off-gas temperature	°C	K-type TC	T-AJ-1	1/hr	
Reheater outlet (carbon bed inlet) off-gas pressure	psig	Rosemount 2088A	AJ1_P2_VAL	1/hr	
Reheater outlet (carbon bed inlet) off-gas flow rate	kg/hr	Micro Motion CFM200M 0-250 kg/hr coriolus mass flow meter	AJ1_F_VAL	1/hr	
Mass of bed product, cyclone samples, and filter fines	kg	Weigh scale	---	Each collection	
All parameters with a PLC tag name are electronically automatically logged under that tag name. Any parameters that do not have a PLC tag name are not electronically logged. Manual logs were maintained by both SAIC and INEEL personnel. At times, the manual log frequency varied from the typical listed frequencies.					

3.3.2 Continuous Off-gas Composition Monitoring

A continuous emissions monitoring system (CEMS) provided on-line off-gas composition measurements for process control, safety, air emissions measurements, and determining the fate of feed constituents that were converted to gaseous compounds. The off-gas composition was measured at two locations in the off-gas system. CEMS 1 was used to measure the off-gas composition at the outlet of the heated filter (upstream of the thermal oxidizer), to characterize the composition of the FBSR off-gas. CEMS 2 was used to measure the off-gas composition at operator-selectable locations at the inlet of the carbon bed or the outlet of any of the three stages of the carbon bed. CEMS-2 sampled only from the location at the inlet to the carbon bed during the Hanford LAW test, providing data that characterizes the off-gas downstream of the oxidizer and upstream of the carbon bed. This location is also downstream of the partial quench and reheater.

Each sampling and conditioning system includes:

- A heated probe through which off-gas is sampled
- A heated filter to remove particulate matter
- Heated sample line to transport hot, filtered sample gas from the heated filter to the chiller system
- An electrical refrigerated chiller system to cool the sample gas, condense water moisture from the sample gas, and separate the condensate with minimal scrubbing of water-soluble gases
- A sample pump
- A backup filter
- Flow monitoring and control manifold with control valves to deliver the cooled, dried, and filtered sample gas to the continuous monitors
- For CEMS 1 only, a carbon filter is located upstream of the flow control manifold, to remove residual condensable hydrocarbons that otherwise foul the analyzers and interfere with CEMS measurements. The THC analyzer withdraws sample gas upstream of the carbon filter in order to most representatively sample these hydrocarbons before they are removed by the carbon filter.

Figures 3.3-1 and 3.3-2 show the physical configurations of the two CEMSs.

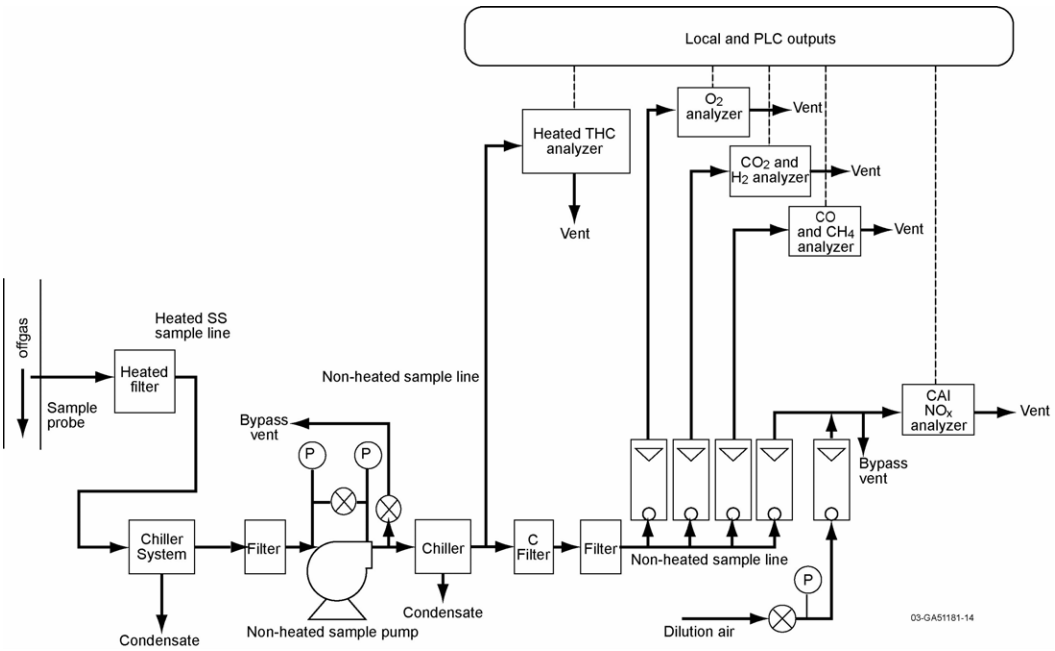

Figure 3.3-1. CEMS 1 for steam reformer off-gas measurements at the filter outlet sample location, upstream of the thermal oxidizer.

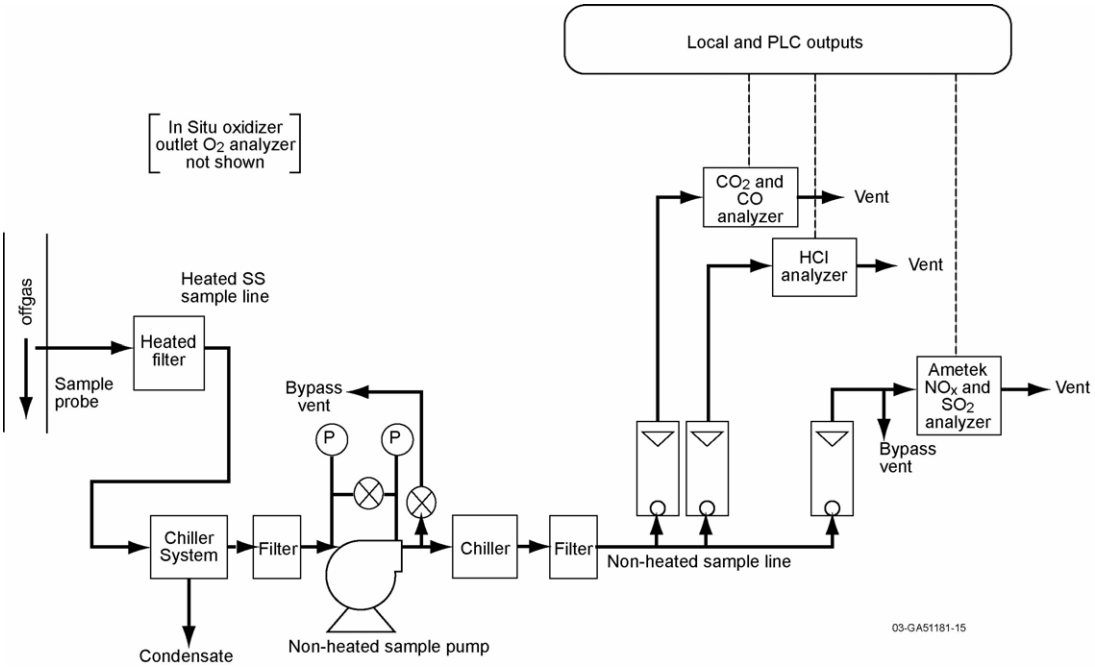

Figure 3.3-2. CEMS 2 for steam reformer off-gas measurements upstream of the carbon bed.

Specifications for the gas analyzers are shown in Table 3.3-2. The analyzers were calibrated with calibration gases daily during the test series. Past experience has shown that CEMS calibrations once per day or even less frequently are usually adequate. During each calibration, the following activities were generally performed:

- The system was leak-checked two ways (a) by checking the response of the O_2 analyzer (a significant O_2 response would indicate a significant amount of air in-leakage upstream of the sample pump), and (b) by running the sample pump with the CEMS inlet plugged and demonstrating no sample gas flow.

- Analyzer zero responses were determined using a zero gas (N_2 gas for all of the analyzers, or N_2 for the O_2 analyzer and air for the other analyzers).

- Analyzer span responses were determined using a calibration gas with the specified gas concentration.

- Interferences of gas species on the detection of other gas species were determined by recording all analyzer responses for each of the calibration gases. With internal corrections for such interferences (such as the interference of CO_2 on the H_2 measurement) no post-test CEMS interference corrections were needed after the test series.

- Calibration data generated prior to any analyzer adjustments applied to CEMS data during the time period prior to the calibration; calibration data generated after analyzer adjustments applied to CEMS data during the time period following that calibration.

- Calibration data was used to generate a composite correction factor for both air dilution and span calibration for the CEMS 1 NO_x analyzer, that require air dilution for operation.

The calibrations showed that the average calibration, drift, linearity, and bias for each test period were within the intended acceptance limits.

Table 3.3-2. Off-gas analyzer specifications.

Gas species	Instrument	Detection principle	Instrument range	Acceptance limits, % FS				Reference method
				Calibration	Drift	Linearity	Bias	
O_2	Servomex 1440 CEMS 1)	Paramagnetism	0-25%	2	3	4	5	40 CFR 60 App. A Method 3A
	In situ ZrO_2 probe (CEMS 2)	Electrochemical						
CO_2	Nova 4230 RM (CEMS 1)	Nondispersive infrared (NDIR)	0-40%					
	CAI (CEMS 2)		0-100%					
H_2	Nova 4230 RM (CEMS 1)	Thermal conductivity	0-5%	---	---	---	---	---
CO	CAI 200 (CEMS 1)	NDIR	0-1% 0-2% (CEMS 1)	5	10	2	---	40 CFR 60 App. A Method 10
	CAI (CEMS 2)		0-500 ppm 0-2,500 ppm (CEMS 2)					
CH_4	CAI 200 (CEMS 1)		0-0.5% 0-1%	---	---	---	---	---
NO, NO_x	Ametek M922 (CEMS 2)	Dispersive ultraviolet (DUV)	0-5,000 ppm	2	3	4	5	40 CFR 60 App. A Method 7E
	Ecophysics CLD 70E (CEMS 1)	Chemiluminescence	0-5,000 ppm					
THC	CAI 300 HFID (CEMS 2)	Flame ionization detection (FID)	0-3% C_1	5	3	---	---	40 CFR 60 App. A Method 25A
HCl	Thermo 15C (CEMS 2)	NDIR with gas filter correlation (GFC)	0-100 ppm to 0-5,000 ppm	---	---	---	---	---

3.3.3 Process Sample Collection

Process sample collection and analysis was performed to determine the fate of feed constituents, determine process mass balances, and evaluate the properties of the solid products. Some sample analyses were performed for process monitoring and control during the test series. Selected samples were also delivered for more comprehensive post-test laboratory analysis at SRNL. Table 3.3-3 shows the samples that were shipped to SRNL and the analyses that were performed. The sample selection matrix was designed to generate samples of feed and product materials sufficient to characterize those materials, perform key mass balances, and determine the fate of feed constituents in the steam reforming process. Test samples were identified with unique sample labels, and sample information was recorded on a sample log.

The scope of onsite analysis included:

- All bed samples were analyzed for particle size distribution (ASTM D 197, "Standard Test Method for Sampling and Fineness Test of Pulverized Coal") bulk density (ASTM B 527, "Standard Test Method for Determination of Tap Density of Metallic Powders and Compounds"), and particle

density (ASTM C 128, “Standard Test Method for Density, Relative Density (Specific Gravity), and Absorption of Fine Aggregate”).

- All bed product, cyclone samples, and filter fines were weighed.
- Selected bed product, cyclone samples, and filter fines were also evaluated using onsite optical microscopy.

Table 3.3-3. Laboratory sample analysis matrix performed at SRNL.

Request for Analysis | Idaho National Engineering Laboratory | [Hanford LAW FBSR test RFA Nov 2.xls]RAF for report

Sample number	Sample date	Sample description	Sample weight, gm	Suggested analyses																Remarks
				Bulk density	Total H_2O/ Calcine	Mois-ture	Optical micro-scope	SEM	XRD	pH	Elemental composition: Organic carbon	Elemental composition: Cations	Elemental composition: Anions	PSD	Redox	PCT	SPFT	PUF	TCLP	
1081 2/2	2-Aug	Hanford LAW simulant	330								1	1	1							To verify the mixture recipe
1082	2-Aug	LAW slurry, 634 g OptiKast/L LAW	368		1															
1086 2/2	2-Aug	208C coco shell carbon	54										1							Blank for carbon bed
1100	2-Aug	Starting bed COT 0	221			1	1				1	1	1							Unscreened bed drain
1101	2-Aug	Bed product COT 12:21	104			1	1				1	1	1							Unscreened dynamic bed sample drains
1103	4-Aug	Bed product COT 39:15 (last before feedrate increase)	86			1	1	1	1		1	1	1	1		1				Unscreened dynamic bed sample drains
1104	5-Aug	Bed product COT 55:30 (1 hr after rate increase)	156			1	1	1	1		1	1	1	1	1	1	1	1	1	1104 is dynamic bed from the sample port. 1123 is unscreened 10x bed drain. If the amount of sample 1104 is not sufficient for all analyses, combine 1123 with 1104 for analysis, even though 1123 is from the bed drain and 1104 is from the bed sample.
1123	5-Aug	Bed product COT 55:30 (1 hr after rate increase)	669																	
1108	5-Aug	Bed nozzle agglomerations COT 65:45	18						1											
1106	5-Aug	Final bed	204			1	1	1	1		1	1	1		1					Final bed. 1106 and 1124 are 2 identical aliquots of the final bed. Use 1106 for analysis if it has enough mass.
1124	5-Aug	Final bed	759																	
1107	5-Aug	Final agglomeration	95	1		1	1	1	1		1	1	1			1				
1109	2-Aug	Cyclone fines COT 11	64			1	1		1		1	1	1	1						
1112	5-Aug	Cyclone fines COT 64:20	67	1		1	1	1	1		1	1	1	1						
1113	2-Aug	Filter fines COT 10	83	1		1		1	1		1	1	1	1						
1115	4-Aug	Filter fines COT 39	99								1	1	1							
1125	4-Aug	Filter fines COT 55:30	687	1		1	1	1	1		1	1	1	1		1				2 containers 1/2 and 2/2
1126	5-Aug	Filter fines 67:30	334																	Similar to 1116; archive
1089	3-Aug	CEMS 1 condensate COT 29:10	130							1			1							
1092	4-Aug	CEMS 1 condensate COT 51:15	129							1	1	1	1							
1094	5-Aug	CEMS 1 condensate post-test	116							1			1							Taken <10 min. after feed off
1090	3-Aug	CEMS 2 condensate COT 29:10	130							1			1							
1093	4-Aug	CEMS 2 condensate COT 51:15	122							1	1	1	1							
1095	5-Aug	CEMS 2 condensate post-test	113							1			1							Taken <10 min. after feed off
1097 2/2	9-Aug	Carbon bed top layer	61										1							
1098 2/2	9-Aug	Carbon bed middle	62										1							
1099 2/2	9-Aug	Carbon bed bottom layer	51										1							
Totals				4	1	10	9		9	6	14	14	22	6	2	4	1	1	1	

1. Desired information from analyses is (a) determine degree of mineralization, types of mineralization and mineralized phases, and leachability of the FBSR bed and fines products, (b) characterize different bed constituents, and (c) elemental analyd information fr products to determine species composition of bulk products and product phases, and fate of feed constituents.

2. Total H_2O by loss on ignition (LOI) at 750°C, consistent with ASTM D3174. Residual solids left from simulant slurries is the calcined product, which is the mass of solid product produced during steam reforming.

3. Moisture at 107±3°C consistent with ASTM D3173.

4. Optical microscope analysis to provide photographs at high enough magnification (10-50x) to discriminate distinct particles. Include a mm scale in photos for size reference.

5. Scanning electron micrograph (SEM) analysis of cyclone catch and filter fines to provide photos of these particles at high enough magnification (up to 5,000-20,000x) to discriminate ~0.1 um particles.

6. SEM-energy dispersive Spectroscopy (SEM-EDS) to determine composition differences of different sectioned particles - for example, to determine if cores of bed particles are unreacted clay.

7. X-ray diffraction (XRD) analysis to determine different mineral phases.

8. Organic carbon content by LOI at 750°C consistent with ASTM D3174, except for the CEMS condensate samples. For those samples, use a liquid total organic carbon (TOC) procedure.

9. Cation analysis preceeded by lithium tetraborate (Li borate) fusion at 1,000 C followed by dissolution in 2% HNO3 solution with 1 ml con HCl on a hotplate.

10. Cations Al, Ca, Cr, Fe, Mg, K, Si, Na, and Ti by inductively coupled plasma emission spectroscopy (ICP-ES); Cations Cs and Re by ICP-mass spectroscopy (ICP-MS) for better detection limits.

11. Anions analysis preceeded by sodium peroxide (Na Per) fusion followed by water uptake to dissolve all anions.

12. Anions CO_3 (inorganic C), Cl, F, NO_2, NO_3, PO_4, and SO_4 by ion chromatography (IC). Iodine by ICP-MS. For solid samples, anion detection limits need to be ~0.01 wt%. For liquid samples, anion detection limits need to be ~0.1 mg/L.

13. Particle size distribution (PSD) by Microtrak to determine size distributions of small particles. The PSD for bed media has been determined by sieve tray analysis (ASTM C92 - 95) during the test.

14. The extent of oxidation is indicated by the ratio of Fe+2 to Fe(total) (Redox test).

15. Product Consistency Test (PCT).

16. Single Pass-Through Flow Test (SPFT).

17. Pressurized Unsaturated Flow (PUF) test.

3.4 Process Input Materials (Selection and Composition)

The TTT steam reforming technology for the treatment of LAW involves converting the liquid waste into an insoluble, mineralized product. Overall, water is evaporated, nitrates and nitrites converted mostly to N_2 and sodium is converted to sodium aluminosilicate. A mineralizing additive, kaolin clay, must be used in addition to a reducing additive (carbon) to achieve this. Kaolin clay is added to provide sufficient reactive Al and Si to combine with alkali elements (primarily Na and K) in the feed to produce nepheline and other aluminosilicate mineral phases in the reformer. Toxic metals and radionuclides are expected to be immobilized in the matrix, either by forming an incorporated mineral phase or by microencapsulation. Carbon was added to provide some heat input to the bed and to form reducing conditions for NO_x destruction. The use of a dense, inert starting material, such as alumina, in a fluidized bed reactor operated at about 725°C facilitates the conversion. The alumina has a high heat capacity, which facilitates heat transfer to the atomized feed, and helps prevent over-quenching in the feed zone. Hot alumina appears to be not readily coated by the product, perhaps due to the Leidenfrost effect.

3.4.1 Starting Bed Media

Starting fluidized bed materials that were considered included dolomite, sintered bauxite beads, nepheline syenite, and sintered calcium silicate. The major criteria considered in evaluating these materials for use were composition, melting point, attrition resistance, particle size distribution, and availability. Composition was important because of the expected bed product composition, and a desire to discriminate between starting bed and product produced from an analytical standpoint. The preferred starting bed particle size is 150 to 300 microns. 70-grit alumina was finally selected as the starting bed media because of its attrition resistance and inertness relative to the product. The INEEL measured HMPD of this starting material was 0.0211 cm and the measured particle density was 3.79 gm/cc. The material vendor (AGSCO Corp.) states that the bulk density is 1.61 – 1.87 gm/cc and the Al_2O_3 content is 99.55%.

3.4.2 Carbon Reductant Additive

Nine different carbon types were investigated for use as a reductant in the experimental program. Characteristics measured on carbon samples were reactivity (thermogravimetric analysis), particle size distribution, attrition resistance, moisture content, loss on ignition, and ash compositional analysis. Appendix C gives details on selection criterion used and rankings of carbons evaluated. A wood-based carbon and a coal-based carbon were selected for use in the pilot scale activities. Initial functional tests performed in July confirmed that the wood based carbon, supplied by Berger Brothers, performed the most efficiently and was selected for use in the LAW experiments. A summary of the carbon reductant properties are shown in Table 3.4-1. Further property information about the Berger Brothers carbon can be found in Jantzen, 2004.

Table 3.4-1. Carbon reductant properties.

Supplier	Berger Brothers, Chicago, IL
Type/Size	Wood base, -0.371", +0.185"
Moisture (% of Sample)	3.13
Ash at 650°C (% of Dried Sample)	5.38
Ash at 750°C (% of Dried Sample)	5.14
Loss on Ignition (% Loss of Undried Sample)	95.0

3.4.3 Mineralizing Additive

Selection of a mineralizing agent (kaolin clay) followed a procedure similar to that of the carbon reductant. Four kaolin clays were investigated. Characteristics measured included phase analysis (X-ray diffraction), particle size distribution, whole element chemistry, and slurry rheological properties. It is important to select a clay type with a Si:Al mole ratio that is in a favorable range, when reacted with the liquid waste, for producing durable mineral phases. Particle size distribution is important such that as much of the clay mass as possible combines with and reacts with the liquid waste. Clay constituents that do not support generation of desirable mineral phases (e.g., quartz) should be minimized. Data measured to support the clay raw material selection is documented [Jantzen, 2004]. The rheological properties of the clay slurry are important since the clay and waste must be combined and injected into the reactor with a minimum expenditure of energy, and piping restrictions should be minimized.

SnoBrite clay was used for the previous experiments performed at Hazen with LAW surrogate material. The mineral product generated during that experiment was documented as having desirable durable properties [Jantzen, 2002]. SnoBrite clay was unavailable for the LAW pilot scale experiments. However, since the properties and composition of OptiKasT clay closely matched those of the SnoBrite clay, OptiKasT clay was chosen as the mineralizing agent in LAW pilot scale experiments. Table 3.4-2 shows the properties of the SnoBrite and OptiKasT clays.

Table 3.4-2. Properties of candidate kaolin clays.

Clay	SnoBrite	OptiKasT
Major phases	Kaolinite (PDF#75-1593) $(Al_2O_3 \cdot 2SiO_2 \cdot 2H_2O)$	Kaolinite (PDF#75-1593) $(Al_2O_3 \cdot 2SiO_2 \cdot 2H_2O)$
Minor phases	Muscovite (PDF#07-0042) $(K, Na)(Al, Mg, Fe)_2 (Si_{3.1}Al_{0.9})O_{10}(OH)_2$ Rutile (TiO_2) possible	Muscovite (PDF#07-0042) $(K, Na)(Al, Mg, Fe)_2 (Si_{3.1}Al_{0.9})O_{10}(OH)_2$
Si:Al atom ratio	1.02	1.04
Total moisture* (wt%)	14.20%	15.15%
Particle size (wt% less than) 10% - 50% - 90%	0.82µm – 5.00µm – 20.8µm	0.74µm – 4.22µm –15.9µm
Particle density	2.77 gm/cc	2.69 gm/cc
* The total moisture content was determined based on total mass loss during a Loss on Ignition (LOI) analysis, during which the sample was heated to 700°C, and includes both moisture sorbed onto the clay and also water of hydration. Determining total moisture based on LOI analysis assumes that the only mass change upon heating to 700°C is due to volatilization of water.		

It was recommended, after team analysis of property data, that 635 gm of as-received OptiKasT clay be added for every liter of simulated LAW. The quantity of clay to be mixed with the LAW simulant was selected such that the expected product composition was within the desired shaded region of the ternary phase diagram (Figure 3.4-1). This region was thought to provide the most favorable final product composition. The clay was added to the simulant in the 200-liter feed tanks as needed to maintain a ready inventory of feed slurry.

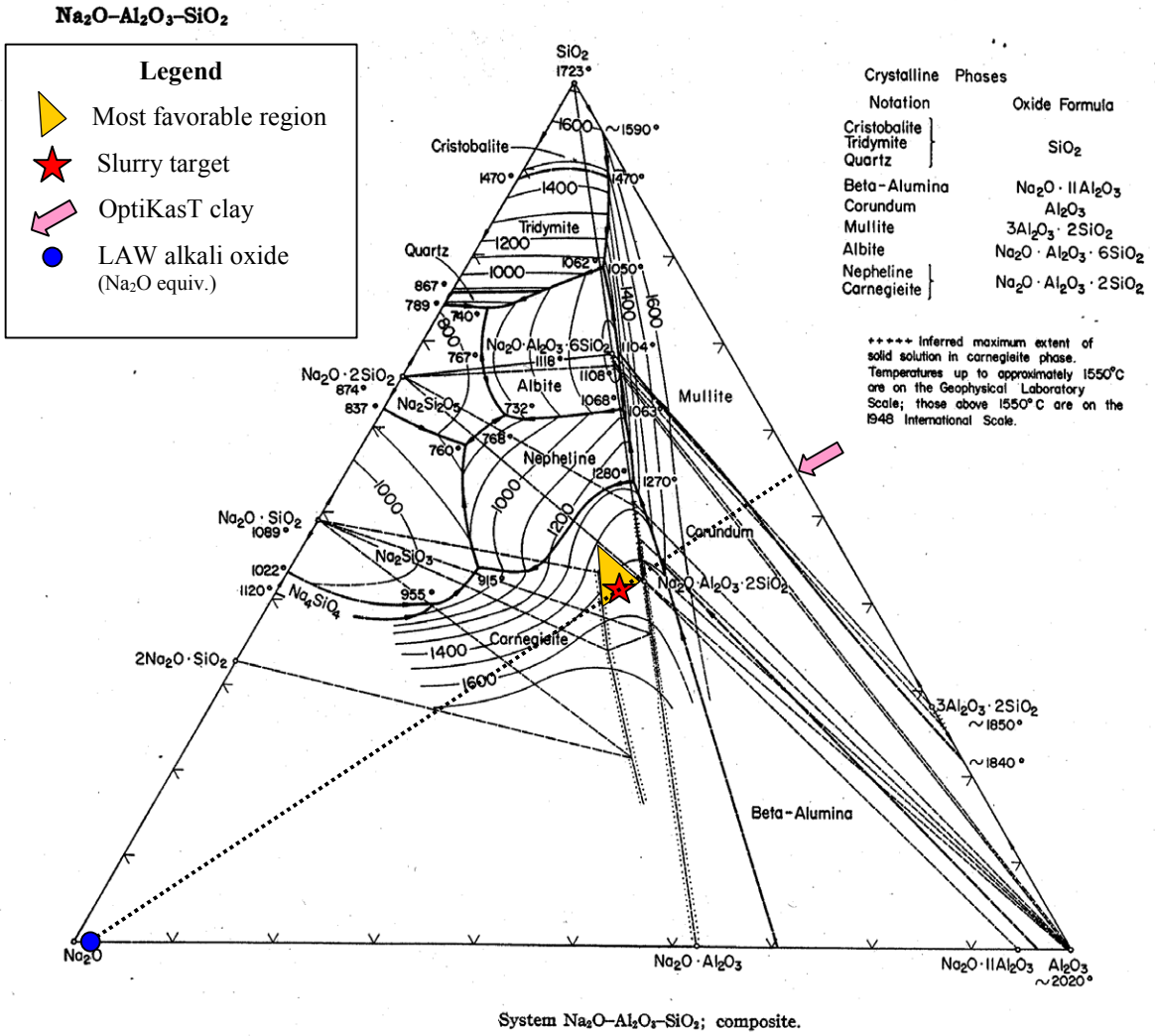

System Na_2O–Al_2O_3–SiO_2; composite.

E. F. Osborn and Arnulf Muan, revised and redrawn "Phase Equilibrium Diagrams of Oxide Systems," Plate 4, published by the American Ceramic Society and the Edward Orton, Jr., Ceramic Foundation, 1960.

Principal References

G. W. Morey and N. L. Bowen, *J. Phys. Chem.*, **28**, 1167–79 (1924).
F. C. Kracek, *J. Phys. Chem.*, **34**, 1583–98 (1930).
N. L. Bowen and J. W. Greig, *J. Am. Ceram. Soc.*, **7**, 238–54 (1924); corrections, ibid., 410.
N. A. Toropov and F. Ya. Galakhov, *Voprosy Petrogr. i Mineralog., Akad. Nauk S.S.S.R.*, **2**, 245–55 (1953).
Shigeo Aramaki and Rustum Roy, *Nature*, **184**, 631–32 (1959).
J. F. Schairer and N. L. Bowen, *Am. J. Sci.*, **254**, 129–95 (1956).
Liberto De Pablo-Galan and Wilfred R. Foster, *J. Am. Ceram. Soc.*, **42**, 491–98 (1959).

Figure 3.4-1. Ternary phase diagram showing clay and target feed compositions.

3.4.4 Hanford LAW Simulant

The simulant used for FBSR testing was prepared from commercially available reagent grade chemicals according to a recommended Hanford LAW composition [Rassat, 2003]. This simulant is

designed to be representative of dissolved radioactive saltcake. The simulant composition is shown in Table 3.4-3. This simulant is a basic solution of (primarily) sodium and potassium salts.

Table 3.4-3. LAW simulant used in the FBSR test.

Species	Target		As Measured		
Metals	**Molarity**	**gm/L**	**Molarity**	**gm/L**	**Δ%**
Al	6.4 E-2	1.7 E+0	6.7 E-2	1.8 E+0	4.7%
Ca	---	---	6.2 E-4	2.5 E-2	---
Cr	1.0 E-2	5.4 E-1	9.6 E-3	5.0 E-1	-7.5%
Cs	7.5 E-8	1.0 E-5	1.1 E-7	1.4 E-5	40%
K	1.2 E-2	4.8 E-1	5.0 E-2	1.9 E+0	301%
Mg	---	---	3.2 E-4	7.8 E-3	---
Na	5.0 E+0	1.2 E+2	5.5 E+0	1.3 E+2	10%
Re	5.2 E-4	9.6 E-2	2.7 E-4	5.0 E-2	-48%
Si	---	---	1.5 E-3	4.1 E-2	---
Non-metals	**Molarity**	**gm/L**	**Molarity**	**gm/L**	**Δ%**
$CH_3CO_2^{-2}$	1.2 E-2	7.0 E-1	---	---	---
$C_2O_4^{-2}$	1.3 E-1	1.2 E+1	---	---	---
CO_3^{-2}	4.8 E-1	2.9 E+1	---	---	---
TIC	---	5.7 E+0	---	5.3 E+0	-7.1%
TOC	---	3.5 E+0	---	3.3 E+0	-4.5%
Cl^-	4.4 E-2	1.6 E+0	4.4 E-2	1.6 E+0	1.1%
F^-	3.2 E-2	6.0 E-1	5.4 E-2	1.0 E+0	70.7%
I^-	1.3 E-5	1.7 E-3	1.6 E-5	2.1 E-3	21.1%
NO_2^-	4.2 E-1	2.0 E+1	4.2 E-1	2.0 E+1	0.0%
NO_3^-	2.5 E+0	1.6 E+2	2.6 E+0	1.6 E+2	2.0%
OH^-	7.4 E-1	1.3 E+1	---	---	---
PO_4^{-3}	4.9 E-2	4.7 E+0	4.7 E-2	4.5 E+0	-3.5%
SO_4^{-2}	9.0 E-2	8.6 E+0	8.7 E-2	8.3 E+0	-3.5%
Water	---	8.7 E+2	---	8.5 E+2	---
Specific Gravity	---	1.23	---	1.2 E+0	---

[Compiled LAW Analytical Data Tables - Nov 8.xls]Simulant and Slurry

The simulant contains a total of 0.14 *M* organic compounds as sodium oxalate ($Na_2C_2O_4$) and sodium acetate (CH_3COONa). These compounds will thermally decompose, in the FBSR, to produce various decomposition products, including THC compounds. Sodium oxalate and acetate will also react with available O_2, NO_x, H_2O, and C to produce additional products including CO, CO_2, H_2, NO, and N_2.

The simulant was analyzed at SRNL to verify the elemental composition. According to the laboratory analysis, all of the major constituents were within 10% of the intended concentrations (Table 3.4-3), although there were no direct analyses for the organic species. Minor constituents, especially potassium and cesium, were apparently impacted by the presence of contaminants in technical grade chemicals used in the chemical makeup of the simulant.

Assuming that the LAW would not dissolve the clay or react with it to evolve NO_x or other volatile compounds, and that the particle density of the clay is 2.69 gm/cc, the theoretical density of the slurry would be approximately 1.50 gm/mL of slurry. The volume increase in the original LAW simulant, due to the volume occupied by the undissolved clay particles, was calculated to be 25%. The projected slurry composition and properties were calculated from analytical data on the LAW simulant and clay (where available) and are shown in Table 3.4-4. Target LAW simulant compositions were used when analytical data were not available for the carbonaceous anions or hydroxide.

Table 3.4-4. Simulant slurry feed properties.

Slurry Properties	Deaerated	With 3 vol% Aeration
Density Estimate	1.50 kg/L slurry	1.46 kg/L slurry
Volume Expansion	1.24 L slurry/L LAW	1.27 L slurry/L LAW
Mass Expansion	1.52 kg slurry/kg LAW	

3.5 Test Procedures and Operating Conditions

Experimental activities were performed by Science Applications International Corporation (SAIC) personnel in accordance with documented operating procedures [SAIC, 2004]. SAIC personnel received experimental direction from BBWI personnel. Communication sheets detailing changes in operating parameters were prepared and initialed by THOR and BBWI personnel as documentation of experimental direction.

The FBSR system is ready for simulant feed operation after starting bed media is charged and preheating is complete. An initial inventory of carbon reductant is established in the bed by adding about 1 kg of carbon. This is done by feeding carbon into the bed at a high rate, ~2 kg/hr, for about ½ hour. During this time the CEMS is monitored to verify the generation of H_2 and attainment of low O_2 concentrations; typically ~0-0.5% (dry, as measured). Water feed is then initiated at a minimum feed rate of about 2 kg/hr. The target O_2 concentration in the fluidizing gas (~15 wt%) can be initiated. Bed temperatures are monitored to verify adequate and not excessive wall heating and heating from carbon oxidation.

The simulant feed slurry is initiated at about 3 kg/hr when a carbon inventory is established in the bed, H_2 generation verified, low O_2 concentrations are apparent, and stable bed operation is observed. The system is then adjusted to achieve and maintain the operating parameters listed in Table 3.5-1 while monitoring all key parameters.

Spreadsheet tools were available for calculating fluidizing gas parameters, carbon stoichiometry, mineral stoichiometry, and simulant makeup. They were to be used as necessary, based on experimental needs and operating conditions.

Table 3.5-1. Key initial operating conditions for the August 2004 LAW FBSR test.

Parameter		Value
Fluidizing Gas	Ratio (U/U_{mf})[(a)]	Initially ~8. Will change as bed particle density and mean diameter data change.
	Gas velocity at the distributor	Maintained ≥0.20 m/s
	Composition: O_2 Steam	10-15 wt%; Adjusted to maintain 0.4 kg O_2/hr. 85-90 wt%
	Fluidizing Gas Temperature	≥ 740°C
	Fluid Gas Distributor	THOR[SM] proprietary.
	Distributor Differential Pressure	15 – 95 in WC, 15 in WC is the minimum. ≥40 in WC during bed charging
Feed, Additives, & Reductants	Feed Nozzle	Redesigned hot face nozzle; modified SprayCo available.
	Slurry feed rate (total)	3.0 kg/hr after the switch from H_2O. Increased to 4.0 kg/hr as stable conditions are observed (~COT = 8:00). To be increased based on process recommendations from TTT. Minimum controllable rate is ≥2 kg/hr.
	Berger Brothers P6 Carbon	2 kg/hr for 30 minutes before slurry feed initiation. 0.8 kg/hr after feed started, adjusted as required to maintain H_2 production and NO_x destruction as recommended by TTT. Minimum controllable rate is ≥0.5 kg/hr.
	OptiKasT clay	635 gm/L LAW
Atomizing Nitrogen	LAW slurry NAR	May vary based on process observations and slurry feed rate. Decreases must be made in steps of 200 or less to avoid disruption in gas flow.
	Atomizing N_2 flow rate	≥ 3.0 kg/hr; typically 4.0 kg/hr[(c)]
Process Conditions	Bed temperature	725°C
	Freeboard temperature	710±5°C
	Reactor wall temperature limit	≤780°C
Bed Parameters	Virgin bed mass	~18 kg white alumina
	Fluidized bed depth	Initially ~ 24"; Normally 25 – 28"
	Reformer pressure at distributor	Atmospheric
	Starting alumina particle size (HMPD)	0.0211 cm; adjusted as needed[(b)]
	Starting alumina particle density	3.79 gm/cc; adjusted as needed[(b)]
Off Gas	Off-gas filter temperature	≥ 400°C

Parameter		Value
Parameters	Oxidizer chamber temperature	1,000ºC
	Partial quench outlet temperature	130°C
	Reheat outlet temperature	140ºC
	Oxidizer outlet O_2 concentration	3% as measured (wet basis)
	Carbon bed temperature[(d)]	<125 ºC

[(a)]U_{mf} = Minimum fluidizing velocity, as calculated by the Wen and Yu correlation [Kunii and Levenspiel, 1991]

[(b)]Based on a virgin bed of 70-grit white alumina.

[(c)]Minimum flow rate controlled at ≥ 2.0 kg/hr.

[(d)]Carbon bed consists of 12 inches of Barneby Sutcliffe 208C, 4X8 mesh, in middle section of bed.

4. TEST RESULTS

The steam reforming demonstration was performed in the INEEL pilot scale fluidized bed test system at the STAR center beginning on August 2 and continuing through August 5, 2004. Test operation was continuous, 24 hours per day, staring at 0900 on August 2 and continuing nonstop until the test was terminated at 0526 on August 5. The total continuous operating time (COT) was 68 hours 26 minutes (68:43 hours). The LAW simulant slurry feed rate ranged between 3 – 5.5 kg/hr.

4.1 Test Conditions, Operations, and Performance

4.1.1 Test Conditions and Operations

The demonstration was designed to operate at the operating conditions described in Section 3.5. However, some operating condition changes were required in order to maximize the process throughput that would achieve high bed turnover, respond to process changes, and maintain stable bed operation (stable particle size and density) for the duration of the test. The key operating changes are summarized in Table 4.1-1. Key process variables are also shown, graphically, in Figure 4.1-1.

The measured density of the slurry varied over time, but was consistently lower than the theoretical density of 1.50 gm/mL. This is attributed to trapped and entrained gases in pores and minute bubbles that could not disengage from the slurry. The quantity of bubbles entrained could have been influenced by the level of the slurry in the feed tank relative to the upper agitator impeller and impeller speed, and perhaps by air dispersed in the slurry by the centrifugal recirculation pump. A slurry density of 1.43 gm/mL (as measured by the coriolis mass flowmeter) corresponds to a 27% volume expansion relative to the LAW supernate resulting from the clay addition, instead of a calculated value of 24% based on the clay particle density. The difference (3%) could be attributed to small, entrained air bubbles.

Initial starting conditions were selected (see Section 3.5) and slurry feed was started at 3 kg/hr (communication sheet #1, test condition 1). After nearly an hour, the carbon addition rate was reduced to avoid excessive carbon accumulation in the bed and filter products (sheet #2, test condition 2).

The bed height did not grow significantly in the first 5 hours of operation, and bed product was not drained, indicating that not much of the feed solids were retained in the bed, but were elutriating to the filter. The slurry feed rate was increased from 3 to 4 kg/hr (test condition 3) after five hours of otherwise satisfactory operation in order increase the process throughput. This change was also intended to decrease the number of fine, atomized slurry droplets so that product would accumulate more in the bed and less on the sintered metal filter because the fluidizing gas and atomizing gas flow rates constant were held constant. This condition was held for over 3 hours without appreciable change in the bed mass or fluidized bed density.

Table 4.1-1. Hanford LAW mineralization test operating parameters.

Communication sheet	Date, start time	COT, hr:min	Duration, hr:min	Input feed rates, kg/hr							Slurry feed rate, L/hr (SR1_F1A_VFR)	Slurry specific gravity (SR1_D1A_VAL)	NAR, sL/L	Bed temperature, °C (SR1_T3_VAL)	Fluidized bed specific gravity (BED_DENSITY)	Fluidizing gas velocity below feed, m/s (FLUIDIZING_FV)
				Atomizing N_2 (SR1_F1B_KGH)	Fluidizing steam (H1_F_PV)	Fluidizing O_2 (SR1_F2_KGH)	Total fluidizing gas	Carbon feed rate setpoint (LF2_FD_RATE)	Corrected carbon feed rate	Feed slurry (SR1_F1A_VAL)						
1	2 Aug 04 09:00	00:00	00:48	3.18	2.85	0.41	3.26	1.00	0.85	3.0	2.1	1.43	1,300	722	1.29 - 1.28	0.247
2	2 Aug 04 09:48	00:48	04:12	3.15	2.85	0.41	3.26	**0.70**	0.59	3.0	2.1	1.44	1,300	722	1.28 - 1.25	0.247
3	2 Aug 04 14:00	05:00	03:12	3.11	2.84	0.41	3.25	0.70	0.59	**4.0**	**2.7**	1.47	**980**	722	1.25 - 1.21	0.247
4, 5	2 Aug 04 17:12	08:12	15:48	**2.59**	**2.33**	0.38	**2.71**	0.70	0.59	4.0	2.8	1.44	**800**	722	1.21 - 0.53	**0.204**
6	3 Aug 04 09:00	24:00	01:30	**2.85**	2.33	0.38	2.71	0.70	0.59	**5.0**	**3.5**	1.43	**700**	722	0.53 - 0.50	0.205
7	3 Aug 04 10:30	25:30	04:34	**3.00**	2.30	0.37	2.67	0.70	0.59	5.0	3.4	1.46	**750**	722	0.50 - 0.46	0.201
8	3 Aug 04 15:04	30:04	09:16	2.93	**1.81**	0.37	**2.18**	0.70	0.59	5.0	3.4	1.49	750	722	0.46 - 0.41	**0.162**
9	4 Aug 04 00:20	39:20	02:00	2.93	1.88	0.38	2.26	**0.80**	0.68	5.0	3.4	1.49	750	721	0.41 - 0.40	0.168
10	4 Aug 04 02:20	41:20	12:55	3.04	**1.25**	0.39	**1.64**	0.80	0.68	5.0	3.5	1.44	750	720	0.40 - 0.39	0.118
11	4 Aug 04 15:15	54:15	11:42	2.88	1.25	0.39	1.64	0.80	0.68	**5.5**	**3.7**	1.49	**670**	723	0.39 - 0.40	0.118
12	5 Aug 04 02:57	65:57	02:29	**3.50**	1.25	0.39	1.64	0.80	0.68	5.5	3.7	1.47	**800**	724	0.40 - 0.36	0.118
Shutdown	5 Aug 04 05:26	68:26														
Test averages				2.91	1.88	0.39	2.26	0.75	0.63	4.7	3.2	1.46	800	722	0.00	0.168

1. Bolded values are setpoint changes.
2. The total fluidizing gas is the sum of the fluidizing steam and the fluidizing O_2.
3. The bed temperature is from thermocouple TC-3.
4. The fluidizing gas velocity is based on only the input fluidizing steam and O2. The gas velocity above the feed zone is higher due to contributions of atomizing gas, vaporized feed, and purges.
5. The carbon feed rate based on the feeder setpoint was corrected after the test based on the gravimetric carbon feed rate determined by the net weight of carbon fed during the test.

[LAW test summary and mass balances Nov 16.xls]Test summary

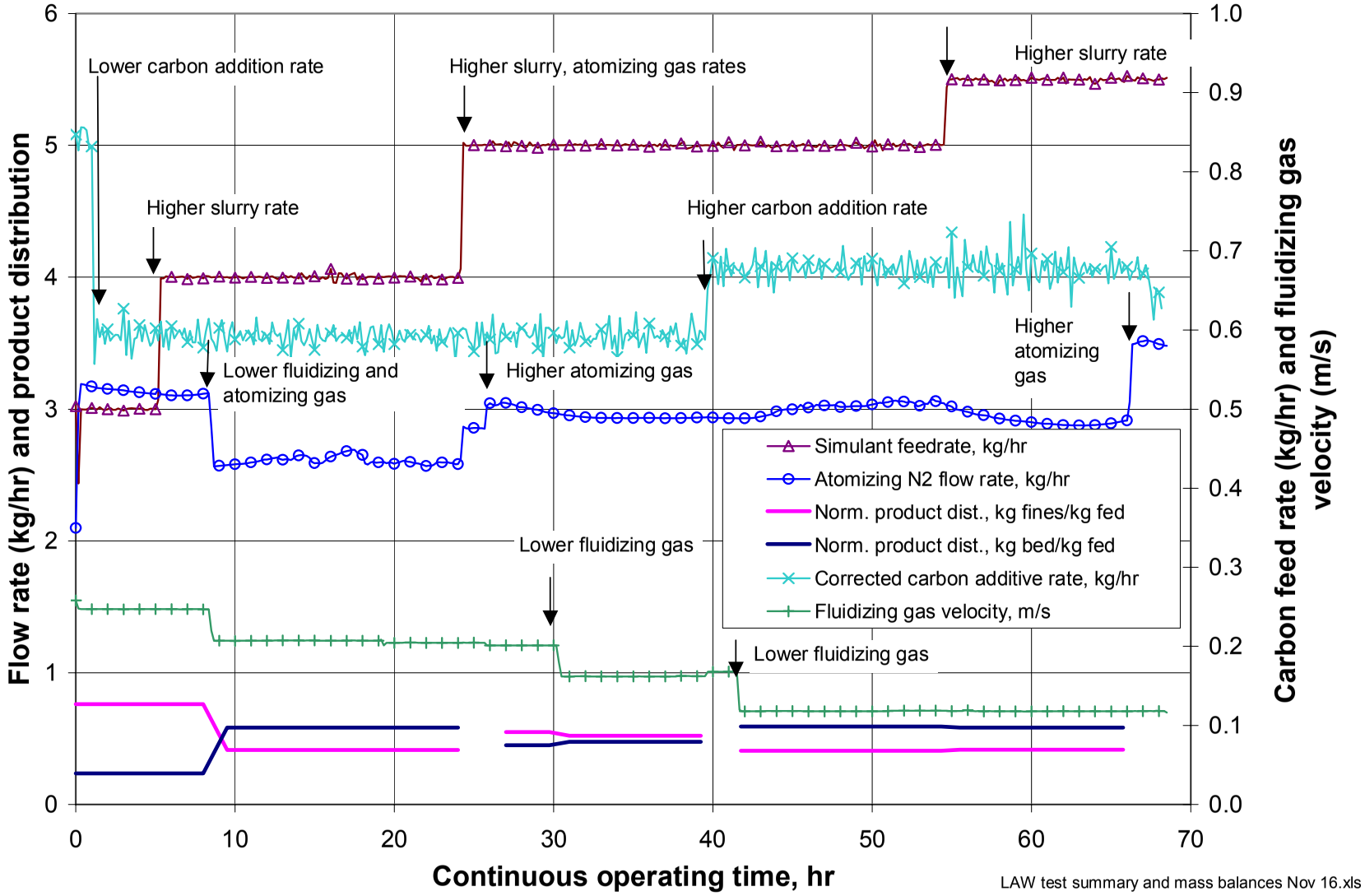

Figure 4.1-1. Process operating conditions.

The product distribution between the bed and the filter fines was still relatively unchanged at about 25% bed and 75% filter fines (Figure 4-1.1) at COT 8, because of the still relatively high fluidizing gas and atomizing gas rates. The fluidizing gas ratio (U_{mf}) was 9.5, only slightly higher than the target value of 8, during test conditions 1-3 and the gas velocity at the distributor was 0.25 m/s. The NAR was 1,300 for test conditions 1 and 2, and 975 for test condition 3. In order to increase the amount of bed product and decrease the amount of fines, by producing a coarser feed droplet population in the bed, the fluidizing gas and atomizing gas flow rates were reduced in test condition 4. The fluidizing gas ratio was decreased to 8, and the NAR was decreased to 800. These changes increased the bed product from 25% to 60%, and decreased the fines from 75% to 40%, of the input feed solids.

The bed mass started to accumulate and bed density began to drop after these changes were made, indicating that product was accumulating in the bed. The bed was sampled and analyzed for particle size distribution and observed for the presence of feed nozzle agglomerates. No fragments of nozzle accretions or other agglomerates were observed. The calculated particle size and density data were entered into the process computer and the fluidizing gas flows adjusted accordingly to maintain a relatively constant fluidization regime (test condition 5).

The slurry feed rate was increased from 4 to 5 kg/hr (test condition 6) at COT 24 in order increase process throughput and also perhaps increase the amount of bed product relative to fines produced. The atomizing gas was not increased proportionately to the slurry feed (which resulted in a reduced NAR value of 700).

A bed sample was obtained shortly after starting test condition 6. Small pea-sized agglomerates were observed along with fingernail shaped "petals" (~1 cm x 1.5 cm). These agglomerates were thought to be due to waste injector nozzle fouling, so the atomizing gas flow rate was increased to improve feed atomization and to preclude formation of larger agglomerates and further injector nozzle fouling at COT 25.5 (test condition 7). The product distribution again changed to about 45% bed product and 55% fines at the higher atomizing gas rate.

The bed particle size distribution measurements indicated a continued decrease from the starting bed harmonic mean particle diameter (HMPD) of 0.211 mm to 0.166 mm by COT 27. The fluidizing steam was reduced at COT 30 (test condition 8) because the harmonic mean particle size and average particle density continued to decline as product accumulated in the bed and as the starting bed medium was displaced. Fluidizing velocities were 20 – 30 times the calculated minimum fluidizing velocity.

The carbon feed rate was increased at COT 39:20 (test condition 9) to counter the rising NO_x concentration. The change in carbon additive feed rate, from 0.7 to 0.8 kg/hr, increased the carbon:oxidant stoichiometry from 350% to 420%. The NO_x concentration gradually decreased at this time, and the concentration of H_2, THC, and CH_4 gradually increased. These changes were gradual because the REDOX reactions in the bed depend not on the instantaneous carbon feed rate, but on the inventory of carbon in the bed. The carbon feed rate increase reversed the depletion of the fluidized bed carbon inventory.

The fluidizing gas rate was again lowered (test condition 10) to reduce bed grinding and encourage the formation and persistence of larger bed particles at COT 41.33. The product distribution also changed to about 60% bed product and 40% filter fines, and the bed HMPD stabilized at about 0.11 to 0.12 mm after this change.

Test condition 10 reduced the fluidizing steam flow so that the distributor differential pressure was reduced to about 10 inches of water column, and slowly drifted even lower to about 7 inches of water column by the end of the test as shown in Figure 4.1-2. The distributor was designed to fluidize denser

and larger bed material than what was obtained during this test. A minimum distributor differential pressure is recommended to (a) ensure balanced fluidizing gas flow distribution to all of the distributor orifices, and (b) to prevent bed particles falling through the distributor orifices into the distributor. Two rule-of-thumb recommendations for the minimum distributor differential pressure are (a) ≥0.5 psig (14 in.W.C.) for deep beds of high-density media [Agarwal, 1962], and (b) greater than 20 – 40% of the total bed differential pressure [Kunii, 1991]. Of the two rules, the latter rule is considered the most significant and has the most data confirming its general applicability.

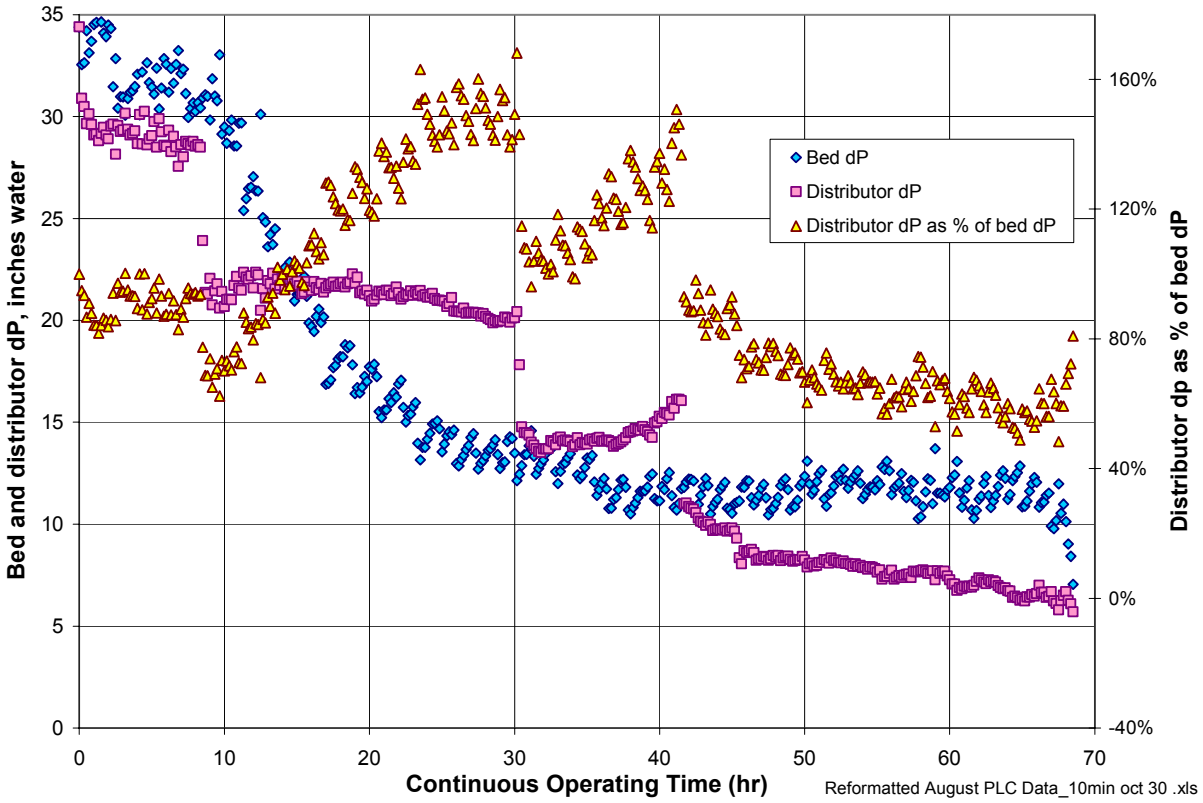

Figure 4.1-2. Distributor differential pressure during the Hanford LAW FBSR test.

The 7 – 10 inch water column differential pressure initiated by the test condition 10 change was lower than the first minimum recommended value of 14 inches of water, but still considerably higher than the second minimum value of at least 20 – 40% of the total bed differential pressure. During the entire test, the distributor differential pressure ranged between 50 – 160% of the total bed differential pressure. While operation after test condition 10 may have put the operation of the distributor at risk of potential poor distribution of fluidizing gas at the bottom of the fluidizing bed, it was considered necessary in order control the product distribution and bed particle size.

The reduction in fluidizing steam resulted in an oxygen concentration of 24 wt% in the fluidizing gas. Over time, after the test condition 10 step change in fluidizing gas flow rate, the distributor

differential pressure continued to slowly decline (from about 10 inches water to about 7 inches water). The decline over time may have been the result of a partially restricted distributor slowly clearing. Examination of the distributor after the run was terminated showed evidence that some portion of the fluidizing gas distributor was partially or totally restricted and a small quantity of black, flaky powder was found in the distributor. The black powder is believed to be oxide scaling that had spalled from the internal piping or distributor surfaces, which may have partially restricted the distributor.

The bed HMPD stabilized between 0.11 and 0.12 mm at COT 35, and the fluidized bed density was fairly constant at 0.38 gm/cc. The majority of the original starting bed had been displaced by product particles (bed turnover >95%) and the process was in relatively stable operation. However, the bed particle size was still smaller than desired. It was decided that the slurry feed rate be increased from 5 to 6 kg/hr, in 0.5 kg/hr increments, while keeping the atomizing gas flow constant to achieve a larger particle size. The feed rate was increased to 5.5 kg/hr (test condition 11) at COT 54.25.

Operational problems associated with diagnosing the failure of a valve on the carbon feeder system preempted plans to increase the feed rate to 6 kg/hr. Cyclical fluctuations were observed in the process pressure and the off-gas temperature. Initial efforts to diagnose the problem with the valve led operators to believe that the filter cake was not clearing off the filter candles properly. Efforts to clear the candles and to dislodge apparent restrictions in the off-gas piping resulted in sudden rises in the bed level and mass (about 15% increases). This is attributed to fines being dislodged from either the cyclone or the freeboard, which returned to the bed. The filter blow-back system was disabled to reduce the load on the filters, but the cyclical pressure fluctuations continued. Further investigation led to the discovery that the frequency of the fluctuations matched the frequency of the valves on the carbon addition system and eventually that a valve had failed open. With the valve open, atmospheric air was drawn into the reformer each time the other valve cycled, resulting in an increased gas flow rate (hence a pressure spike) and additional oxygen in the system which accounted for the temperature fluctuations.

Reducing the system vacuum so that the fluidized bed at the level of the carbon feed inlet was essentially at atmospheric pressure temporarily mitigated the air influx through the carbon feed system. This enabled continued, safe operation for the remainder of the test.

The cyclone was operated with the recycle auger reversed for a period of time to “clear” out excess fines in order to increase the bed particle size. Removal of sufficient fines collected by the cyclone and recycled to the bed would result in an increase of the average particle size of the remaining bed media. Nearly 1.2 kg of fines were removed at COT 54.33. The particle size of a bed sample collected about one hour later did not indicate any significant increase in bed particle size, so another 1.9 kg were removed at COT 60.33. The bed HMPD increased to 0.164 mm after this second fines removal.

Bed drains and samples started showing evidence of an increased number of agglomerates, including tear-shaped, pea-sized, thin-walled forms that contained a loose powder in the interior. These were considered indicative of undesired agglomeration in the bed. The atomizing gas flow rate was increased (test condition 12, COT 65.95) in an attempt to correct what appeared to be poor atomization brought on by nozzle accretions interfering with the spray pattern.

The bed temperatures, starting at about COT 67, especially the location measured by TC3 that penetrates up through the bottom receiver to a location just a few inches below the feed spray zone, began to be erratic and diverge from the prior temperature baseline and from temperatures indicated by other bed TCs. This temperature spiking and variation signaled a general failure of mass and heat transfer in the bed, typically caused by a general defluidization or agglomeration of the bed. The simulant feed was stopped, the test ended, and shut-down procedures initiated at COT 68:26.

Bed vessel inspections after the test showed that much of the bed mass had formed a semi-spherical mass large enough to form a loose bridge across the bed above the feed zone (Figure 4.1-3). The front surface of the feed nozzle is visible on the inner wall at the 3-o'clock position in this figure. The cyclone recycle port is visible at about the 7-o'clock position. This single bridging mass appeared to be a composite of several, separate bed agglomerations in the reactor bed. Some hollow tubes of fired product were found in the bed, including one in the bridged powder, about two inches above the feed zone.

Figure 4.1-3. Bridged solids above the feed port, looking up through the bottom of the fluidized bed vessel.

Much of the rest of the bed media that was not in the bridging monolith consisted of small and large agglomerations that bridged above the bed drain tube and could not be drained out of the bed. These agglomerations are visible sitting on top of the distributor after the distributor flange was unbolted and the distributor was lowered from the bottom of the bed vessel for inspection (Figure 4.1-4).

Figure 4.1-4. Bed agglomerations on the distributor.

Figure 4.1-5 shows the FBSR bed and wall temperatures and the difference between the two temperatures plotted chronologically through the run. For convenience, different markers are used to indicate the differential temperatures for the different slurry feed rates. The data indicate that heat transfer from the wall to the bed was impacted by the displacement of starting bed media by aluminosilicate product, leading to an increasing differential between the wall and bed temperatures up to approximately COT 25.

At about COT 51, the bed temperature dropped several degrees. No definitive explanation is available for the temperature drop, but operators thought that the system ceased controlling temperatures with input from T3, and switched heater control input to thermocouple T4. Thermocouple T3 continued to give reliable temperature measurements. The wall temperature was increasing during the period when the bed temperature fell and increased again after control input was switched from T3 to T4.

In retrospect, the sudden drop in bed temperature, coupled with an increase in wall temperature (T20), indicates a change in heat transport mechanisms, such as a change in bulk emulsion convection or fouling of the heat transfer surfaces. However, no evidence of fouled surfaces was observed during the "postmortem" examination (Figure 4.1-3). Changes in the emulsion convection may have been caused by maldistribution of fluidizing gases as a result of distributor restrictions or accumulation of debris (agglomerations) on/around the distributor, accretions on the vessel wall, or changes in the behavior of the powder from Geldart Group B to Group A (Kunii, 1991). Regardless of the cause for the step change in the bed differential temperature, the event at COT 51 appears to be the initiating event leading to eventual bed defluidization.

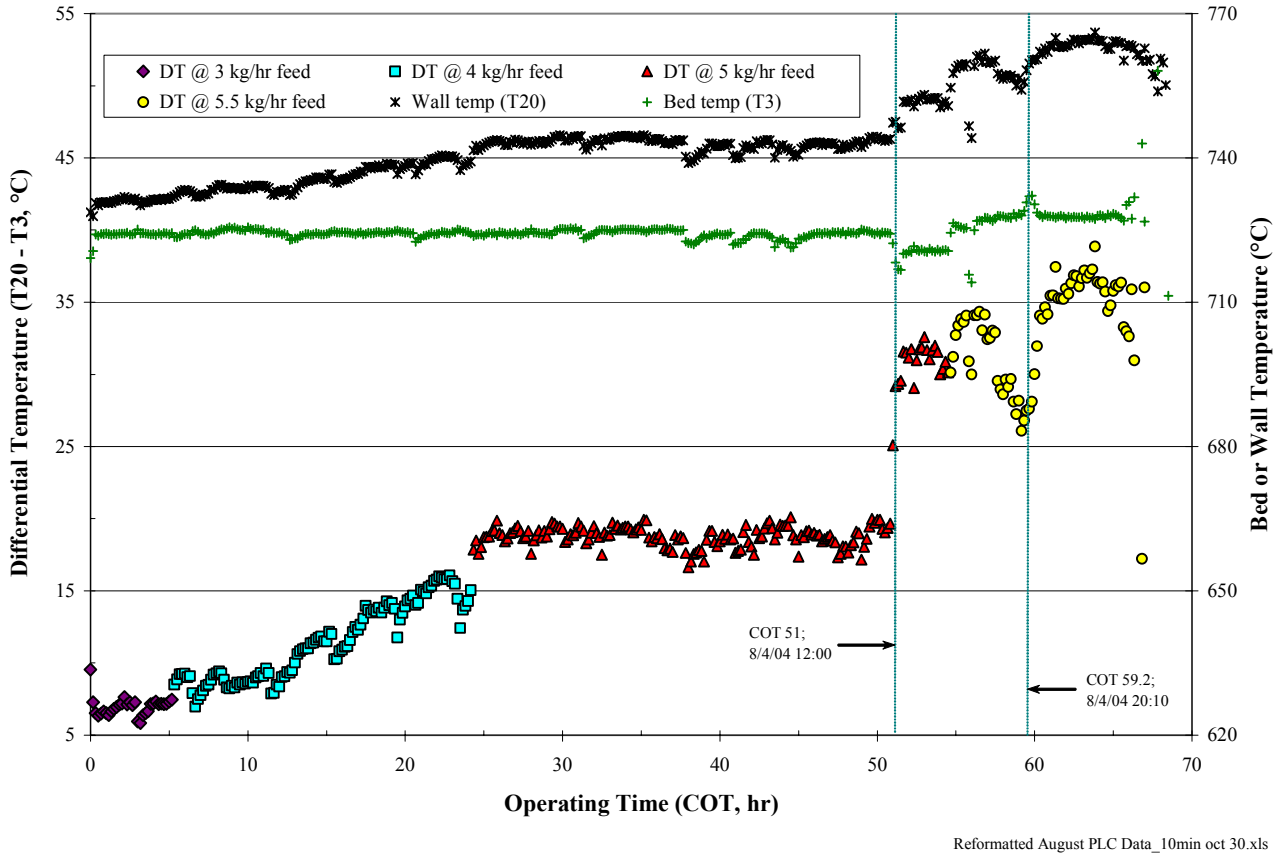

Figure 4.1-5. FBSR bed and wall temperature profiles vs. COT.

Shortly after increasing the slurry feed rate to 5.5 kg/hr (COT 54:12), a shuttle valve on the carbon feeder airlock failed open, allowing air to infiltrate the reformer. The decrease in the differential temperature near COT 56 suggests that the valve failed open at that time. The infiltrating air reacted exothermically with carbon and combustible gases, which increased heat input to the bed and decreased the demand on the bed heaters. The infiltration was mitigated at about COT 59 by slowly increasing the reformer pressure, at the carbon injection point, over a period of several minutes, to nearly match ambient atmospheric pressure. The decline in air infiltration resulted in an increasing demand on the bed heaters as evidenced by the increasing differential temperature. Overall trends in wall, bed, and differential temperatures do not appear to have been affected by the change in pressure other than that attributed to reduced air infiltration.

It is postulated that the agglomerations, which terminated the test, were caused by a combination of several possible contributing factors. The slurry waste feed rate (5.5 kg/hr) may have been too high for the operating conditions, resulting in excessive cooling and eventually agglomerating the bed media in the feed spray zone. The atomizing gas rate (<3 kg/hr, NAR 670), maintained as low as considered possible to minimize bed grinding and control fines generation, may have been too low to adequately atomize the liquid feed slurry. Dynamics between feed droplets and bed particles may have caused periodic growth of agglomerations attached to or near the nozzle, which could further interfere with feed atomization. The fluidized bed density, which started at about 1.4 g/cc but decreased to about 0.4 g/cc as the aluminosilicate product replaced the starting bed media, may have been too low to prevent the feed spray from spraying across the bed and hitting the far wall, or too low to provide the needed thermal inertia in

the bed to prevent excessive bed particle cooling in the spray zone. The fluidizing gas velocity, decreased from a starting velocity of 0.25 m/s to 0.12 m/s to control fines generation, was still up to 30 times higher than the minimum value needed to maintain fluidization, but may have been low enough that heat and mass transfer in the spray zone was insufficient to prevent excessive bed particle cooling. The low distributor differential pressure may have led to poor distribution of the fluidizing gases and uneven fluidization in the lower portion of the bed, including the feed zone.

4.1.2 Fluidized Bed Performance

One of the objectives of this test was to obtain a stable bed in the steam reforming reactor. The fluidized bed mass, density, height, particle size, and product distribution would be controlled within acceptable limits for stable operation as noted in the test objectives.

The bed particle size, bulk density, and particle (true) density are key operating parameters and characteristics of the bed product. Bed product was frequently harvested from the reactor to maintain fluidized bed depth within an acceptable range. This was accomplished by removing the bed product via either a bottom drain below the distributor or a sample port that extends into the fluidized ("live") region of the bed. Bed media taken from the "live" region through the sample port are believed to be more representative of the fluidized media and were used for bed particle density and size determinations.

The mean particle size determination was performed during the test by obtaining about 15 – 35 grams of bed media sampled from the fluidized region and passing the material through a series of standard sieve screens. The mass fraction of solids that accumulated on each screen (m_i) and the mean particle diameter of the size fraction (d_i) were used to compute the mass-mean and harmonic-mean particle diameters (MMPD and HMPD). Process fluidizing calculations were based on the HMPD, which approximates the mean diameter of a sphere with an equivalent surface to volume ratio as the bed particles. The mass of fine particles influence the HMPD calculation more strongly than the masses of the larger particles.

$$\mathrm{MMPD} = \sum_{i=1}^{n} m_i d_i$$

$$\mathrm{HMPD} = \left[\sum_{i=1}^{n} \left(\frac{m_i}{d_i} \right) \right]^{-1}$$

The size fraction diameter (d_i) was defined as the geometric mean of the apertures for the sieve upon which the solids reside and the preceding, adjacent sieve ($d_i = \sqrt{a_i a_{i-1}}$). The diameter of the solids fraction that accumulated on the top screen was taken as the geometric mean of the sieve aperture and that of the next larger size sieve in the series. The fraction diameter for pan fraction of solids was taken as half of the aperture size of the last (preceding) sieve ($a_n/2$).

Figures 4.1-5 through 4.1-7 show how the MMPD and HMPD changed as bed turnover resulted in conversion of the bed from the starting bed of alumina particles to a bed made primarily of mineralized product particles. The bed inventory decreased from an initial mass at the test start of about 16 kg (as seen by the PLC) to a mass of about 5.6 kg that was relatively constant once the bed turnover was essentially complete at about COT 35 (95% turnover). This degree of bed turnover occurred by the time about 145 kg of LAW slurry simulant was fed. The fluidized bed density, bulk density, and particle

density also decreased to relatively stable values of about 0.4 gm/cc, 0.7 gm/cc, and 2 gm/cc (see Figure 4.1-6), respectively as the bed turnover exceeded reached 95%.

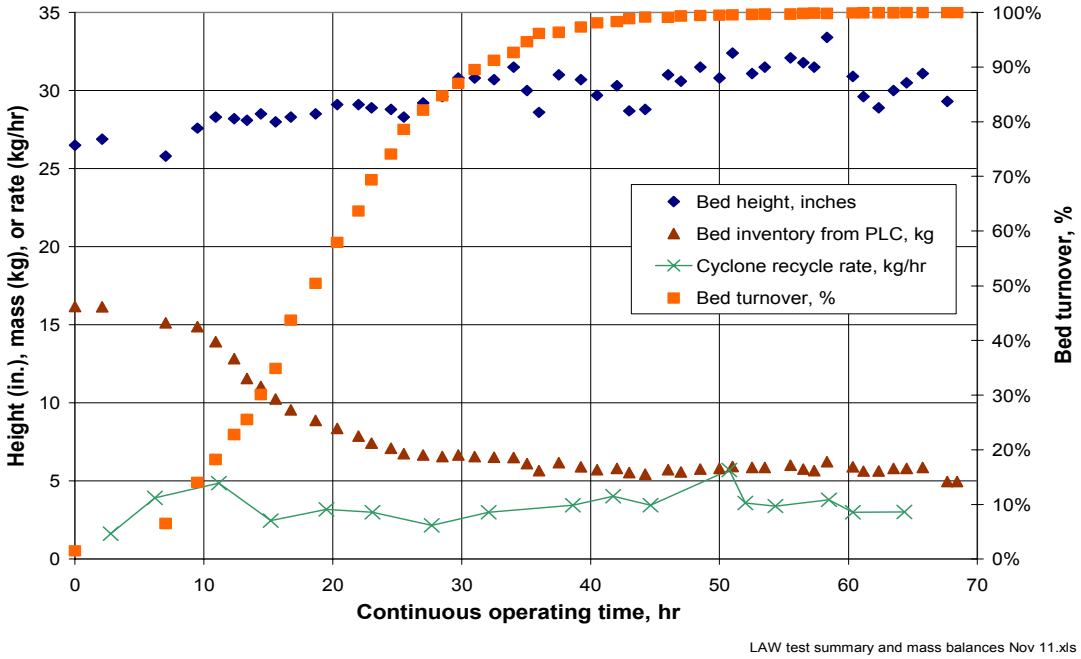

Figure 4.1-6. Bed height, inventory, and cyclone recycle rate.

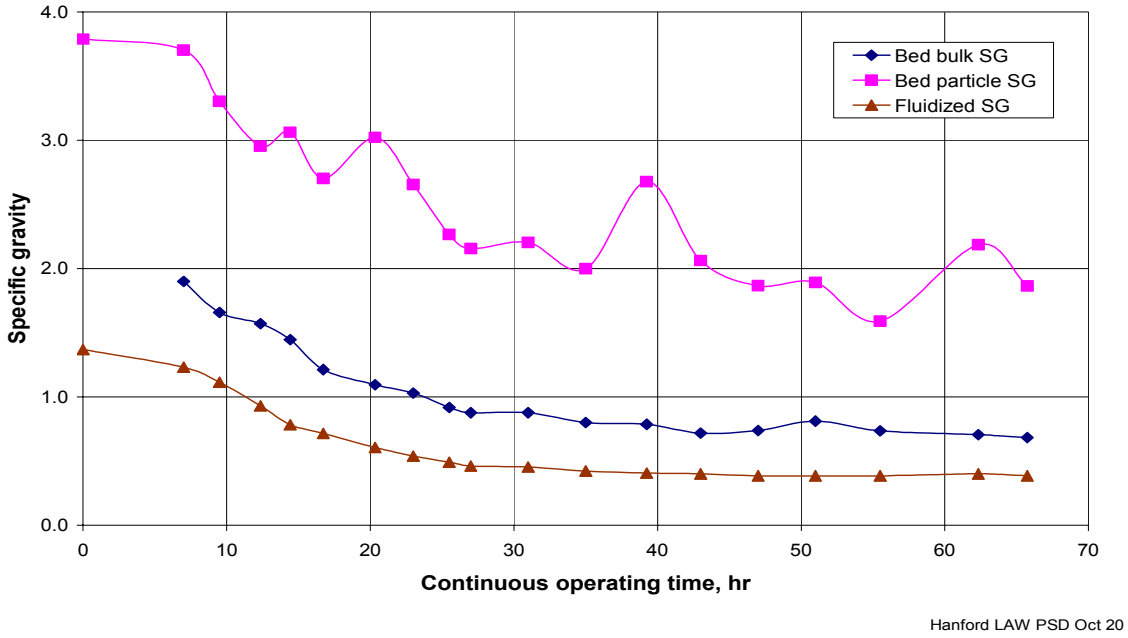

Figure 4.1-7. Bed bulk specific gravity, particle specific gravity, and fluidized specific gravity.

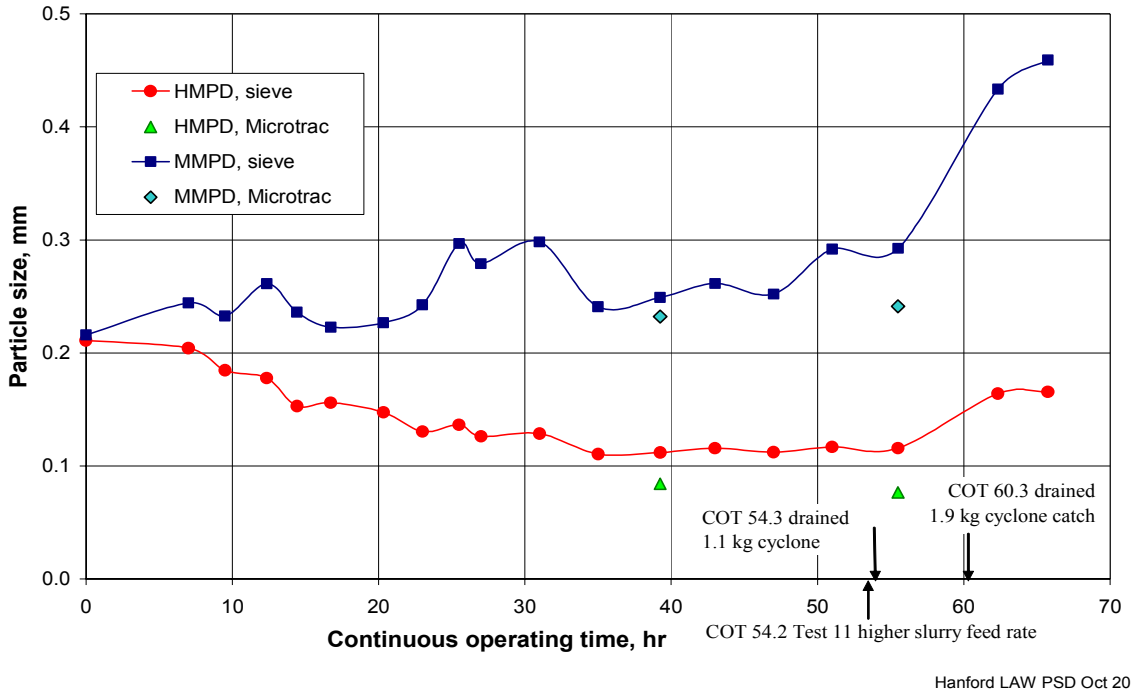

Figure 4.1-8. Bed media particle size.

Frequent removal of bed product was required to maintain the bed height within a nominal range of about 26-30 inches (within the maximum height of the fluidized bed section of 30 inches) as the bed density decreased. The bed height was allowed to range up to about 33 inches, as the bed density decreased, extending up into the bottom flange of the transition section between the 6-inch diameter bed section and the 12-inch diameter disengaging section. This bed depth did not compromise bed mass calculations or get into the expanded region where bed fluidization characteristics could change.

Two bed samples were also analyzed after the test using a laboratory Microtrac S3000 particle size analysis instrument. The Microtrac results are shown with the sieve tray results on Figure 4.1-7. The Microtrac data, when reduced using the geometric mean diameters for each stage, as was done for the sieve tray analysis [ASTM, 2002 and Kunii, 1991], is slightly lower than the sieve tray data. This is because the Microtrac instrument is capable of particle sizing to below 0.001 mm, and so is more sensitive than the sieve tray analysis, with the smallest tray size of 325 mesh (0.052 mm).

The particle bulk density was measured by pouring 20 – 30 cc of sampled bed media into a 100-ml graduated glass cylinder and settling the material by rapping the cylinder against the table or by setting the cylinder on a vibrator. The sample was flooded with water to obtain an estimate of the void volume between the particles and an estimate of the particle density after recording the bulk density. The measurement was an estimate, because gas bubbles would form in the wetted bed media that could not be disengaged with tapping or vibrating. Nevertheless, the values obtained were useful to follow a general (relative) trend in the particle characteristics as time progressed.

The bed particle size distribution gradually decreased from a harmonic mean particle diameter (HMPD) of about 0.21 mm to a relatively stable value of about 0.11 mm after the bed turnover reached

95%. The mass mean particle diameter (MMPD) increased from 0.22 mm to an average of 0.26 mm during the same time period. The HMPD decreased as the amount of fines in the bed increased. The MMPD increased because, simultaneous with the increase in the amount of fines, the amount of larger particles also increased.

The stable bed density and particle size values were lower than desired for this test. Several test condition changes during the test (increasing the slurry feed rate, lowering fluidizing gas rate, and lowering the atomizing gas rate) were made to try to increase both the bed particle size and density. In addition, some of the fines recycled back to the bed by the cyclone were harvested at two different times in larger amounts than needed to determine the cyclone recycle rate, in order to remove some of the recycled fines from the system, thereby increasing the average bed particle size.

Eventually, some combination of either the cyclone fines harvesting, lower gas flow rates, or the slurry feed rate increase from 5 to 5.5 kg/hr, (without increasing the atomizing gas flow rate) resulted in a bed particle size increase. At the time when the test was terminated due to bed agglomerations, the bed HMPD had increased to about 0.17 mm and the bed MMPD increased to about 0.46 mm. However, the changes that were made to control bed density and particle size combined with the lower fluidized density seemed to be contributing factors in the defluidizing agglomeration that caused the test termination.

4.2 Solid Product and Fines Characterization

A sample of the fluidized bed material at COT 0 is depicted in an optical photograph shown in Figure 4.2-1. The starting alumina bed media looks like broken pieces of glass, all of fairly uniform size. These pieces have sharp edges and angular surfaces, and are nearly transparent. Carbon reductant particles in the bed are very dark, angular particles that range in size up to several mm. Additional optical photographs (Figures 4.2-2 through 4.2-4) show how the starting alumina bed was replaced over time with product bed. The scale shown in these photographs is 1 mm. Essentially no starting bed material is visible by COT 55:30 (Figure 4.2-4). Individual particles have a popcorn-like appearance.

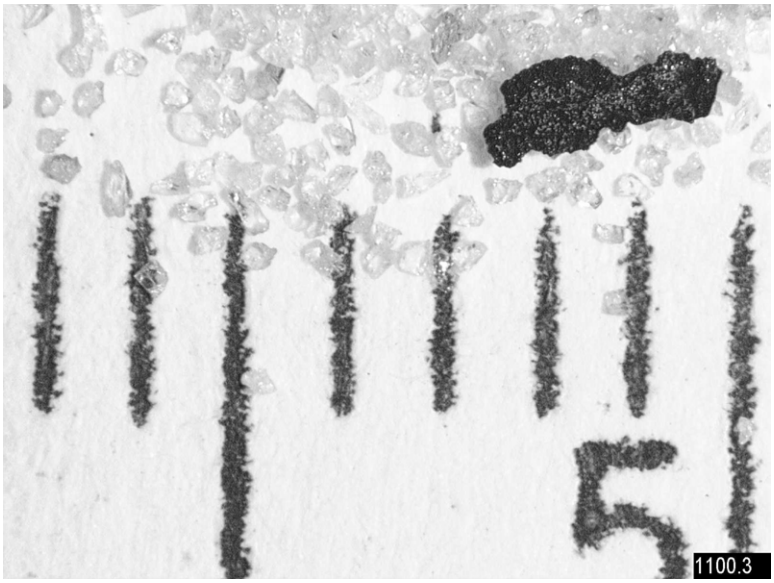

Figure 4.2-1. Photograph of the starting bed material at COT 0

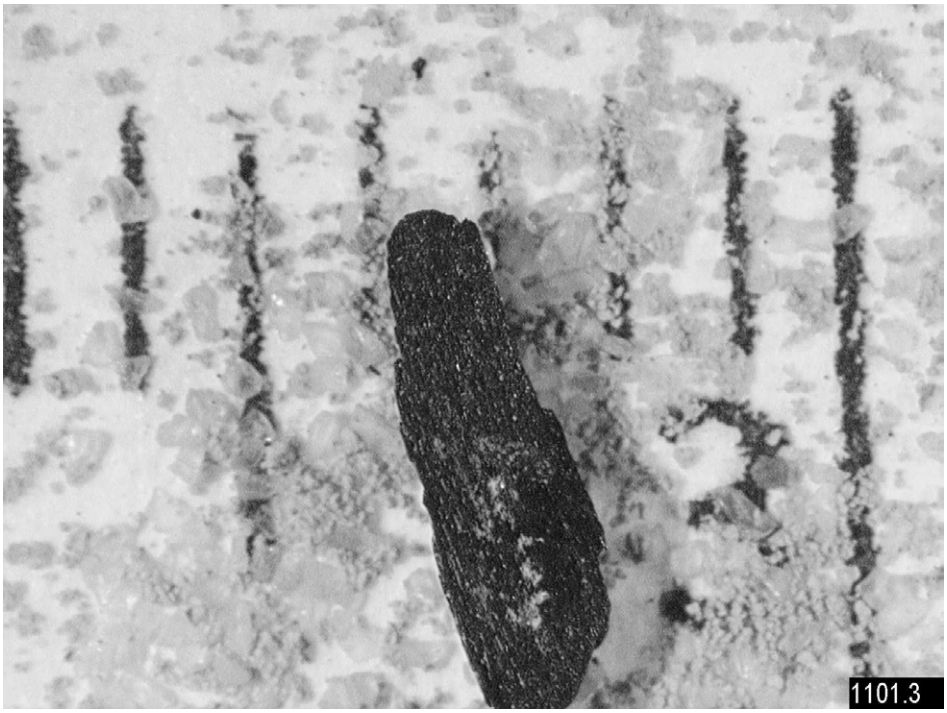

Figure 4.2-2. Photograph of the bed material at COT 12:21.

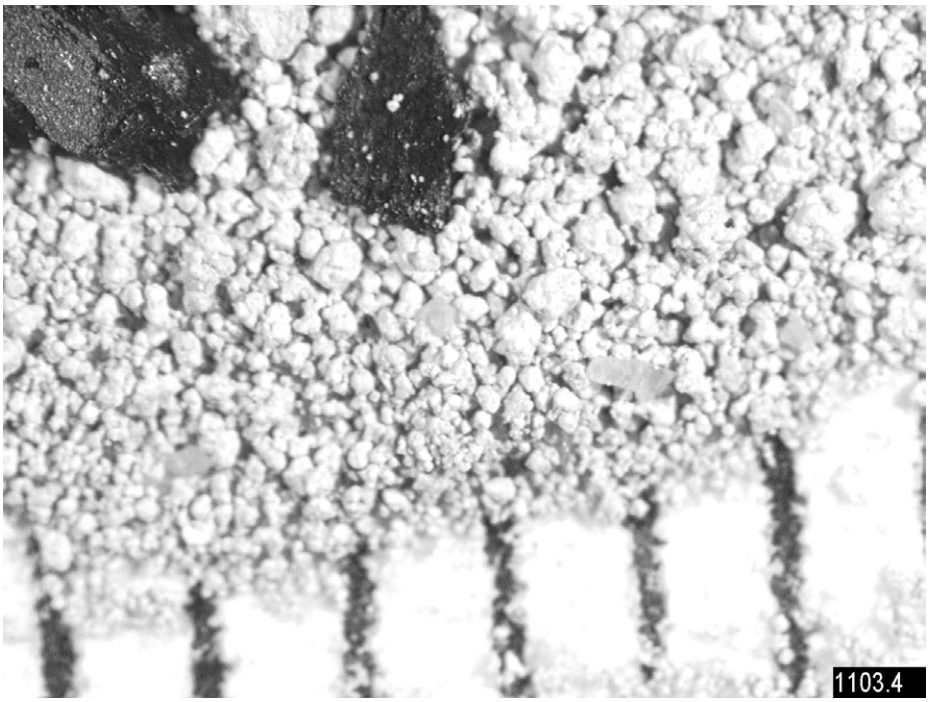

Figure 4.2-3. Photograph of the bed material at COT 39:15.

Figure 4.2-4. Photograph of the bed material at COT 55:30.

The starting alumina bed media was eventually replaced by particles of mineralized product as the test progressed. The very narrow particle size distribution for the starting alumina bed broadened during the test to include significant amounts of particles less than 0.1 mm, and significant amounts of particles greater than 0.3 mm, as shown in Figure 4.2-5. The particle size distribution was relatively stable at about 24% of the bed mass less than 0.1 mm and about 24% of the bed mass greater than 0.3 mm when bed turnover approached 99% (COT 55.5). The mass of <0.1 mm bed material decreased to 13%, the mass of >0.3 mm bed material increased to 43%, and the mass of >1 mm material increased from about 6% to 11% after operating at a higher LAW simulant slurry feed rate, and with lower fluidizing and atomizing gas flow rates at the end of the test. Some of the larger bed particles were small, 1-2 mm agglomerations that had increased as a result of the final operating conditions of the test.

Figure 4.2-6 shows how the bed MMPD and HMPD varied over the operating period. The HMPD decreased from 0.211 mm to 0.166 mm and the MMPD increased from 0.216 mm to 0.459 mm over the coarse of the experiment. The bed bulk density decreased from 1.90 to 0.68 g/cc and the particle density decreased from 3.79 to 1.87 g/cc, as shown in Figure 4.1-6, during the experiment.

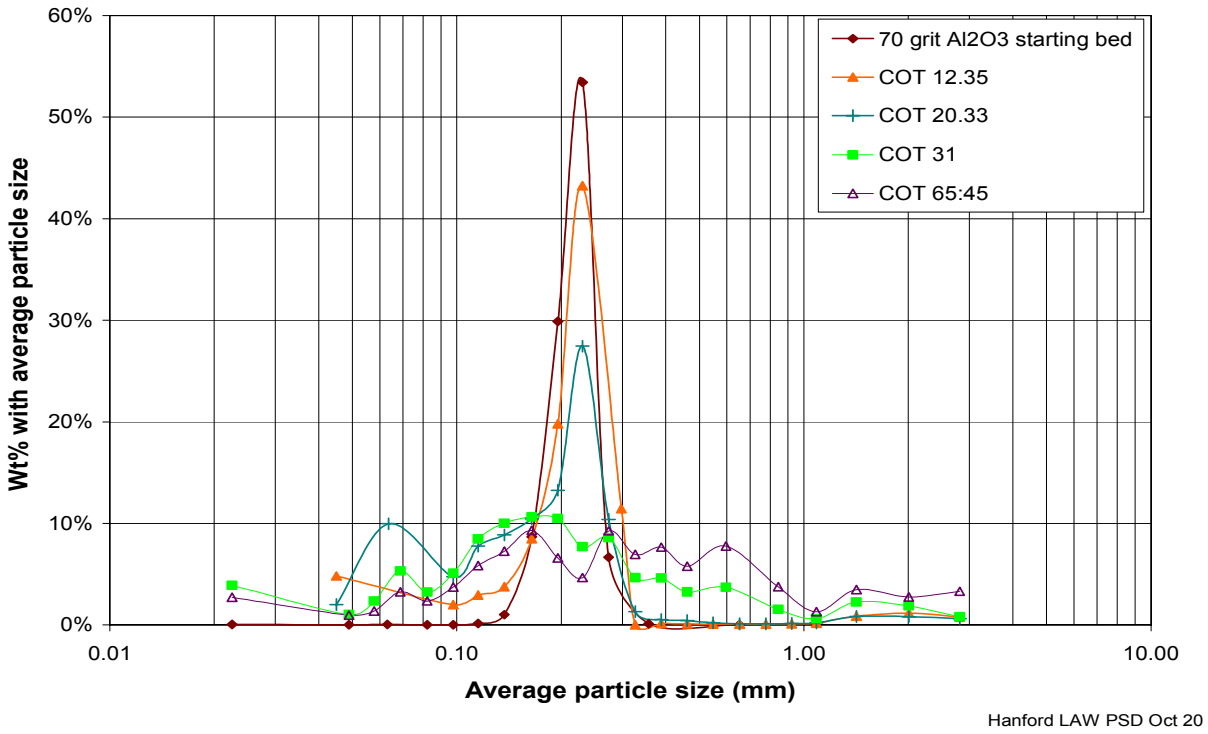

Figure 4.2-5. Measured bed particle size distributions over the operating period.

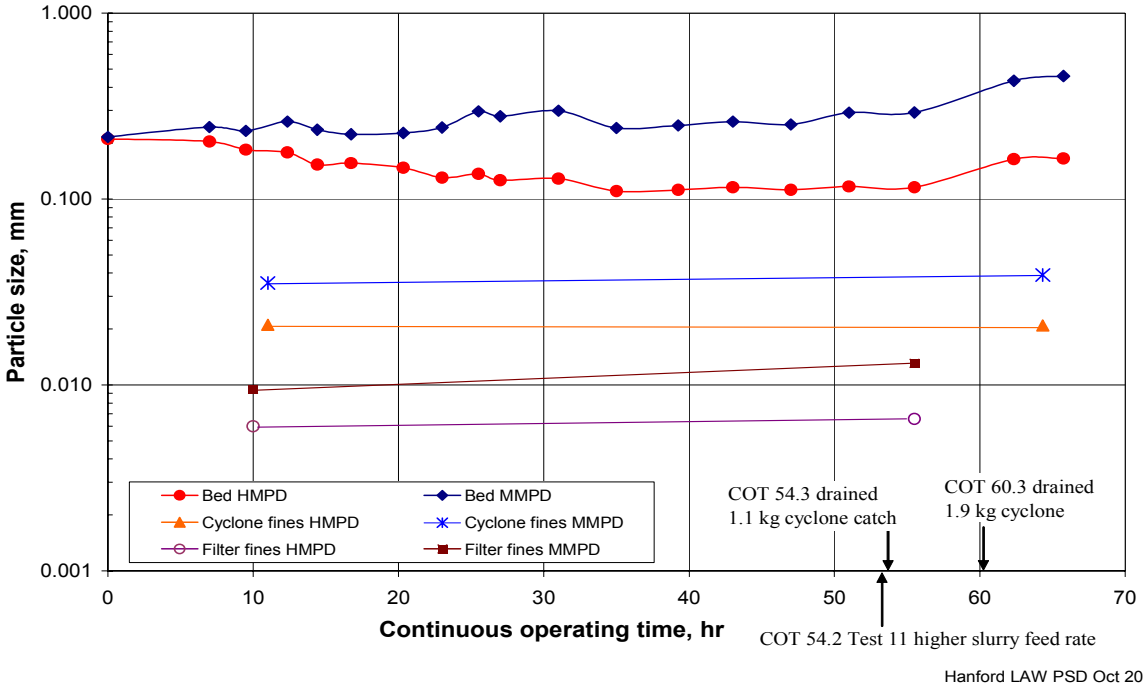

Figure 4.2-6. Average particle sizes for the FBSR solid products.

Fines elutriated from the bed and collected in the cyclone were continuously recycled back to the bed, except when the cyclone recycle rate was measured or cyclone recycle samples were collected. Some of the recycled fines were deliberately harvested to increase the bed mean particle size and not returned to the bed in an effort to increase the HMPD late in the test. Fines passing through the cyclone were collected by the heated sintered metal filters, and periodically removed as product. Figures 4.2-7 and 4.2-8 are optical photographs showing the cyclone and filter fines on a scale of 1 mm. These photographs are typical of the products seen during the experiment. The small black particles in the photos are un-reacted carbon. The filter fines have the consistency of talc, the individual particles clump together, but are relatively easy to collect.

Particle size distribution of the cyclone and filter fines was measured at two different times, one early in the test and one late in the test. The size distribution of these particles is shown in Figures 4.2-6 and 4.2-9. The size of the cyclone particles is, on average, about 5 times smaller than the bed product. The filter fines are about 4 times smaller in diameter than the cyclone fines.

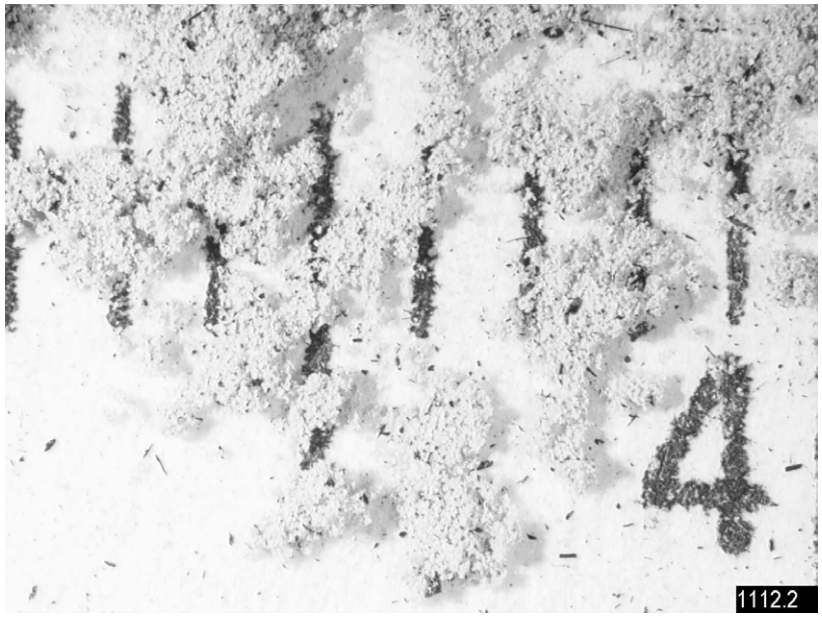

Figure 4.2-7. Photograph of the cyclone fines material at COT 64:20.

Figure 4.2-8. Photograph of the filter fines material at COT 55:30.

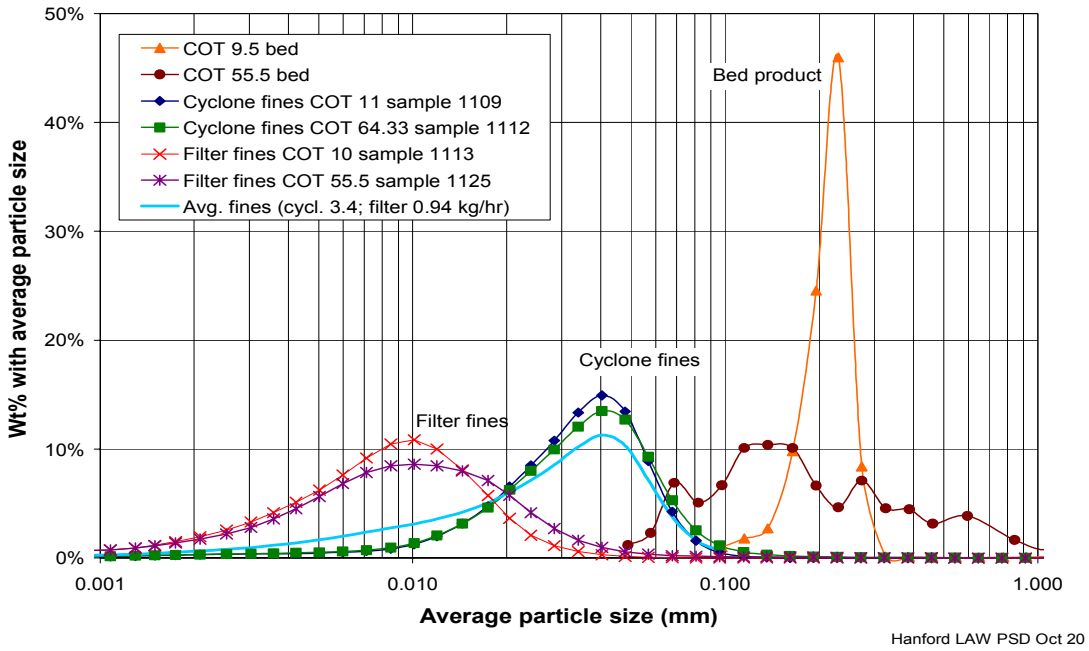

Figure 4.2-9. Particle size distributions for solid products at progressive continuous operating times.

Bed particle morphology can be seen with higher scanning electron microscope (SEM) magnifications of a larger bed particle. Much smaller particles are visible (Figure 4.2-10) on the surfaces of the larger product particles, much like sand particles are visible in sandstone. This photograph is of the final bed product. The bar located at the bottom of the photo, in the middle, represents a distance of 3.28 microns. This photograph shows that the product particles do not generally consist of coatings of product

that grew, onion-skin style, on the alumina particles (like typically occurs in SBW calcination and in SBW steam reforming to a carbonate product). Instead, the solid product from the feed tended to form separate particles. Individual particles, on the surface of a larger particle, range from less than 1 um to several um in diameter. At this magnification, the small individual particles appear angular, indicating crystalline structure.

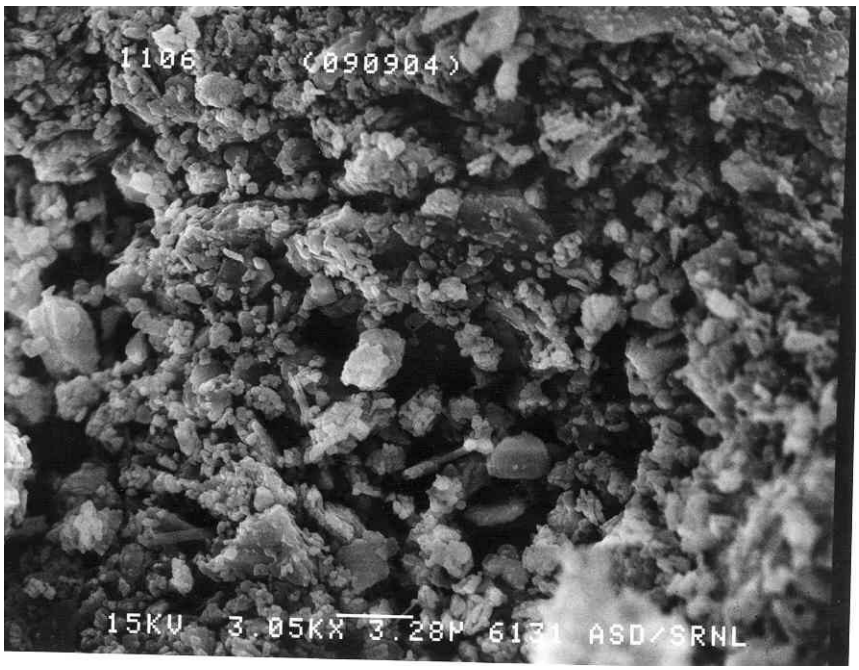

Figure 4.2-10. SEM photograph of the final bed.

The morphology of the cyclone fines can be seen in Figure 4.2-11. This SEM photograph indicates that the cyclone fines appear to be generally smaller versions of the bed product particles. The scale in the photograph is shown by the bar located at the bottom of the photo, in the middle, which represents a distance of 12.5 microns. Individual particles range in size from 10-60 microns, consistent with the measured particle size distribution. Much smaller, sub-micron particles are visible on the surfaces of larger particles at this magnification.

The morphology of the filter fines is shown in Figure 4.2-12. The scale in the photograph is shown by the bar located at the bottom of the photo, in the middle, which represents a distance of 9.8 microns. Particles ranging in size from 1-20 um are visible, also consistent with the measured particle size distribution. Some of the larger particles appear to be loose agglomerations of smaller particles.

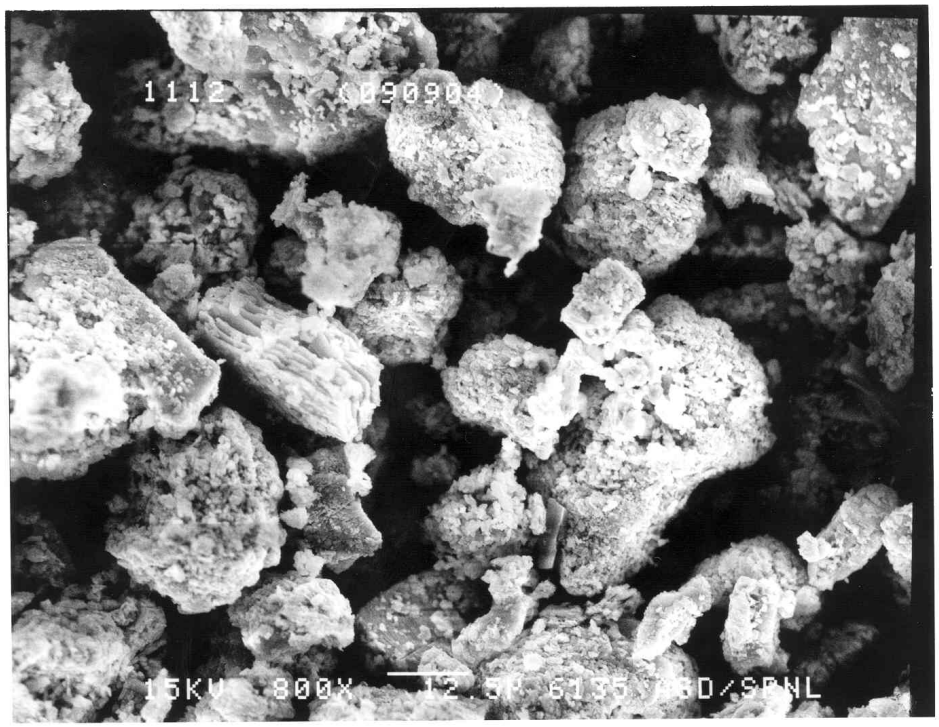

Figure 4.2-11. SEM photograph of cyclone fines sample at COT 64:20.

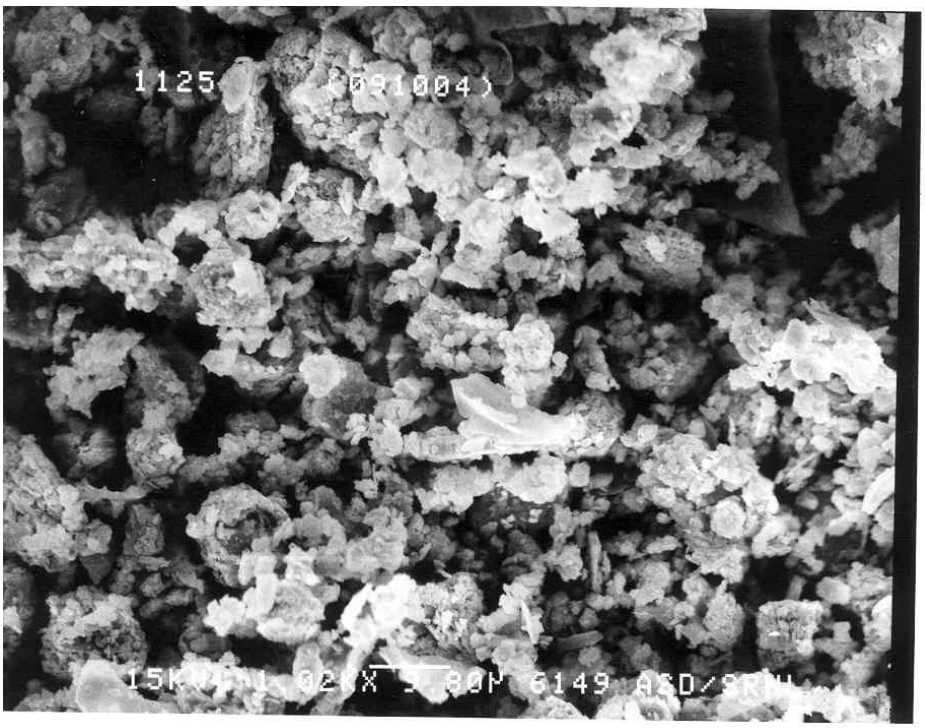

Figure 4.2-12. SEM photograph of filter fines sample 1125 (COT 55:30).

Bulk densities of the filter fines product are listed in Table 4.2-1. The filter fines product density did increase slightly during the operating period, and the carbon content (~4 wt%) does not significantly affect the bulk density. Tapping the sample, consistent with ASTM B 527, significantly consolidates the sample, decreasing the volume about 35%, and increasing the bulk density about 35%.

Table 4.2-1. Bulk densities of the filter fines.

Description	Bulk density (g/mL)	
	Untapped	Tapped
Filter Fines (including un-reacted carbon) at COT 10	0.288	0.476
Filter Fines (including un-reacted carbon) at COT 55:30	0.310	0.517
Filter Fines (carbon roasted out) at COT 55:30	0.33	0.5

Results of x-ray diffraction analyses on the solid products are summarized in Table 4.2-2. The major phase in the products formed in the FBSR is carnegieite. There is some nepheline present, and a minor amount of nosean, in the bed products. The cyclone samples showed a major phase of carnegieite, with a minor amount of nepheline (no nosean). The filter fines showed a major phase of carnegieite and trace amounts of nepheline (no nosean).

Table 4.2-2. Summary of mineral phases observed in the FBSR solid products.

Description	$Na_{7.15}(Al_{7.2}Si_{8.8}O_{32})$ Nepheline (Si rich) PDF# 79-0993	$NaAlSiO_4$ Carnegieite PDF #11-0220	$Na_6[Al_6Si_6O_{24}](Na_2SO_4)$ Nosean PDF# 73-1734	TiO_2 Anatase PDF# 21-1272
Bed Product COT 39:15	Some	Major	Minor	Trace
Bed Product COT 55:30	Some	Major	Minor	Trace
Final Bed	Some	Major	Minor	Trace
Cyclone fines COT 11:00	Minor	Major	None	Trace
Cyclone fines COT 64:20	Minor	Major	None	Trace
Filter fines COT 10:00	Trace	Major	None	Trace
Filter fines COT 55:30	Trace	Major	None	Trace

Table 4.2-3 shows the XRD results for a bed sample at COT 27 that was sieved into fractions (-80 mesh, filter fines, -70, +80 mesh, and +70 mesh). An interesting observation is that the coarse material (+70 mesh) shows major amounts of carnegieite and nosean with lesser amounts of nepheline. This material appears to have an increased reaction yield, resulting in a greater amount of the desired nosean

phase. This leads to the possibility that the atomization of the feed led to a "spray drying effect" and the rapid formation of small, metastable minerals (carnegieite). The spray drying effect may have inhibited chemical reactivity, particle growth, and perhaps accounted for the morphology observed in the SEM photographs. In instances where particles did undergo particle growth (i.e. +70 mesh particles), the necessary reactions did occur to form the favorable nosean phase.

Table 4.2-3. Phase analysis for different sieve fractions of COT 27 product bed.

Description	$Na_{7.15}(Al_{7.2}Si_{8.8}O_{32})$ Nepheline (Si rich) PDF# 79-0993	$NaAlSiO_4$ Carnegieite PDF #11-0220	$Na_6[Al_6Si_6O_{24}](Na_2SO_4)$ Nosean PDF# 73-1734	TiO_2 Anatase PDF# 21-1272
COT 27 Bed Fines (-80 mesh)	Minor	Major	Trace	Trace*
COT 27 Filter Fines	Minor	Major	None	Trace
COT 27 Bed -70, +80 mesh	Minor	Major	Minor	Trace*
COT 27 Bed Coarse (+70 mesh)	Minor	Major	Major	Trace

*Trace amounts of corundum (Al_2O_3) were also seen in these samples.

A more detailed analysis of the solid products will be reported separately by SRNL. That analysis will include data regarding performance of the products when subjected to the Product Consistency Test (PCT) and the Single Pass Flow Through (SPFT) Test. Chemical composition of the solid products is detailed in Section 4.4.

4.3 Off-Gas Characterization and Off-Gas System Performance

The off-gas system downstream of the FBSR heated filter includes the thermal oxidizer for destroying H_2, CO, and total hydrocarbons (THC) from the FBSR, a water-spray partial quench to cool the hot oxidizer outlet off-gas, a reheater to ensure off-gas temperature control, and a carbon bed. The partial quench cooled the off-gas to about 130°C, cool enough for the downstream carbon bed. The carbon bed was used in this test only to capture any halogen gases (HCl, Cl_2, etc) and SO_2 that may be in the off-gas for mass balance purposes, since no Hg was added to the Hanford LAW simulant.

4.3.1 Off-Gas Composition at the Steam Reformer Heated Filter Outlet

The average off-gas composition (wet basis) at the outlet of the heated filter is shown in Table 4.3-1 for each test condition. The wet basis composition was calculated from the dry, as-measured composition by (a) correcting for zero and span calibration error/drift, and (b) normalizing the dry composition to a wet basis using the off-gas moisture content. The moisture content at the filter outlet location was not directly measured but was calculated from the fluidized bed input flow rates of fluidizing steam, evaporated water from the simulant, water from NaOH in the simulant, and water from oxidation of hydrogen-bearing sodium acetate in the feed. The amount of water from the NaOH (under 0.02 kg/hr)

and from oxidation of sodium acetate (under 0.01 kg/hr) in the feed was very small relative to the amount of H_2O from the fluidizing steam (~2 kg/hr average) and evaporated water (~2 kg/hr average) from the simulant.

The trends in the heated filter outlet off-gas composition are shown in Figure 4.3-1. This figure shows the continuously-monitored composition averaged over 10-minute time periods. Occasional gaps in the data trends occur when the instruments were off-line for calibrations. The trends over time indicate graphically how the gas composition varied during the test period. Concentrations of reduced gas species (H_2, CO, THC, and CH_4) were relatively high at COT 0. Only carbon was fed to the FBSR, without any simulant feed, prior to COT 0. This established an initial inventory of carbon in the fluidized bed to ensure that FBSR conditions were sufficiently reducing when simulant feed was started.

Various test condition changes were made as the test progressed. These changes were made to adjust the NO_x-reduction stoichiometry, the simulant feed rate, feed atomization, or bed fluidizing conditions.

After COT 0, when the simulant feed was started, off-gas concentrations of reduced gas species decreased, and the NO_x concentration increased, as expected. The carbon addition rate was decreased at COT 0:48, which further lowered the concentrations of reduced gas species, and allowed the NO_x concentration to further increase. These changes occurred because the REDOX stoichiometry changed when O_2 was introduced to the fluidizing gas, the feed containing nitrites and nitrates was initiated, and the carbon feed rate was reduced.

The carbon filter in the CEMS 1 sampling system may have contributed to the initially low NO_x concentrations, and the gradual NO_x concentration increase over time. A carbon filter is not typically used in CEMS sampling systems, but it was needed in the CEMS 1 sampling system to remove heavier, condensable hydrocarbon species that fouled CEMS 1 in prior testing activities. The carbon filter effectively removed condensable hydrocarbon species, but it can also tend to adsorb some of the acid gases, and NO_x in the sample gas. The carbon filter might have sorbed some NO_x, reducing the measured NO_x concentrations, until the carbon became relatively saturated with NO_x. Prior test programs have shown that, after an initial time period, the carbon filter no longer appreciably sorbs NO_x, and the measured NO_x values accurately reflect the actual NO_x values.

NO_x concentrations monotonically increased from about 1,000 ppm (wet) at COT 1 to about 3,800 ppm at COT 35. This monotonic increase was due to gradual depletion of apparently high levels of carbon inventory in the bed at COT 0, the lower COT 0:48 carbon feed rate, lower fluidizing gas and atomizing gas rates (which lowered the amount of diluent gases), and the higher simulant slurry feed rate. The carbon:oxidant stoichiometry decreased from 900% to 350% between COT 0 and COT 39:20. Refer to Section 4.4.3 for discussion with regard to the carbon:oxidant stoichiometry.

The carbon feed rate was increased at COT 39:20 to counter the rising NO_x concentration. The change in carbon additive feed rate, from 0.7 to 0.8 kg/hr, increased the carbon:oxidant stoichiometry from 350% to 420%. The NO_x concentration gradually decreased at this time, and the concentration of H_2, THC, and CH_4 gradually increased. These changes were gradual because the REDOX reactions in the bed depend not on the instantaneous carbon feed rate, but on the inventory of carbon in the bed. The carbon feed rate increase reversed the depletion of the fluidized bed carbon inventory.

The slurry feed rate was increased from 5 to 5.5 kg/hr at COT 54:15. Shortly thereafter, at about COT 57, one of the carbon feeder air lock valves stuck open. An influx of air entered the bed every time the other carbon feeder air lock valve opened, reacting with and decreasing reduced gas species concentrations, which impaired NO_x destruction and caused the NO_x levels to rise. At about COT 60, the

FBSR pressure was adjusted to be nearly atmospheric, rather than negative. This reduced the amount of air influx, and began to correct the FBSR off-gas composition. The concentrations of reduced gas species began to rise, and NO_x levels began to decrease.

The CO concentration stayed relatively constant after an initial downward trend between COT 0 and COT 15, while the concentrations of more oxidized gas species (NO_x) and more reduced gas species (H_2, THC, and CH_4) varied. CO, being an intermediate gas species between the reduced gases THC and CH_4, and the oxidized gas CO_2, remained relatively constant because, as conditions became more oxidizing, and some of the CO was converted into CO_2, and some of the more reduced gas species were converted to CO. Less CO was formed in favor of higher concentrations of reduced gas species when conditions became more reducing, but the formation of slightly less CO_2 replaced some of the lost CO.

Table 4.3-1. Off-gas composition (wet basis) at the outlet of the FBSR heated filter.

Test COT, clock time, and operating condition	Gas composition, wet basis											Mole weight
	O_2, % AE1_A1_O2_WB_ADJ	CO_2, % AE1_A3_CO2_WB_ADJ	CO, % AE1_A5_CO_WB_ADJ	H_2, % AE1_A2_H2_WB_ADJ	THC, ppm AE2_CST1_THC_WB_ADJ	CH_4, ppm AE1_A6_CHX_WB_ADJ	NO, ppm ---	NO_x, ppm ---	H_2O, % AE1_H2O_FRAC	N_2, % AE1_N2_WB_ADJ	Total, %	
COT 0, 0900, 1, test start	0.02	3.59	0.50	3.04	2,247	1,598	---	71	61.9	31.4	100.5	21.7
COT :48, 0948, 2, lower carbon feedrate	0.01	4.05	0.55	2.30	1,474	1,127	339	340	61.1	32.5	100.6	22.1
COT 5:00, 1400, 3, higher slurry feedrate	0.00	3.76	0.45	1.81	1,200	948	---	618	64.7	29.7	100.5	21.8
COT 8:12, 1712, 4 and 5, lower fluidizing steam	0.04	3.67	0.29	1.28	1,029	760	769	703	65.1	29.9	100.3	21.8
COT 24:00, 0900, 6, higher slurry feedrate	0.08	3.53	0.26	1.09	943	757	---	881	67.2	28.2	100.3	21.7
COT 25:30, 1030, 7, higher atomizing gas flowrate	0.05	3.50	0.25	1.02	900	695	932	954	67.7	27.8	100.3	21.6
COT 30:04, 1504, 8, lower fluidizing steam flowrate	0.06	3.73	0.22	0.82	807	608	1,211	1,283	66.1	29.4	100.3	21.9
COT 39:20, 0020, 9, higher carbon feedrate	0.08	3.65	0.19	0.65	754	512	1,437	1,427	65.4	30.3	100.3	22.0
COT 41:20, 0220, 10, lower fluidizing steam flowrate	0.05	3.79	0.24	0.94	949	689	891	808	64.4	30.8	100.3	22.0
COT 54:15, 15:15, 11, higher slurry feedrate	0.01	4.06	0.23	1.06	992	817	584	587	66.5	28.4	100.2	21.8
COT 65:57, 0257, 12, higher atomizing N2 flowrate	0.01	3.94	0.23	1.46	972	794	289	293	64.2	30.4	100.3	21.9
COT 68:26, 0526, shutdown												
Test averages	0.04	3.79	0.28	1.19	1,007	768	899	764	65.3	29.7	100.3	21.8

Notes:

1. The CEMS data were recorded by the PLC, and automatically adjusted for zero, span error, and moisture content. All measurements were made on a dry basis.
2. PLC tag numbers in the column headers indicate the source of the data. No tag number indicates that the data was calculated from other PLC data.
3. The PLC calculations were checked by hand and compared with concentrations recorded on data sheets.
4. The THC analyzer sample gas was split from the other sample gas upstream of the CEMS 1 carbon filter, so the THC measurements were not affected by hydrocarbon sorption by the carbon filter.
5. The NO and NO_x results were corrected for 4x dilution of the sample gas (by air). The air dilution was required for chemiluminescent CEM operation to provide excess O_2 needed for operation of the NO_x converter. No sample gas dilution was performed for the other analyzers.
6. NO data is not available for some test conditions. The NO_x analyzer was only in the NO_x mode during those times.
7. NO_x data is not available for some test conditions. The NO_x analyzer was only in the NO mode during those times.
8. The moisture content and gas molecular weight were determined based on input mass flowrates and calculated gasified or reacted products.
9. The N_2 concentration was determined by difference on a dry basis and then converted to wet basis.
10. The N_2 flowrate determined from the calculated N_2 concentration (by difference) and the FBSR outlet gas flowrate averaged 5.9 kg/hr, which agrees well (within 3.6%) of the total N_2 flowrate into the FBSR. The total N_2 flowrate into the FBSR averaged 6.4 kg/hr (from PLC tag V1_F1_VAL) less the average N_2 flowrate (0.29 kg/hr) into the oxidizer stage 2 (B1_F7_VAL).
11. The sum of the gas concentrations, near 100%, indicates good data quality.

[Reformatted August PLC Data_10min oct 30.xls]CEM 1 table

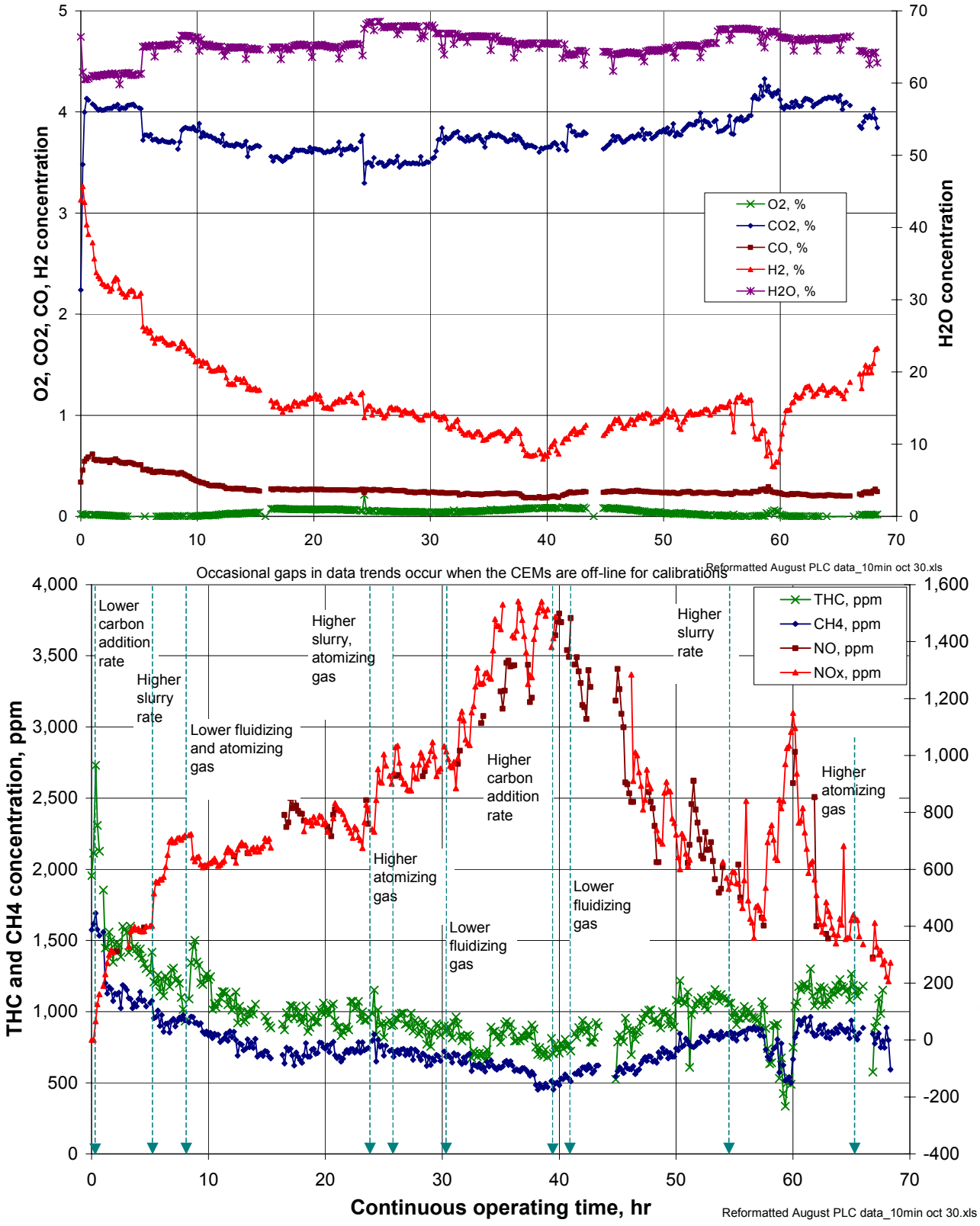

Figure 4.3-1. Wet basis off-gas composition at the FBSR heated filter outlet.

4.3.2 Off-gas Composition Downstream of the Oxidizer

The average off-gas composition (wet basis) downstream of the thermal oxidizer, partial quench, and reheater is shown in Table 4.3-2 for each test condition. All of the CEMS 2 measurements were made on a dry basis, after condensing off-gas moisture from the off-gas, except for the O_2 measurement. The O_2 measurement was made using a heated extractive ZrO_2 electrochemical sensor, on a wet basis, for thermal oxidizer process control. Except for the O_2 measurement, the wet basis composition was calculated from the dry, as-measured composition by (a) correcting for zero and span calibration error/drift and (b) normalizing the dry composition to a wet basis using the off-gas moisture content. The O_2 measurement required no calibration corrections and was measured on a wet basis. The moisture content downstream of the oxidizer and partial quench was not directly measured, but was calculated from the input flow rates of water into the process, and calculated amounts of water produced from oxidation reactions.

The CEMS 2 off-gas measurements were continuous, and recorded automatically by the PLC. Off-gas concentration trends in the oxidizer outlet off-gas composition are shown in Figure 4.3-2. This figure shows the continuously-monitored concentrations averaged over 10-minute time periods. The trends over time indicate graphically how the gas composition varied during the test series.

The O_2 concentration was very constant, controlled well by the oxidizer control system. Moisture and CO_2 concentrations were also very constant. The concentrations of these species were relatively insensitive to individual process changes considering the multiple sources of both H_2O and CO_2 in the oxidizer off-gas. Small step-function changes in the moisture content occurred when the slurry feed rate or fluidizing gas flow rates were changed. Changes in FBSR operating conditions had little impact on the oxidizer outlet off-gas moisture content because much of the total off-gas moisture in the oxidizer outlet gas was the product of auxiliary fuel combustion and the partial quench water spray. The moisture content contributed at this point due to feed slurry content, fluidizing gas, and FBSR gas reactions (6.5 scfm average) was only about 24% of the total moisture (27 scfm average) in the off-gas downstream of the oxidizer and partial quench.

The oxidizer operated very efficiently to oxidize H_2, CO, THC, and CH_4 in the FBSR off-gas to CO_2 and H_2O. The average CO concentration measurement downstream of the oxidizer was slightly below zero (-2.5 ppm). The calibrated operating range of this nondispersive infrared (NDIR) analyzer was 0-300 ppm (wet basis). This negative average value is about 1% of the calibrated full-scale range, well within typical and acceptable ranges of measurement error of up to 2% of the full-scale value. The true CO concentration was probably between 0 and 6 ppm, considering a maximum measurement error range of $\pm$2% of the full-scale range. A maximum CO concentration of 6 ppm (wet basis), when converted to 7% O_2, dry basis, would be 9 ppm; well within the EPA Hazardous Waste Combustor (HWC) Maximum Achievable Control Technology (MACT) standard of 100 ppm for CO.

The HCl and SO_2 concentration measurements were also slightly less than zero, averaging –0.5 ppm and –0.2 ppm, respectively. The ranges of maximum HCl and SO_2 concentrations were calculated based on typically acceptable instrument errors. Maximum HCl values could range to about 6 ppm (wet basis), based on a nominal 0-500 ppm range for this analyzer. This corresponds to a concentration of about 9 ppm (dry, corrected to 7% O_2), well within the HWC MACT standard of 21 ppm for HCl.

The oxidizer outlet NO_x concentration generally trended similar to the FBSR filter outlet NO_x concentration, only over a much lower concentration range. The oxidizer outlet NO_x concentration peaked at about COT 35, like the FBSR filter outlet NO_x concentration did. The oxidizer outlet NO_x concentration slowly trended downward when the carbon addition rate was increased at COT 39:20, just like the FBSR filter outlet NO_x concentration did.

Table 4-3-2. Off-gas composition (wet basis) downstream of the oxidizer and upstream of the carbon bed.

Test COT, clock time, and operating condition	Gas composition, wet basis											Mole weight
	O_2, % B1_A1_O2_WB_ADJ	CO_2, % AE2_A1_CO2_WB_ADJ	CO, ppm AE2_A1A_CO_WB_ADJ	NO, ppm AE1_CST2_NO_WB_ADJ	NO_2, ppm AE1_CST2_NO2_WB_ADJ	NO_x, ppm AE1_CST2_NOX_WB_ADJ	SO_2, ppm AE1_CST2_SO2_WB_ADJ	HCl, ppm AE2_A2_HCL_WB_ADJ	H_2O, % AE2_H2O_FRAC	N_2, % AE2_N2_WB_ADJ	Total, %	
COT 0, 0900, 1, test start	3.00	4.86	-0.8	48	2	51	---	-0.3	42.0	50.8	100.7	24.7
COT :48, 0948, 2, lower carbon feedrate	3.00	5.02	-4.0	71	-3	68	4.3	-0.3	40.4	52.2	100.7	24.8
COT 5:00, 1400, 3, higher slurry feedrate	3.00	5.02	-9.9	89	-4	85	---	-0.3	41.7	51.6	100.7	24.7
COT 8:12, 1712, 4 and 5, lower fluidizing steam	3.00	5.01	-2.3	77	2	79	3.9	-0.3	41.3	51.3	100.6	24.8
COT 24:00, 0900, 6, higher slurry feedrate	3.00	4.84	-0.7	84	1	85	---	-0.3	43.3	49.5	100.7	24.5
COT 25:30, 1030, 7, higher atomizing gas flowrate	3.00	4.81	-3.2	103	-3	100	-3.6	-0.3	44.2	48.7	100.7	24.4
COT 30:04, 1504, 8, lower fluidizing steam flowrate	3.00	4.97	-5.8	118	-4	114	-4.2	-0.3	42.4	50.3	100.7	24.6
COT 39:20, 0020, 9, higher carbon feedrate	3.00	4.85	1.7	88	15	103	3.1	-0.3	42.0	50.8	100.7	24.7
COT 41:20, 0220, 10, lower fluidizing steam flowrate	3.00	5.04	0.0	78	2	80	-1.9	-0.1	41.2	51.4	100.6	24.8
COT 54:15, 15:15, 11, higher slurry feedrate	3.00	5.04	-2.6	67	-8	58	-5.1	-0.2	42.3	50.3	100.7	24.6
COT 65:57, 0257, 12, higher atomizing N2 flowrate	3.00	4.97	0.1	56	-4	52	-1.4	0.1	42.4	50.3	100.7	24.6
COT 68:26, 0526, shutdown												
Test averages	3.00	4.99	-2.5	81	-1	80	-0.5	-0.2	41.9	50.8	100.7	24.7

Notes:

1. The CEMS data were recorded by the PLC, and automatically adjusted for zero, span error, and moisture content. All measurements were made on a dry basis.
2. PLC tag numbers in the column headers indicate the source of the data. No tag number indicates that the data in that column was calculated after the test, from other PLC data, and not taken directly from the PLC.
3. The moisture content and gas molecular weight were determined based on input mass flowrates and calculated gasified or reacted products.
4. The N_2 concentration was determined by difference on a dry basis and then converted to wet basis.
5. The sum of the gas concentrations, near 100%, indicates good data quality.
6. The PLC calculations were checked with hand calculations and compared with concentrations recorded on data sheets during the test.

[Reformatted August PLC Data_10min oct 30.xls]CEM 2 table

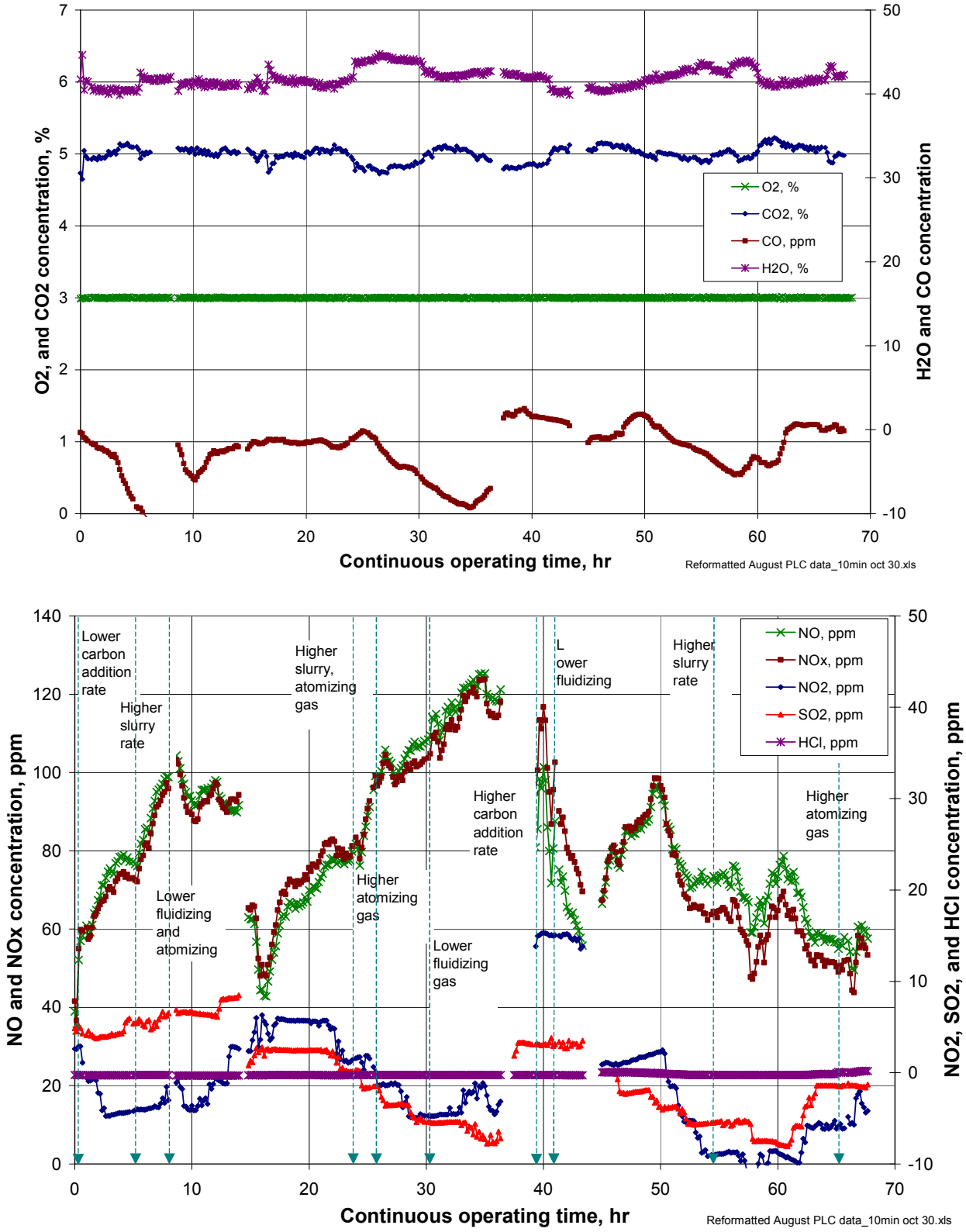

Figure 4.3-2. Wet basis off-gas composition downstream of the thermal oxidizer.

The Ametek DUV analyzer used to measure oxidizer outlet NO_x concentrations simultaneously measures and records NO, NO_2, and NO_x concentrations. The measured NO_2 concentration ranged between about –10 ppm and 15 ppm, and averaged –1 ppm. The reported NO and NO_x concentrations were essentially identical.

4.3.3 NO_X Destruction

The nitrates and nitrites in the simulant react with the reductant in the FBSR, converting the N in the nitrates to predominantly N_2, and potentially other nitrogen gas species such as NO, N_2O, HCN, and NH_3. While only NO and NO_2 are measured by the FBSR outlet CEMS, grab samples in prior steam reformer tests have indicated the presence of both HCN and NH_3 in the FBSR outlet gas. The presence of gas species such as NH_3 that, upon sorption in water form basic solutions containing such ions as NH_4^+ and OH^-, is confirmed by the pH measurements of the CEMS 1 condensate that averaged 9.2, even though the CEMS 1 condensate also contained sorbed nitrates and carbonate that would otherwise have driven the pH below 7. CEMS condensate from fully oxidized off-gas downstream of the oxidizer is typically less than 7 (averaging 3.3 for the CEMS 2 condensate) because of sorbed CO_2 (that forms carbonic acid) and trace amounts of other acid gas species.

Table 4.3-3 shows NO_x destruction based on the amount of NO_x (NO and NO_2) measured in the off-gas compared to the amount of nitrate and nitrite in the feed. NO_x destruction trends during the test series are shown in Figure 4.3-3. The calculated steam reformer NO_x destruction averaged about 92% for the test series. Average NO_x destruction for specific test conditions ranged from as low as 87% during Test Condition 9, (after the simulant slurry rate was increased to 5 kg/hr, but before the carbon reductant rate increase during Test Condition 9 impacted the carbon inventory in the bed) up to 97% (during Test Condition 12, after the carbon reductant rate was increased and time allowed for carbon inventory in the bed to increase). Higher NO_x destruction at over 98% was achieved in the first hour of test operation, but this may have been biased because of the high initial carbon inventory in the bed and the initially low off-gas NO_x readings in the first few minutes following test startup (due possibly to some sorption of NO_x in CEMS 1 carbon filter).

NO_x destruction was also determined for the entire steam reforming test system, using the NO_x measurements downstream of the thermal oxidizer. These NO_x destruction values show how a complete, integrated system performs to destroy nitrates in the feed and NO_x in the off-gas. The total system NO_x destruction ranged between 93–97% for the different test conditions, compared to a range of 87–97% (neglecting startup) for the steam reformer NO_x.

The nominal oxidizer NO_x concentration, when there was no NO_x in the FBSR off-gas prior to COT 0, was about 35 ppm (wet basis). This was thermal NO_x formed in the oxidizer. The oxidizer will tend to destroy NO_x contained in the entering gas to reach its baseline of 35 ppm. Early in the test series (Test Conditions 1 and 2), when the FBSR NO_x concentrations were still below 350 ppm (wet basis), the total system NO_x destruction was less than the FBSR NO_x destruction because of the thermal NO_x produced in the oxidizer. Starting in Test Condition 3, and continuing until Test Condition 12, the NO_x concentration in the FBSR off-gas was high enough so that, even considering the thermal NO_x formed in the oxidizer, there was a net reduction in NO_x as conditions in the oxidizer tended to drive the oxidizer outlet NO_x concentration toward the baseline level of about 35 ppm. The oxidizer outlet NO_x missions were less than the sum of the baseline oxidizer thermal NO_x emission and the FBSR NO_x emission, although the oxidizer outlet NO_x levels never were as low as 35 ppm as they were at the test start.

Table 4.3-3. NO_x destruction for the Hanford LAW test series.

Test COT, clock time, and operating condition	FBSR carbon stoichiometry, %	At the FBSR filter outlet			At the oxidizer outlet			NO_x destruction in the oxidizer, %
		NO_x MTEC, ppm wet	NO_x, ppm wet	NO_x destruction, %	NO_x MTEC, ppm wet	NO_x, ppm wet	Total NO_x destruction, %	
		---	---	---	---	AE1_CST2_NOX_WB_ADJ	---	
COT 0, 0900, 1, test start	901%	7,074	143	98.0	994	60	94	-167
COT :48, 0948, 2, lower carbon feedrate	564%	7,233	340	95.3	982	68	93	-51.6
COT 5:00, 1400, 3, higher slurry feedrate	423%	8,528	618	92.8	1,239	85	93	---
COT 8:12, 1712, 4 and 5, lower fluidizing steam	435%	9,098	703	92.3	1,390	79	94	20.2
COT 24:00, 0900, 6, higher slurry feedrate	348%	9,896	881	91.1	1,598	85	95	39.4
COT 25:30, 1030, 7, higher atomizing gas flowrate	352%	10,238	954	90.7	1,609	100	94	32.8
COT 30:04, 1504, 8, lower fluidizing steam flowrate	352%	10,802	1,283	88.1	1,676	114	93	37.8
COT 39:20, 0020, 9, higher carbon feedrate	416%	10,668	1,427	86.6	1,686	103	94	54.6
COT 41:20, 0220, 10, lower fluidizing steam flowrate	412%	10,960	808	92.6	1,757	80	95	31.4
COT 54:15, 15:15, 11, higher slurry feedrate	375%	11,682	587	95.0	1,887	58	97	32.9
COT 65:57, 0257, 12, higher atomizing N2 flowrate	375%	11,175	293	97.4	1,926	52	97	-1.5
COT 68:26, 0526, shutdown								
Test averages	412%	10,196	772	92.4	1,601	80	95	22.3

Notes:

1. The CEMS data were recorded automatically by the PLC, and automatically adjusted for zero, span error, and moisture content. All measurements were made on a dry basis.
2. The NO_x Maximum Theoretical Emission Concentration (MTEC) is the calculated concentration in the off-gas that would exist if all NO_2 and NO_3 in the feed were converted to NO_x in the off-gas, without any other NO_x formation or destruction.
3. PLC tag numbers in the column headers indicate the source of the data. No tag number indicates that the data in that column were calculated after the test, from other PLC data, and not taken directly from the PLC.
4. Total NO_x destruction at the oxidizer outlet is calculated based on the oxidizer outlet NO_x concentration compared to the calculated NO_x MTEC at that location. This conservatively includes thermal NO_x formed in the oxidizer in the NO_x destruction calculation.
5. The NO_x destruction in the oxidizer calculation is based on the difference between the FBSR NO_x destruction and the total NO_x destruction downstream of the oxidizer, and indicates when the oxidizer actually reduces the amount of NO_x in the FBSR outlet gas.

[Reformatted August PLC Data_10min oct 30.xls]NOx dest table

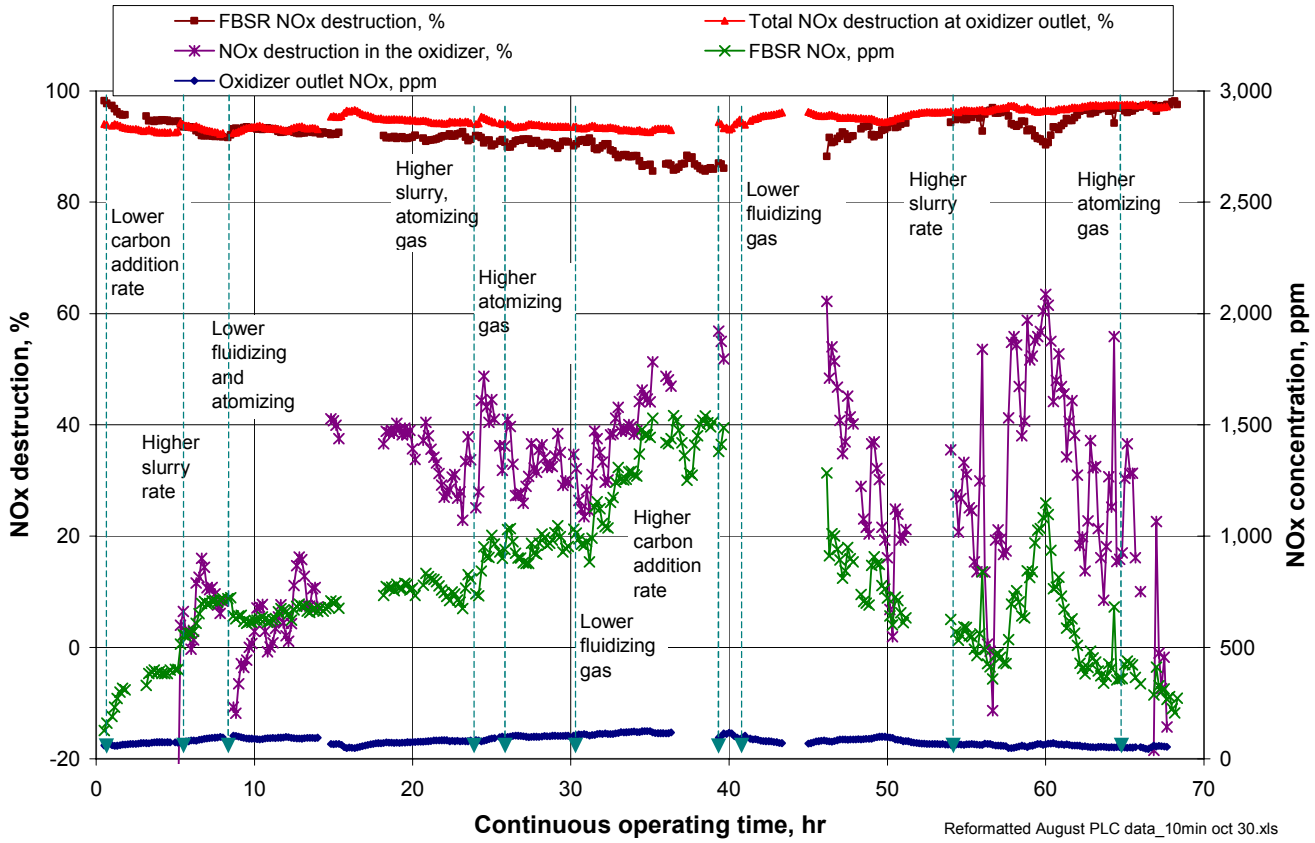

Figure 4.3-3. NO_x destruction trends for the Hanford LAW test series.

There was a net formation of NO_x in the oxidizer due to thermal NO_x formation when the FBSR outlet NO_x level was less than about 350 ppm. There was a net NO_x destruction in the oxidizer when the FBSR outlet NO_x levels exceeded about 350 ppm. The NO_x destruction by the oxidizer averaged almost 55% when the FBSR NO_x level averaged just over 1,400 ppm during Test Condition 9. The average NO_x reduction for the entire test series was 22%.

The NO_x destruction results for this test easily met the test objective of at least 80% NO_x destruction. NO_x destruction approaching 99% or higher was demonstrated under certain test conditions. The FBSR NO_x destruction is compared to the C:oxidant stoichiometry and the off-gas H_2 concentration in Figures 4.3-4 and 4.3-5. These figures show that for higher carbon stoichiometries, the H_2 concentration and NO_x destruction are higher.

Two indicators of high (>90%) NO_x destruction are:

- Whenever the C:oxidant stoichiometry exceeded 375%

Whenever the wet basis FBSR H_2 concentration exceeded 1% (dry basis H_2 concentration exceeded 2.5%)

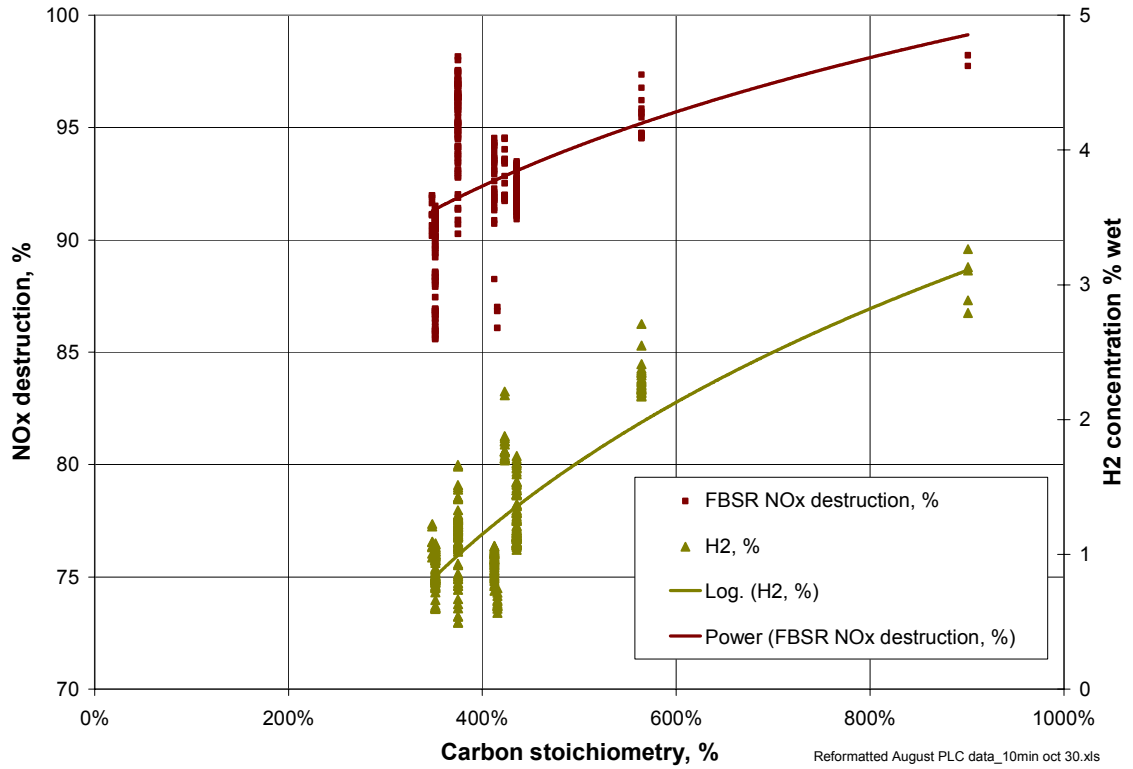

Figure 4.3-4. FBSR NO_x destruction and H_2 concentration compared to carbon stoichiometry.

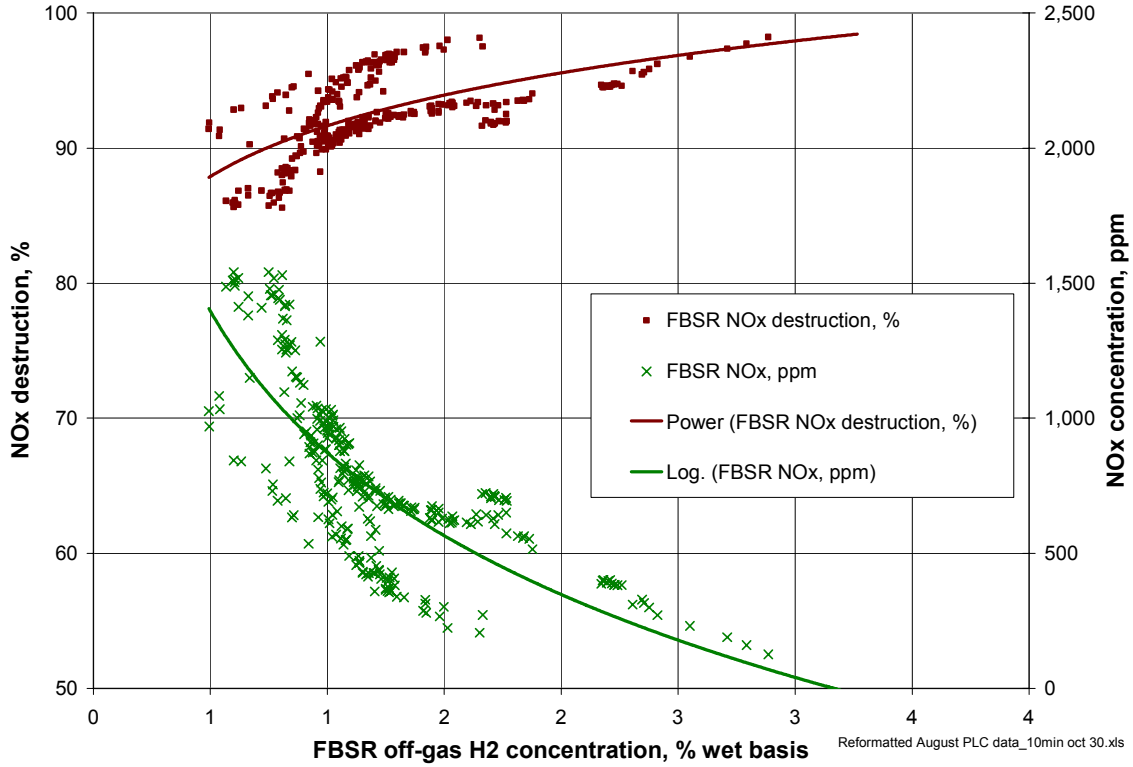

Figure 4.3-5. FBSR NO_x destruction compared to the FBSR off-gas H_2 concentration.

Either of these are valid indicators as long as the carbon inventory in the bed is at a relatively steady state. Test Condition 9 is an exception because, even though the stoichiometry based on the feed rate exceeded 375%, the FBSR H_2 concentration was less than 1% (wet basis) and the FBSR NO_x destruction was only 87%. The carbon inventory in the bed was allowed to become depleted for some hours prior to Test Condition 9.

A dip in the FBSR NO_x destruction occurred between about COT 57 and COT 62. The NO_x destruction decreased because the FBSR outlet NO_x levels increased; simultaneously, the H_2 level decreased below 1% (wet). These changes occurred because one of the carbon feeder air lock valves stuck open during this time. An influx of air entered the bed every time the other valve opened, reacting with and decreasing reduced gas species concentrations, which impaired NO_x destruction. NO_x destruction returned to higher levels, as NO_x levels dropped and H_2 levels rose, when the air inleakage was controlled by increasing the FBSR operating pressure.

4.3.4 Off-gas Control Components Performance

Some FBSR operating parameters, and key off-gas system operating parameters, are shown in Table 4.3-4. The cyclone differential pressure averaged only 0.5 inches water, which is much lower than a nominal cyclone differential pressure of about 5 inches for good cyclonic particle size separation. However, the bed product, cyclone catch, and filter catch particle size data suggests that the cyclone did, in fact, remove elutriated fines with reasonable efficiency. The particle size distributions of the recycled fines were, on average, about 0.035 mm MMPD, about 8 times smaller than the COT 55.5 bed product particle size of 0.292 mm MMPD. The filter fines, at 0.011 mm MMPD, were about 3 times smaller in diameter than the cyclone fines. The average cyclone efficiency was about 80%, at a measured cyclone recycle rate of about 3.4 kg/hr and an average filter fines capture rate of about 0.94 kg/hr.

The heated, sintered metal filter bank performed very well to capture elutriated fines that passed through the cyclone. No fines were detected in downstream equipment such as the oxidizer, where fines might sediment out of the off-gas, the carbon bed, where fines might be trapped in interstitial spaces in the bed, or in the CEMS filters.

The oxidizer is physically configured with three different stages, to enable operation in a staged non-selective, non-catalytic NO_x reduction (NSNCR) mode. The three-stage system was operated in a fully oxidizing mode, since NO_x was efficiently destroyed in the FBSR. Auxiliary fuel (natural gas) and air were added through a burner in stage 1. If other reduced gas species, such as H_2S, are formed in the FBSR, then those gas species are also oxidized in this stage (H_2S to SO_2, for example). This stage was operated in an oxidizing (rather than NO_x-reducing) mode, with approximately 105% stoichiometric air. Reduced gas species H_2, THC, CH_4, and CO were fully oxidized in this stage at an operating temperature of 1,000°C. The hot stage 1 off-gas passed through stage 2 (designed for NSNCR operation to quench the stage 1 gas to a temperature below 800°C) and through stage 3 (designed for NSNCR operation as an oxidizer to fully oxidize the NSNCR off-gas). No quench water was added in stage 2, and only a small amount of air (to cool the air nozzles) was added in stage 3. The O_2 content in the stage 3 off-gas averaged 3.0% (wet basis).

The stage 1 temperature was controlled at 1,000°C, and no temperature control was required in stages 2 and 3. The stage 3 off-gas averaged 706°C. The stage 1 residence time was 3.0 seconds, conservatively high for good engineering practice, to efficiently oxidize organic materials. The total residence time in stages 1-3 was 5.8 seconds. The low CO content of the oxidizer outlet off-gas, averaging –2.5 ppm (wet basis), and ranging up to 6 ppm (wet basis) based on the accuracy of the CO analyzer at such low CO concentrations, confirms highly efficient oxidation of organic compounds. The

calculated combustion efficiency of the oxidizer was 99.99% using a CO concentration of 6 ppm and an average CO_2 concentration of 4.99% (wet basis).

The partial quench used water spray evaporation to cool the oxidizer off-gas to a temperature cool enough for the downstream carbon bed. A mist eliminator downstream of the partial quench was designed to capture any residual water mist in the event that an upset of the partial quench resulted in excessive off-gas cooling and un-evaporated water droplets in the off-gas. The partial quench operated within its control range for the duration of the test, and cooled the off-gas to an average temperature of 130^{o}C. An electric reheater was used to slightly reheat the off-gas to an average of 138^{o}C so that, after some minimal heat losses, the carbon bed operating temperature averaged 119^{o}C.

The middle section of the carbon bed contained 4x8 mesh Barneby Sutcliffe 208C carbon to capture any trace quantities of acid gases in the off-gas. Samples of the carbon were analyzed for Cl, I, F, and SO_4 content. No Cl, F, I, or SO_4 was detected in the carbon bed samples, confirming the low HCl and SO_2 CEMS measurements, and the low CEMS condensate measurements (See Table 4.4-2).

Table 4.3-4. Key operating parameters for the FBSR and off-gas system.

Test COT, clock time, and operating condition	Feed slurry rate, kg/hr SR1_F1A_VAL	Total N_2 gas input flowrate, kg/hr V1_F1_VAL	Super-heater H_2 steam outlet temp, C H2_T_VAL	Cyclone diff pressure, inches water C1_PD_VAL	Cyclone outlet gas temp, C C1_T3_VAL	Filter diff pressure, inches water F1_PD_VAL	Filter outlet gas temp, C F1_T2_VAL	FBSR filter outlet H_2O flowrate, kg/hr H2O_BEFORE_OXI_KGH	Calculated FBSR filter outlet gas flowrate, kg/hr TOTAL_KGH_BEFORE_OXI	FBSR filter outlet gas flowrate, scfm ---	Natural gas flow to oxidizer, kg/hr B1_F1_VAL	Air flowrate to oxidizer stage 1, kg/hr B1_F2_VAL	Air flow to oxidizer stage 3, kg/hr B1_F5_VAL	N_2 purge flow to oxidizer stage 2, kg/hr B1_F7_VAL
COT 0, 0900, 1, test start	2.9	6.73	740	0.0	450	7.3	448	7.53	14.9	9.7	2.72	59.8	6.00	0.28
COT :48, 0948, 2, lower carbon feedrate	3.0	6.49	730	0.4	484	11.9	420	7.01	14.2	9.1	2.78	61.2	6.64	0.30
COT 5:00, 1400, 3, higher slurry feedrate	3.9	6.47	728	0.7	502	11.8	383	8.19	15.4	10.0	2.81	61.7	6.75	0.31
COT 8:12, 1712, 4 and 5, lower fluidizing steam	4.0	6.20	728	0.6	492	8.5	362	7.97	14.9	9.6	2.70	59.4	5.47	0.28
COT 24:00, 0900, 6, higher slurry feedrate	4.8	6.35	728	0.6	493	7.1	361	9.01	16.1	10.5	2.75	60.5	5.61	0.28
COT 25:30, 1030, 7, higher atomizing gas flowrate	5.0	6.39	723	0.6	515	7.8	355	9.23	16.3	10.7	2.79	61.4	6.07	0.30
COT 30:04, 1504, 8, lower fluidizing steam flowrate	5.0	6.38	686	0.5	496	7.2	355	8.56	15.6	10.1	2.74	60.4	5.53	0.29
COT 39:20, 0020, 9, higher carbon feedrate	5.0	6.60	693	0.5	495	7.5	357	8.60	15.9	10.2	2.76	60.8	5.31	0.27
COT 41:20, 0220, 10, lower fluidizing steam flowrate	5.0	6.57	613	0.5	480	7.1	363	8.22	15.5	10.0	2.70	59.4	5.24	0.29
COT 54:15, 15:15, 11, higher slurry feedrate	5.5	6.33	564	0.4	475	7.4	372	8.72	15.8	10.2	2.69	59.1	5.64	0.30
COT 65:57, 0257, 12, higher atomizing N2 flowrate	5.5	7.07	565	0.5	470	7.1	369	8.79	16.6	10.8	2.68	58.9	5.52	0.28
COT 68:26, 0526, shutdown														
Test averages	4.7	6.41	665	0.5	488	8.1	368	8.33	15.5	10.0	2.72	59.9	5.64	0.29

[Reformatted August PLC Data_10min oct 30.xls]flowrate table

Table 4.3-4. Key operating parameters for the FBSR and off-gas system (continued).

Test COT, clock time, and operating condition	Oxidizer stage 1 temp, C B1_T1_VAL	Oxidizer stage 2 temp, C B1_T2_VAL	Oxidizer stage 3 temp, C B1_T3_VAL	Partial quench water flowrate, kg/hr PQ1_F1_VAL	Partial quench outlet gas temp, C PQ1_T1_VAL	Reheater outlet gas pressure, psia AJ1_P2_VAL	Reheater outlet gas temp, C AJ1_T1_VAL	Total input gas flowrate, kg/hr TOTAL_KGH_AFTER_PQ	Total input gas flowrate, scfm SCFM_AFTER_PQ	Measured total off-gas flowrate, k/hr AJ1_F1_VAL	Measured total off-gas flowrate, scfm AJ1_F1_SCFM	Ratio, measured/ calculated total off-gas rates AJ1_F1_OGMR_CALC	Carbon bed diff pressure, inches water GAC1_PD_VAL	Carbon bed temp, C GAC1_T_VAL
COT 0, 0900, 1, test start	1,000	848	734	17.4	130	10.8	138	101	58.0	112	64.2	1.11	2	117
COT :48, 0948, 2, lower carbon feedrate	1,000	855	745	16.4	130	10.6	138	101	57.7	117	66.7	1.16	2	119
COT 5:00, 1400, 3, higher slurry feedrate	1,000	857	747	17.0	130	10.7	138	104	59.4	120	68.6	1.16	2	119
COT 8:12, 1712, 4 and 5, lower fluidizing steam	1,000	848	731	15.4	130	11.2	138	98	56.0	110	62.8	1.12	2	117
COT 24:00, 0900, 6, higher slurry feedrate	1,000	844	719	17.5	130	11.5	138	103	59.2	113	64.9	1.10	2	118
COT 25:30, 1030, 7, higher atomizing gas flowrate	1,000	842	709	18.9	130	11.5	138	106	61.2	117	67.9	1.11	2	120
COT 30:04, 1504, 8, lower fluidizing steam flowrate	1,000	832	684	16.6	130	11.5	138	101	58.0	113	65.1	1.12	2	120
COT 39:20, 0020, 9, higher carbon feedrate	1,000	830	679	16.3	130	11.6	137	101	58.1	113	64.7	1.12	2	118
COT 41:20, 0220, 10, lower fluidizing steam flowrate	1,000	832	691	15.2	130	11.6	138	98	56.1	109	62.1	1.11	2	118
COT 54:15, 15:15, 11, higher slurry feedrate	1,000	830	683	16.0	130	11.7	139	99	57.0	111	63.6	1.11	2	120
COT 65:57, 0257, 12, higher atomizing N2 flowrate	1,000	832	692	16.2	130	11.9	138	100	57.5	109	62.4	1.09	2	118
COT 68:26, 0526, shutdown														
Test averages	1,000	839	706	16.1	130	11.4	138	100	57.3	112	64.1	1.12	2	119

1. PLC tag numbers indicate the source of the data. No tag number indicates that the datawas calculated after the test, from other PLC data, and not taken directly from the PLC.
2. Standard temperature is 68°F, standard pressure is 1 atmosphere. N_2 was used to atomize the quench water.
3. The superficial volume, velocity, and residence time is calculated from the bed volume assuming 100% void space.
4. Residence time calculations were made using the average oxidizer outlet offgas flowrate less the average partial quench water flowrate, which is 51.4 scfm.
5. The average residence time in Stage 1 was 3.0 seconds. The volume of Stage 1 is (14.8 ft3) was based on a inside diameter of 21 inches and a length of 74 inches, not including the conical reducing section at the inlet of the quench section.
6. The average residence time in Stage 2 was 0.3 seconds. The volume of the quench stage (1.1 ft3) was based on the volume of the frustum (8 inches long), the throat length (10 inches), and the throat inside diameter (8 inches).
7. The avg residence time in Stage 2 was 2.5 seconds. The volume of the oxidizing stage (9.22 ft3) was based on an inside diameter of 21 inches and a length of 46 inches.

[Reformatted August PLC Data_10min oct 30.xls]flowrate table

4.4 Process Mass Balance & Elemental Partitioning

The feed slurry, when sprayed into the bed, dries and undergoes evaporation, thermal decomposition, and other reactions that denitrate and solidify the solid forming feed constituents. The cumulative masses of slurry feed, carbon additive, and calculated solid product from the slurry are shown in Figure 4.4-1. These input masses are very consistent and controlled, with slight changes in the slope of the cumulative feed when feed rate changes were made during the test. The total output masses are shown in Figure 4.4-2.

4.4.1 Overall Mass Balance and Product Distribution

The total input solid masses were the starting bed media, calcine from the SBW feed, and the carbon reductant. Total output solid masses were the bed product, the mass of the cyclone recycle material that was sampled (and not returned to the bed), and the filter fines catch. The output bed product was the sum of the mass of bed removed at the end of the test and the mass of bed material removed at discrete times during the test from either the bed drain port or the bed sample port. Bed media was removed during the test to control the bed height as calcined feed added to the bed mass, to obtain samples for analyses, to periodically inspect the bed media for appearance, and agglomerations, and to provide a pathway for such agglomerations, if they occurred, to be removed from the bed.

The cumulative solid product feed was zero at the test start. The cumulative total outputs were slightly above zero, because (a) part of the bed mass (1.9 kg) was drained from the bed just before the test start in order maintain the bed height in the right range as carbon reductant was added, and (b) 0.4 kg of starting bed media had elutriated to the filter and was removed. But the total input solid mass, that included the starting bed, was already 20 kg. At the end of the test, cumulative total output, including the final bed mass after the test, reached 148 kg, which, allowing for measurement errors, was essentially the same as the total input solid mass of 146 kg.

The solid product distribution and mass balance closure are shown in Table 4.1-1. The solid mass balance closure is quite good for this test, indicating a total measurement error or process losses of about 2 wt% of the input solid masses. This amount of error is within reasonable error bounds for the various measurements used to provide data for the mass balance calculations – the slurry feed rate, the amount of calcine product in the slurry, and the recovery and measurement of product bed, cyclone, and filter masses.

The distribution of FBSR product to the bed product and the filter fines was very close to 50:50 regardless of whether the amount of unreacted carbon was included in the calculations. About 50% of the FBSR product stayed in the bed, and about 50% of the product formed fines sufficiently small to pass through the cyclone into the heated filter. The product distribution between the bed and the filter fines varied within a range of about 25-60% bed product and 40-75% filter fines distribution during the test based on the FBSR operating parameters. For the first 8 hours of the test, during test conditions 1-3, the product distribution was about 25% bed and 75% filter fines, because of the relatively high fluidizing gas and atomizing gas rates. When both the fluidizing gas and atomizing gas flow rates were reduced in test condition 4, the product distribution changed to about 60% bed product and 40% filter fines. When the atomizing gas rate increased again for the higher simulant feed rate of test condition 7, the product distribution again changed to about 45:55 bed product and filter fines. When the fluidizing gas rate was lowered for test condition 8, the product distribution changed to about 50:50. When the fluidizing gas rate was again lowered for test condition 10, the product distribution also changed to about 60% bed product and 40% filter fines. Decreasing gas flows decreases the amount of "jet" grinding that occurs as the high velocity gases accelerate bed particles into each other, increases the initial feed droplet size, and increases the efficiency of the freeboard section with regard to disengaging entrained fines.

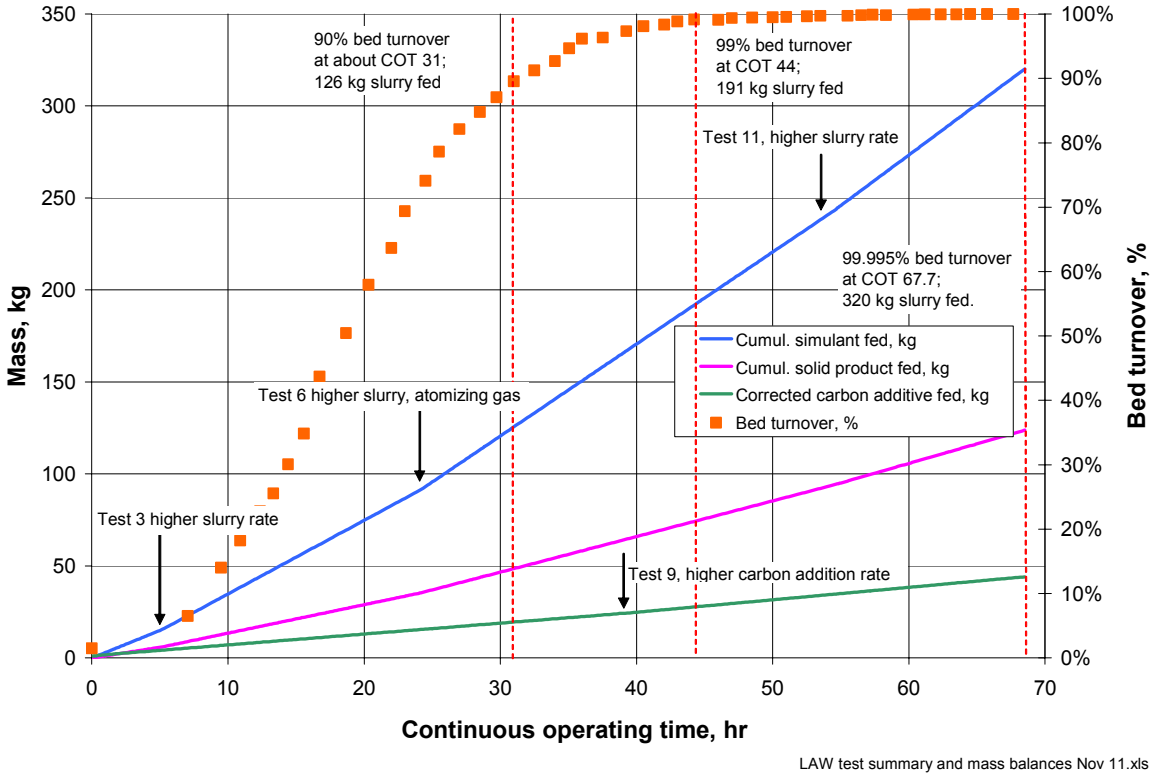

Figure 4.4-1. Cumulative input feed masses.

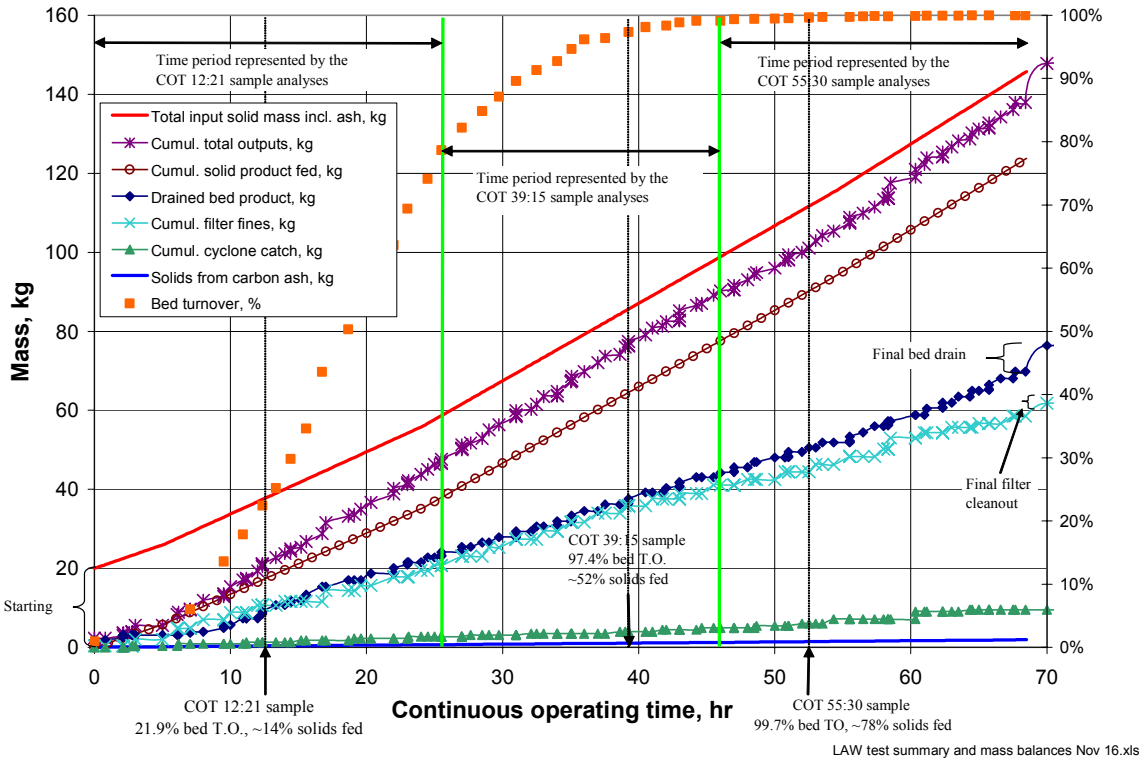

Figure 4.4-2. Cumulative product masses.

Table 4.4-1. Solid product distribution and mass balance closure for the Hanford LAW FBSR test.

FBSR input masses			FBSR output masses	
Input streams	Wt frac. or wt%	Input mass, kg	**Output streams**	Output mass, kg
Starting alumina bed, kg:		17.7	Cumulative drained bed, kg:	74.5
Total feed slurry input from PLC, kg:		320	Cumulative cyclone catch, kg:	9.6
kg solid product/kg slurry:	0.387		Cumul. filter fines, kg:	61.4
Total calcined product:		123.8	Total output solids, kg:	145.4
Mass of carbon added to the carbon feed hopper, kg:		43.9	Drained bed excluding starting bed and unreacted carbon, kg	53.9
Ash content of carbon additive, wt % as received:	5.0%			
Percent of carbon additive that was gasified (calculated from total carbon input and residual unreacted carbon):	88.7%		Cyclone catch excluding unreacted carbon, kg:	9.3
Total solids (ash) from carbon additive (calculated from carbon ash content, total carbon additive, and % gasified carbon), kg:		1.9	Mass of filter fines not including organic carbon, kg:	59.5

Total unreacted carbon determined from product sample analyses			Total output solids excluding starting bed and unreacted carbon, kg:	122.7
Average unreacted carbon in bed product:	3.3%	2.5		
Average unreacted carbon in cyclone catch:	2.4%	0.2		
Average unreacted carbon in filter fines:	3.7%	2.3		
Total unreacted carbon:		5.0		
Total input solids, kg:		148.4		
Total input solids excl. starting bed and unreacted carbon, kg:		125.7		

Solids mass balance closure		
Solid mass balance closure, total output mass/total input mass:	98%	

Solid product distribution excluding starting bed		
Percent to bed product & cyclone recycle (incl. unreacted C)	52%	
Percent to filter fines (incl. unreacted C)	48%	

Carbon feed rate check		
Mass of carbon added to the carbon feed hopper, kg:		43.9
Cumulative carbon fed based on PLC, kg:		51.9
Accuracy of cumulative carbon added from PLC (feeder) compared to cumulative gravimetric carbon input, % error:	18.2%	

[LAW test summary and mass balances Nov 16.xls]product mass balance table

The product to fines ratio average was about 1 to 1 by mass, well below the desired ratio of 3.5 to 1 noted in the test objectives. No emphasis was placed on process parametric or configuration changes to improve the product to fines ratio other than recycling the cyclone catch to the bed and keeping the overall superficial gas velocity as low as could be reasonably achieved. Improved cyclone efficiency could reduce the quantity of fines that escape recycle to the bed, but more extensive changes in the process (mechanical or chemical) will likely be necessary to achieve the desired ratio. This may include changing the mechanism and location of fines re-introduction or improvements to the mineralizing chemistry and kinetics to improve cohesion of the product particles.

Table 4.4-1 shows two mass flow rates for the carbon reductant additive. The mass of carbon added to the carbon feed hopper is the difference between the masses of total additions and the mass recovered from the hopper at the end of the run, and represents an accurate measure of the total carbon additive to the process. The cumulative carbon feed based on the PLC is less accurate because it is determined by the sum of small differences between relatively large numbers. Consequently, the carbon

additive flow rate computed by the PLC is about 18% higher than indicated by the actual net amount of carbon added to the feed hopper.

4.4.2 Elemental Mass Balance and Distribution

A mass balance and distribution of key feed elements was accomplished by numerically integrating the bed turnover estimate to account for the fractions of starting bed and mineralized product in each of three samples taken during the run (Table 4.4-2). The calculated compositions of the mineral phases were assigned to the products harvested during the three periods represented by the samples as shown in Figure 4.4-2. The masses for Cs, Mg, Na, Re, and Cl, which were not detected in the first bed sample (COT 12:21), were assigned the mass-weighted average composition of the mineralized product as measured in the latter two samples (COT 39:15 and 55:30) and pro-rated according to the mass fraction of mineralized product in the sample. The result of the computations is shown in Table 4.4-3. Estimated values are shown as gray boxes for clarity.

Table 4.4-2. FBSR effluent stream elemental compositions.

	Sample number	Sample date	Sample description	Units	Al	Ca	Cr	Cs	Fe	K	Mg	Na	P	Re	S	Si	Ti	Cl	F	I	NO_2	NO_3	PO_4	SO_4
Input	na		Hanford LAW simulant - Target Composition	g/l	1.72		0.541	1.0E-5		0.485		115	1.52	0.09608	2.89			1.55	0.60	0.0017	19.5	156	4.67	8.65
	1081	2-Aug	Hanford LAW simulant - Measured Composition	g/L	1.80	0.025	0.500	1.4E-5		1.95	0.008	127	1.48	0.0496	2.89	0.041		1.57	1.03	0.0021	19.5	159	4.51	8.34
	na		OptiKast kaolin clay	Wt%	22.70	0.02			0.26	0.06	0.01	0.02	0.02			24.65	1.06							
	na		Berger Bros. P6 carbon ash	Wt%	0.16	48.24			0.30	2.75	1.48	0.14	0.46		0.27	0.70	0.01				0.27			
	1100	2-Aug	Starting bed COT 0	Wt%	53.0	0.1	<0.01		0.1	<0.01	<0.01	<0.01	<0.01		<0.01	0.4	<0.01							
Products	1101	2-Aug	Bed product COT 12:21	Wt%	48.6	0.219	0.021		0.057	0.095	<0.01	<0.01	0.054		0.044	3.07	0.122							
	1103	4-Aug	Bed product COT 39:15 (last before feedrate increase)	Wt%	17.4	1.27	0.091	1.4E-4	0.183	0.270	0.033	15.3	0.208	5.6E-3	0.289	16.7	0.741	0.175	<0.1	<1E-05	<1E-05	<0.01		
	1104	5-Aug	Bed product COT 55:30 (1 hr after rate increase)	Wt%	17.2	1.65	0.080	1.1E-4	0.186	0.253	0.040	15.0	0.196	4.1E-3	0.245	16.7	0.709	0.130	<0.1	<1E-05	<1E-05	<0.01		
	1106	5-Aug	Final bed	Wt%	18.7	0.66	0.101	1.6E-3	0.239	0.495	0.031	16.3	0.217	8.5E-3	0.243	19.2	0.759	0.319	<0.1	<1E-05	<1E-05	0.039		
	1107	5-Aug	Final agglomeration	Wt%	18.1	0.55	0.097	5.6E-4	0.195	0.499	0.032	16.2	0.213	7.1E-3	0.246	20.7	0.768	0.310	<0.1	<1E-05	<1E-05	<0.01		
	1109	2-Aug	Cyclone fines COT 11	Wt%	19.0	1.15	0.077	5.8E-4	0.195	0.373	0.029	16.1	0.164	4.9E-3	0.123	20.1	0.748	0.132	<0.1	<1E-05	<1E-05	<0.01		
	1112	5-Aug	Cyclone fines COT 64:20	Wt%	18.7	1.21	0.076	7.6E-4	0.217	0.231	0.031	16.6	0.175	4.4E-3	0.174	20.1	0.750	0.088	<0.1	<1E-05	<1E-05	<0.01		
	1113	2-Aug	Filter fines COT 10	Wt%	18.2	1.57	0.078	1.3E-3	0.161	0.461	0.051	16.2	0.200	8.2E-3	0.306	20.0	0.743	0.160	<0.1	<1E-05	<1E-05	0.036		
	1115	4-Aug	Filter fines COT 39	Wt%	18.3	1.30	0.064	2.4E-3	0.171	0.349	0.036	16.2	0.189	3.5E-3	0.276	20.5	0.760	0.122	<0.1	<1E-05	<1E-05	0.037		
	1125	4-Aug	Filter fines COT 55:30	Wt%	18.4	1.27	0.069	1.7E-3	0.173	0.255	0.039	16.5	0.196	4.0E-3	0.383	20.1	0.763	0.101	<0.1	<1E-05	<1E-05	<0.01		
Effluents	1089	3-Aug	CEMS 1 condensate COT 29:10	mg/L				2.5E-4						<1E-4				<10	<10		<10	52		255
	1092	4-Aug	CEMS 1 condensate COT 51:15	mg/L	0.067	0.019	<0.005	0.003	0.067	0.181	<0.001	<0.008		5.0E-4		0.077		<10	<10	0.0082	<10	<10		130
	1094	5-Aug	CEMS 1 condensate post-test	mg/L				1.3E-4						<1E-4				<10	<10		<10	126		400
	1090	3-Aug	CEMS 2 condensate COT 29:10	mg/L				<1E-4						<1E-4				<10	<10		160	<10		29.2
	1093	4-Aug	CEMS 2 condensate COT 51:15	mg/L	0.073	0.009	<0.005	<1E-4	0.025	0.176	<0.001	<0.008		<1E-4		0.020		<10	<10	3.1E-4	<10	<10		10.6
	1095	5-Aug	CEMS 2 condensate post-test	mg/L				1.5E-4						1.2E-4				<10	<10			<10		45.7
GAC	1097	9-Aug	Carbon bed top layer	Wt%														<0.1	<0.1			<0.1	<0.1	1.32
	1098	9-Aug	Carbon bed middle	Wt%														<0.1	<0.1			<0.1	<0.1	0.13
	1099	9-Aug	Carbon bed bottom layer	Wt%														<0.1	<0.1			<0.1	<0.1	1.09

[Compiled LAW Analytical Data Tables - Nov 8.xls]Oxides, Elements, and Anions

Table 4.4-3. Elemental mass balance

Material description	Qty	Al (kg)	Ca (kg)	Cr (kg)	Cs (kg)	Fe (kg)	K (kg)	Mg (kg)	Na (kg)	P (kg)
Hanford LAW simulant	179 L	0.32	0.004	0.089	2.5E-6		0.348	0.001	22.7	0.265
OptiKasT kaolin clay	114 kg	25.78	0.024			0.294	0.071	0.014	0.03	0.025
Carbon ash	1.95 kg	0.00	0.939			0.006	0.053	0.029	0.00	0.009
Starting alumina bed	18.1 kg	9.60	0.010			0.012				
Total Input		35.7	0.978	0.089	2.5E-6	0.312	0.472	0.044	22.7	0.298
Harvested bed (COT 0 - COT 25:50)	22.2 kg	7.83	0.160	0.019	1.9E-5	0.007	0.085	0.006	2.32	0.049
Harvested bed (COT 25:51 - COT 46:00)	20.1 kg	3.23	0.262	0.019	3.0E-5	0.038	0.055	0.007	3.20	0.043
Harvested bed (COT 46:01 - COT 68:25)	32.2 kg	5.53	0.532	0.026	3.6E-5	0.060	0.081	0.013	4.81	0.063
Cylcone samples	9.56 kg	1.80	0.113	0.007	6.4E-5	0.020	0.029	0.003	1.56	0.016
Filter catch (COT 0 - COT 25:50)	20.3 kg	3.69	0.318	0.016	2.7E-4	0.033	0.094	0.010	3.28	0.041
Filter catch (COT 25:51 - COT 46:00)	20.3 kg	3.71	0.263	0.013	5.0E-4	0.035	0.071	0.007	3.28	0.038
Filter catch (COT 46:01 - COT 68:25)	20.8 kg	3.81	0.263	0.014	3.6E-4	0.036	0.053	0.008	3.43	0.041
Total Output		29.6	1.91	0.114	1.3E-3	0.228	0.468	0.054	21.9	0.291
Recovery		83%	195%	127%	50671%	73%	99%	124%	96%	97%

Material description	Qty	Re (kg)	S (kg)	Si (kg)	Ti (kg)	Cl (kg)	F (kg)	I (kg)	NO_2 (kg)	NO_3 (kg)
Hanford LAW simulant	179 L	8.9E-3	0.516	0.007		0.281	0.183	3.7E-4	3.49	28.4
OptiKasT kaolin clay	114 kg			28.0	1.20					
Carbon ash	1.95 kg		5.2E-4	0.0014	1.8E-5				5.2E-4	
Starting alumina bed	18.1 kg			0.0067						
Total Input		8.9E-3	0.517	28.0	1.20	0.281	0.183	3.7E-4	3.49	28.4
Harvested bed (COT 0 - COT 25:50)	22.2 kg	7.3E-4	0.040	2.52	0.110	0.023				
Harvested bed (COT 25:51 - COT 46:00)	20.1 kg	1.2E-3	0.060	3.45	0.153	0.037				
Harvested bed (COT 46:01 - COT 68:25)	32.2 kg	1.3E-3	0.079	5.36	0.228	0.042				
Cylcone samples	9.56 kg	4.4E-4	0.014	1.92	0.072	0.010				
Filter catch (COT 0 - COT 25:50)	20.3 kg	1.7E-3	0.062	4.07	0.151	0.033				0.007
Filter catch (COT 25:51 - COT 46:00)	20.3 kg	7.1E-4	0.056	4.17	0.154	0.025				0.007
Filter catch (COT 46:01 - COT 68:25)	20.8 kg	8.2E-4	0.079	4.17	0.158	0.021				
Total Output		6.9E-3	0.390	25.7	1.03	0.190	ND	ND	ND	0.015
Recovery		77%	76%	92%	85%	68%	0%	0%	0%	0.05%

[LAW test summary and mass balances Nov 16.xls]Chemical mass balance table

The quantity of Cs recovered in the product is not consistent with what was known to have been added. Possible sources of additional Cs include residues in the reactor from previous steam reforming campaigns and "tramp" contamination of the simulant stock chemicals and additives. It is expected that reactor residues would have been manifested as inconsistent sample results. Whereas the sample results do not appear to vary widely from each other, the presence of unanalyzed tramp Cs in the carbon and kaolin clay is suspected.

Mass balance closure for the major constituents is excellent for sodium and silicon and good for aluminum. Mass balance closure for the minor elements seems acceptable considering their low abundance and analytical uncertainties.

About 76% of the total input sulfur was accounted for in the solid products. SO_2 was not detected in the FBSR off-gas downstream of the oxidizer. While other gaseous S species such as COS or CS_2 might have existed upstream of the oxidizer, these would probably have been oxidized to SO_x in the oxidizer. If the maximum detection limit for SO_2 was 6 ppm (like the HCL measurement), then the maximum amount of S in SO_2 would have been 12% of the input S to the FBSR, indicating that less than 12% of the input S is accounted for by the SO_2 CEM measurements. Some of the SO_2, if present in the off-gas, could have been captured as sulfate in the CEMS 2 condensate, and not measured by the SO_2 CEM. The CEMS 2 condensate was analyzed for sulfate to determine if, and how much, of SO_2 in the off-gas was collected in the CEMS condensate. A small amount of SO_4 was detected in the CEMS 2 condensate, corresponding to 4.3% of the input S. Using the detected SO_4 in the CEMS condensate, and

the maximum SO_2 detectable by the SO_2 CEM, between 4.3% and 16% of the input S could have partitioned to the off-gas. Including the 16% maximum amount of S that could have partitioned to the off-gas, the combined S mass balance closure is 92%. Most of the S in the simulant was retained in either the bed product or fines.

About 68% of the total input Cl was accounted for in the solid products. HCl was not detected in the FBSR off-gas. Considering potential instrument error, the maximum HCl level that could have existed in the sample gas without detection was 6 ppm. The range of 0-6 ppm HCl in the off-gas measured by the HCl CEM represents 0-24% of the input Cl to the FBSR, indicating that less than 24% of the input Cl is accounted for by the off-gas CEM measurements. Some HCl, if present in the off-gas, could have been captured in the CEMS 2 condensate, and not measured by the HCl CEM. The CEMS condensate was analyzed for Cl to determine if, and how much, of Cl in the off-gas was collected in the CEMS condensate. No Cl was detected in the CEMS 2 condensate, at a detection limit of 10 mg/L. The maximum amount of Cl that might have been captured in the CEMS 2 condensate prior to the HCl CEM measurement was 8% of the input Cl using this detection limit.

The carbon bed was analyzed for Cl, and no Cl was detected at a detection limit of 0.1 wt%. At this detection limit, the maximum amount of Cl that could have been captured in the carbon bed was 21% of the input Cl, based on the mass of just the top layer of sampled carbon. The combined results of the carbon bed, CEMS, and CEMS condensate analyses indicate that the maximum partitioning of Cl to the off-gas rather than to the bed product or fines was less than 32% of the total input Cl. The actual amount of Cl that evolved to the off-gas was probably considerably less than 32% of the input Cl. Including the 32% maximum amount of S that could have partitioned to the off-gas, the combined C mass balance closure is 100%. Most of the Cl in the simulant was retained in either the bed product or fines.

No F or I were detected in the solid products. The F detection limit was 0.1 wt%, and the I detection limit was 0.1 mg/kg (0.1 ppm by weight). The maximum amount of F that could be present in the solid products, based on the detection limit, is 0.15 kg, 84% of the input F amount. The maximum amount of I that could be present in the solid products, based on the detection limit, is 1.5E-5 kg, only 4% of the input I amount. The CEMS could not detect either F or I species. However, if HF or HI were present in the off-gas, at least some of these species would have been captured in the CEMS condensate. No F was found in the CEMS condensate, at a detection limit of 10 mg/L. A small amount of I (0.00034 mg/L average) was detected in the CEMS condensate. No F was detected in the carbon bed samples. The carbon bed samples were not analyzed for I.

Using the detection limit of 10 mg/L for F in the CEMS 2 condensate, the maximum F in the off-gas (as HF) would have been 13% of the input F. Using the average detected amount of I in the CEMS 2 condensate, an average of 0.2% of the input I partitioned to the off-gas.

The combined solid product and off-gas analyses suggest that although no F was detected in the solid products, most of the F in the simulant still partitioned to the solid product. Up to 84% of the input F could have partitioned to the solid products to just reach the solid product analytical detection limit. The iodine mass balance closure results are inconclusive. The I detection limit for the solid products suggests that not more than 4% of the input I partitioned to the solids, but the off-gas analyses suggest that not more than 0.2% of the input I partitioned to the off-gas.

Table 4.4-4 shows the distribution of key elements between the bed product and the filter fines, including an overall average concentration in the product and fines. Note that the fines to product ratio for the powder masses includes residual carbon and starting bed in the computation and does not reflect the mass partitioning of the mineralized LAW alone. The computation of the quantities of Re, Cs, Na, and Cl have been adjusted by estimates of the elemental concentrations in the COT 12:21 bed sample as

discussed above. The fines-to-product ratio of the mean concentrations (wt%) for each element gives an indication of how the elements partitioned. When this ratio is >1, proportionally more of the element was found in the filter fines fraction. Ratios near 1 indicate that the elements partitioned equally, and ratios <1 would indicate that the element was found preferentially in the bed product.

The data indicate that aluminum and chromium partitioned somewhat preferentially to the bed product; calcium, phosphorous, and chlorine distributed evenly on a weight percent basis. Rhenium, sodium, and potassium appear to partition somewhat to the fines, but not as significantly as do silicon and sulfur. Cesium clearly partitions preferentially to the filter fines.

Table 4.4-4. Key element partitioning.

	Powder		Re			Cs			Re/Cs
	Mass	%Mass	Mass	%Mass	Conc.	Mass	%Mass	Conc.	w/w
Bed + cyclone product	84.1 kg	58%	3.7E-3 kg	54%	0.004%	1.5E-4 kg	12%	0.0002%	24.6
Filter fines	61.4 kg	42%	3.2E-3 kg	46%	0.005%	1.1E-3 kg	88%	0.0018%	2.8
Fines-Product ratio	0.73	---	0.87	---	1.2	7.5	---	10.3	---

	Al			Na			Si		
	Mass	%Mass	Conc.	Mass	%Mass	Conc.	Mass	%Mass	Conc.
Bed + cyclone product	18.4 kg	62%	21.9%	11.9 kg	54%	14.2%	13.2 kg	52%	15.8%
Filter fines	11.2 kg	38%	18.3%	10.0 kg	46%	16.3%	12.4 kg	48%	20.2%
Fines-Product ratio	0.61	---	0.83	0.84	---	1.1	0.94	---	1.3

	Ca			Cl			Cr		
	Mass	%Mass	Conc.	Mass	%Mass	Conc.	Mass	%Mass	Conc.
Bed + cyclone product	1.1 kg	56%	1.27%	0.11 kg	59%	0.134%	7.0E-2 kg	62%	0.084%
Filter fines	0.8 kg	44%	1.37%	7.8E-2 kg	41%	0.127%	4.3E-2 kg	38%	0.070%
Fines-Product ratio	0.79	---	1.1	0.70	---	1.0	0.61	---	0.84

	K			P			S		
	Mass	%Mass	Conc.	Mass	%Mass	Conc.	Mass	%Mass	Conc.
Bed + cyclone product	0.25 kg	54%	0.298%	0.17 kg	59%	0.203%	0.19 kg	49%	0.229%
Filter fines	0.22 kg	46%	0.354%	0.12 kg	41%	0.195%	0.20 kg	51%	0.322%
Fines-Product ratio	0.87	---	1.2	0.70	---	0.96	1.03	---	1.4

[LAW test summary and mass balances Nov 16.xls]Chemical mass balance table

4.4.3 Reductant Utilization

Solid carbon was used as a reductant to provide sufficiently reducing conditions to convert nitrates and nitrites in the simulant to N_2. The carbon was fed through a series of lock-out valves that alternated opening and closing, allowing discrete amounts of carbon into the fluidized bed at a relatively high frequency, while preventing any air influx into the bed, or fugitive emissions from the bed. The valves were purged with a small quantity of N_2 that entered the bed with the carbon.

Sufficient carbon was added to ensure an excess of carbon relative to the amount needed to (a) react with the added O_2 in the fluidizing gas, (b) react with the nitrates and nitrites in the simulant feed, and (c) react with steam. FBSR off-gas measurements that show practically zero O_2, excess H_2 and THC,

and over 90% NO_x destruction, confirm that the carbon added to the steam reformer produced overall reducing conditions, and that the carbon:O_2 and carbon:NO_x reactions almost quantitatively remove the O_2 and NO_x in the system. Some of the solid carbon fed to the steam reformer was removed unreacted from the steam reformer in the bed product, in cyclone fines samples, and in the filter fines.

The carbon:oxidant stoichiometry was defined, in the context of this test, as the ratio of available carbon compared to the total available O_2 and NO_x, assuming that carbon would react first with available fluidizing O_2 according to the theoretical equation

$$C + O_2 \rightarrow CO_2$$

CO is an expected reaction product of the carbon reaction with O_2 in the FBSR. Carbon can also react with other species, especially H_2O, to produce H_2, CO, and CO_2. But the ratio of CO compared to CO_2 measured in the FBSR off-gas indicates that on average over 90% of the C is oxidized to CO_2 rather than CO. This is even after accounting for the formation of CO_2 when sodium carbonate in the feed decomposes, and accounting for the amount of CO_2 produced when the organic species in the Hanford LAW simulant are oxidized to produce CO_2.

The 100% stoichiometric amount of C required to react with the O_2 (to form CO_2) is mathematically subtracted from the total C additive input. The remaining C is the amount available to react with NO_x from the feed simulant according to the assumed theoretically efficient reactions to form N_2 and CO_2:

$$5C + 4MNO_3 \rightarrow 2M_2O + 2N_2 + 5\ CO_2$$

$$3C + 4\ MNO_2 \rightarrow 2M_2O + 2N_2 + 3CO_2$$

In reality, a variety of byproducts (such NO, CO, THC, and H_2) can result from reactions of the carbon reductant with O_2, NO_x, and H_2O. Residual amounts of these byproducts in the off-gas represent process inefficiencies in the conversion of C to CO_2 and the conversion of NO_x to N_2. The target carbon:oxidant stoichiometry is generally set to be considerably higher than 100% for this reason. The difference between the stoichiometry during the FBSR test and 100% stoichiometry represents the sum of "gasification inefficiencies", which includes (a) the amount of C that gasified to CO and THC instead of CO_2, (b) the amount of C that reacted with H_2O and produced intermediate products like H_2 that were not completely used to convert nitrates and nitrites to N_2, and (c) solid carbon that exits the FBSR unreacted in the bed product, cyclone fines samples, and the filter fines.

The Hanford LAW feed simulant contains small concentrations of two organic compounds, sodium oxalate and sodium acetate. The most simplified and efficient overall reactions of these species with O_2 and NO_3 are:

$$Na_2C_2O_4 + 0.5O_2 \rightarrow Na_2O + 2CO_2$$

$$Na_2C_2O_4 + 0.33NO_3 \rightarrow Na_2O + 2CO_2 + 0.17N_2$$

$$2NaCH_3CO_2 + 6O_2 \rightarrow Na_2O + 4CO_2 + 3H_2O$$

$$9NaCH_3CO_2 + 12NO_3 \rightarrow 4.5Na_2O + 18CO_2 + 13.5H_2O + 6N_2$$

The total amount of these reductants is small compared to the total NO_3 and NO_2. Assuming that all available O_2 is consumed by reaction with the carbon additive, and not available for reaction with the

oxalate and acetate, and assuming that byproducts of inefficient oxalate and acetate reaction are not formed, the most NO_3 that can be consumed by the combined acetate and oxalate is only 8% of the total NO_3. Therefore, for simplicity, the oxalate and acetate are not included in the carbon:oxidant stoichiometry calculations since their contribution to the nitrate reduction stoichiometry is small compared the contribution by the added carbon reductant.

The stoichiometric amount of carbon added during the test period, relative to the amount of carbon needed to react with the O_2 and NO_x, is shown in Table 4.4-5 for each test condition. The stoichiometry changed whenever the carbon feed rate was changed, or when the simulant feed rate was changed. The overall stoichiometry was always reductant-rich to ensure sufficiently reducing conditions in the fluidized bed for efficient NO_x destruction.

Table 4.4-5. Calculated carbon:oxidant stoichiometry during test operation.

Communication sheet	Date, start time	COT, hr:min	Duration, hr:min	Calculated carbon stoichiometry
1	2 Aug 04 09:00	00:00	00:48	901%
2	2 Aug 04 09:48	00:48	04:12	564%
3	2 Aug 04 14:00	05:00	03:12	423%
4, 5	2 Aug 04 17:12	08:12	15:48	435%
6	3 Aug 04 09:00	24:00	01:30	348%
7	3 Aug 04 10:30	25:30	04:34	352%
8	3 Aug 04 15:04	30:04	09:16	352%
9	4 Aug 04 00:20	39:20	02:00	416%
10	4 Aug 04 02:20	41:20	12:55	412%
11	4 Aug 04 15:15	54:15	11:42	375%
12	5 Aug 04 02:57	65:57	02:29	375%
Shutdown	5 Aug 04 05:26	68:26		
Test average				412%

[LAW test summary and mass balances Nov 16.xls]carbon stoic

The equation used to calculate the carbon:oxidant stoichiometry is:

Stoich, % = (corrected reductant feed rate – 0.408 x O_2 feed rate)/(0.0251 x slurry feed rate) x 100%

The coefficients 0.408 and 0.251 are stoichiometric coefficients from the above C, O_2, and nitrate/nitrite equations, converted to a mass basis, accounting for the amount of carbon in the carbon additive (91.9 wt%), the corrected reductant feed rate, and the concentrations of total nitrate and total nitrite in the feed slurry. The units of the reductant, O_2, and slurry feed rates are kg/hr.

The carbon mass balance closure and distribution to the output streams are shown in Table 4.4-6. Most of the input carbon was from the carbon in the solid carbon additive. Relatively small amounts of organic carbon (in the sodium acetate and sodium oxalate), and inorganic carbon (in the sodium carbonate) were included in the simulant feed. Carbon outputs included carbon in the solid output

streams (the bed product, the cyclone fines samples, and the filter fines), carbon in the measured CO_2, CO, and THC concentrations in the FBSR off-gas, carbon in the CEMS 1 condensate, and carbon captured in the CEMS 1 carbon filter. Carbon in the CEMS 1 condensate includes carbon in carbon-bearing species that were in the FBSR off-gas, but were scrubbed from the off-gas with the water condensate upstream of the CEMS 1 analyzers, and so were not included in the CEMS 1 analysis. Carbon-bearing species captured in the CEMS 1 carbon filter were also removed from the CEMS 1 sample gas upstream of the CEMS 1 analyzers (except for the THC analyzer, which was located upstream of the carbon filter).

The overall carbon mass balance closure, at 88%, indicates reasonably good accounting of carbon in the FBSR, considering that the combined accuracy of all of the different flow rate and concentration measurements and estimates was approximately plus or minus 10%.

Most of the effluent carbon (about 86%) was in the off-gas CO_2, CO, or THC, when the amounts of carbon represented by the measured CO_2, CO, THC, carbon in the CEMS 1 condensate, and carbon captured in the CEMS 1 carbon filter were summed. Only 14% of the carbon was found as organic carbon (residual unreacted carbon additive) in the solid products. About 71% of the organic carbon input to the fluidized bed was converted to fully oxidized CO_2, even though the C:oxidant stoichiometric ratio averaged 412%. This was because the C:oxidant stoichiometry was based on the $C:O_2$ and $C:NO_x$ overall reactions, and did not account for the amount of carbon gasified to CO, CO_2, and other gas species through reactions with steam. While over four times more carbon was added than was needed to stoichiometrically react with O_2 and NO_x, much of the "extra" carbon was utilized in other steam reforming reactions, and was necessary to provide adequately reducing conditions to efficiently destroy NO_x.

Table 4.4-6. Carbon distribution for the Hanford LAW FBSR mineralization test series.

		Carbon mass inputs, kg			Carbon mass outputs, kg C							
					Solid outputs					C in off-gas at the filter outlet		
		Total solid carbon additive	Carbon from solid carbon additive	Carbon from simulant	Bed product	Cyclone samples	Filter catch	C in the CEMS 1 condensate	C captured in the CEMS 1 carbon filter	CO_2	CO	THC
Totals of individual streams	Total organic (reduced) carbon (TOC)	43.9	39.0	0.6	2.5	0.2	2.3	3.4	0.0	0.0	1.6	0.6
	Total inorganic (fully oxidized) carbon (TIC)	0.0	0.0	1.0	0.0	0.0	0.0	0.0	3.4	21.9	0.0	0.0
Input or output	TOC	39.6			5.0			5.6				
	TIC	1.0			0.0			25.3				
Total input or output		40.7			35.9							
Total carbon mass balance closure, %		88.3										

	Distribution of C amoung the FBSR effluent streams, weight % of total output C							
	Solid outputs					C in off-gas at the filter outlet		
	Bed product	Cyclone samples	Filter catch	C in the CEMS 1 condensate	C captured in the CEMS 1 carbon filter	CO_2	CO	THC
TOC	7.0	0.6	6.4	9.4	0.0	0	4.5	1.6
TIC	0.0	0.0	0.0	0.0	9.4	61.1	0.0	0.0
TOC	14.0			15.5				
TIC	0			70.5				
Totals	100.0							

Notes:

1. The mass of total solid carbon additive fed to the fluidized bed used for carbon mass balance calculations was determined gravimetrically from the mass of carbon added to the feeder hopper, not the amount determined by the PLC. The gravimetric amount is more accurate than the total amount fed based on the PLC.
2. The carbon content of the carbon reductant was estimated at 88.9%, determined from the SRNL moisture and loss-on-ignition analyses (3.1% and 95%, respectively), and allowing for 1% each residual H, N, and O that may be present in this wood-based carbon.
3. The carbon added in the simulant was calculated using the target oxalate, acetate, and carbonate values.
4. Prior analyses have shown that negligible inorganic carbon is present in any of the FBSR mineralized effluents.
5. The organic carbon content of the bed product was determined using 3.3 wt% average organic C concentration in 76.4 kg.
6. The organic carbon content of the cyclone samples was determined using 2.4 wt% average organic C concentration in 9.7 kg.
7. The organic carbon content of the filter fines was determined using 3.7 wt% average C content in a total of 61.8 kg.
8. Organic carbon was detected in the CEMS 1 condensate samples. Inorganic carbon was not detected, indicating minimal sorption of CO_2 in the CEMS 1 condensate. This TOC represents TOC that was not detected as CO_2, CO, or THC by the CEMS 1, and so is accounted for separately in addition to the total C determined based on CO2, CO, and THC recorded by CEMS 1.
9. TIC or TOC captured in the carbon filter includes carbon in carbon-bearing species that passed through the CEMS 1 chiller, but were captured in the CEMS 1 carbon filter used to protect the CEMS 1 analyzers from fouling by condensible hydrocarbons. The THC analyzer was located upstream of the carbon filter to avoid capture of THCs prior to THC analysis, but both CO and CO2 analyzers were downstream of the carbon filter. The amount of TIC and TOC captured by the carbon filter was not measured. The amount of TOC captured in the carbon filter was assumed to be zero; the amount of TIC captured in the carbon filter was estimated to be equivalent to the amount of total carbon captured
10. The C measured in the FBSR offgas was determined using the average filter outlet off-gas flowrate and concentrations of CO_2, CO, and THC. THC is reported as CH_4.

[Reformatted August PLC Data_10min oct 30.xls]carbon MB

5. CONCLUSIONS/RECOMMENDATIONS

The INEEL's pilot scale fluidized bed processing test system at the STAR facility was successfully operated during the first week of August 2004 to conduct a continuous processing test of the TTT mineralized steam reforming process technology on simulated waste materials representative of Hanford LAW.

The pilot scale test generated a large amount of real-time process operating conditions data and process materials data. The data has been compiled and has undergone considerable analysis leading to the test results presented herein. Considerable further analyses are possible, however, to generate increased understanding of the technology and response to changes in key process parameters. Additional data analyses, coupled with additional, controlled process technology tests, such as bed thermal profile tests to determine reactor/bed responses to key input parameter changes, would be extremely useful for future model-based process optimization studies, as well as improving the test system instrumentation/diagnostics understanding for future experimental process optimization tests.

Several different, important FBSR process mechanisms and complex interactive situations cannot be well understood from the currently available data and analyses alone. Considerable additional controlled testing and model-based evaluations of both the local and global heat transfer, fluid dynamics, and reaction rate driven chemistry conditions are needed to better understand controlling mechanisms and parameters and provide for predictive means for scaling and optimizing process parameters. It is recommended that these efforts be pursued to provide a more effective design bases for a potential future production process.

The following are key conclusions and recommendations from the pilot scale fluidized bed LAW mineralized steam reforming processing test results.

1) The pilot scale test achieved a total of 68.4 hrs of cumulative/continuous processing operation, and resulting mineralized products, before termination in response to a bed de-fluidization condition. The process achieved essentially complete bed turnover within approximately 40 hrs (greater than 98% replacement of the starting bed with mineralized product solids) and operated for the remaining hours essentially under relatively steady bed product and process conditions. This did not meet the test objective of operating for >80 hours at a feed rate of ~ 4 kg/hour, but effectively satisfied an underlying objective of 100% bed turnover.

2) The pilot scale test produced a significant quantity of representative FBSR mineralized solid product materials, samples of which have been analyzed for chemical/physical properties, and can be used to compare/validate equivalency with small lab-scale mineralizing chemistry studies/tests by SRNL. The total amount of simulated LAW feed and additives processed was approximately 364 kg and the total solid products mass was approximately 145 kg indicating a total mass reduction within the process of 219 kg, or about 60%. The total input of solids includes 43.9 kg of carbon and about 142 kg clay. Therefore, about 178 kg of LAW surrogate resulted in about 148 kg of solid product, a mass reduction of about 19%. The net solid waste product material mass and volume are of course of interest for any subsequent processing or direct handling and disposal activities. The bed product to fines collected mass ratio was about 1 to 1. This value did not achieve the desired value of 3.5 to 1 as stated in the test objectives, and further optimization and/or development is needed to achieve this objective.

3) The majority (estimated >95 wt%) of the total mineralized process product solids were of a form expected during stable, steady mineralized process operations. These consisted of small (typically 0.2 – 0.3 mm), generally granular solids in the bed product, or much smaller granular

solids in the fines product (typical diameter 0.01 mm). Elutriated fines that were captured in a cyclone (upstream of the heated filter) and were recycled to the fluidized bed averaged about 0.04 mm in diameter. Only a small amount of the total product in the bed was undesirable larger solid pieces, either from nozzle deposit/accretions break-off (typical diameters from 6 to 12 mm) or the very large de-fluidized bed agglomerates (typical dimensions of several inches) which occurred rapidly near the end of the test.

4) The majority of the desired mineralized bed product material consists of small granular product with a rough "popcorn like" appearance. The granules appear to be collections of much smaller micron size particles, which have been successively deposited onto the surface of existing larger bed product granules/particles. The rather haphazard, bumpy, and porous appearance might be characterized as a "very rough powder coating" deposit. This appears to be consistent with what might be expected from successive deposits of an atomized spray of room temperature slurry onto the high temperature bed product granule surfaces. The small slurry mixture droplets (100 micron average) consist of simulant solution containing a large number of insoluble solid clay particles of various sizes (4 micron average, range 0.4 to 40 microns), which have been pre-mixed, soaked, and perhaps partially pre-reacted with the LAW solution. The deposited slurry evaporates/boils and the contained metal nitrates break down and react with reformer gases and the soaked clay particles as heat transfer occurs on the hot granule surfaces. A spray droplet of 100 micron mean size would contain 3125 clay particles of 4 micron average size for the LAW slurry mixture (20% volume fraction clay, 80% simulant solution). The pre-soaked clay particles will undergo the slowest heat uptake. Various lower to intermediate temperature LAW reaction products, such as the alkali-hydroxides, may persist locally at near molten temperatures (400°C range) for some time. This phenomenon may provide a sticky phase that holds the clay particulate to the larger particle surface until surface reaction/binding occurs; while regions of droplet film without clay particles will boil away, likely under film boiling conditions, and may or may not react similarly with the larger mineralized product granule surface. The results of XRD analyses indicate that reactivity/particle growth was likely inhibited by the effects described above.

5) A very small amount of bed product consisted of slightly larger granules on the order ¼ inch to ½ inch (6 mm to 12 mm) characteristic diameter. The larger pieces appeared routinely throughout the test after roughly the first 20 hours of operation. It was clear that these resulted from break-off of minor product deposits/accretions grown on the remaining cool nozzle surface from the shape, appearance and timing. Previous tests had experienced much more severe nozzle accretions. The redesigned nozzle was clearly successful in achieving a significant reduction in formation and size of nozzle surface deposits/accretions. The redesigned bottom receiver drains were effective in removing these larger particles as a part of normal bed/sample drains and they had no noticeable detrimental affect on fluidized bed processing operations.

6) Much larger agglomerations of bed product were produced near the end of the process run, and led to bed defluidization. It is difficult to determine the root cause(s) and dominating parameters of the bed defluidization from the test conditions/results, since there were several planned and unplanned changes to operating/system conditions that occurred within the same general time frame (within the last ten hours of operation). However, it appears from the post-operational inspection appearance of the final bed and inner vessel that the most likely cause was over-quenching of the bed in the nozzle spray cone deposition region due to the combination of the increase in slurry feed flow to 5.5 kg/hr, along with a reduced fluidizing gas (sensible heat source) input, at a time when the bed consisted solely of lower density mineralized product having less thermal capacity and lower heat transfer rate characteristics (lower thermal conductivity). These effects conspired to cause over-quenching/cooling of the bed region in the vicinity of the nozzle spray zone and a relatively rapid runaway deposition and collective agglomeration growth of bed particles in that

zone. Bed mixing and heat transfer conditions worsened as larger particles and agglomerates formed, with continued feed liquid spray deposit resulting in rapid local agglomerate growth and eventual near blockage of the bed just above the nozzle location that required a process shutdown.

7) NO_x was satisfactorily destroyed throughout the process run. Average NO_x destruction of the steam reforming process (upstream of the thermal oxidizer) averaged 92% and was near 96% much of the time, effectively meeting the test objective of greater than 80% destruction. The average NO_x destruction after the thermal oxidizer was 99.95%. Responsiveness of NO_x generation/ destruction in the steam reforming process was as expected, being directly proportional to carbon feed rate/inventory changes which drive the attendant proportional production of H_2 and CO that are thought to participate in NO_x reduction reactions. A catalyst to enhance NO_x destruction was not required or utilized. The carbon feed rate was set well below that utilized in previous tests, leading to fewer un-reacted carbon fines carryover to the filter. Cyclone recycle was effective in achieving capture and return of larger carbon fines to the bed for reaction and more efficient use.

8) The mineralized steam reforming process is intended to immobilize the LAW metal-nitrates as oxides in a stable product solid consisting largely of sodium/potassium-alumina-silicate target mineral phases of various structures. The mineral phases are formed as a result of the clay additive and are intended to capture and retain (stabilize) the alkali metals (Na, K), target radionuclides (Tc) and potentially selected toxic metals and anions. Test results show that nitrates and nitrites in the waste feed were essentially destroyed and that the bed and fines products largely consisted of desired target mineral phases. The major phase found in the bed product was carnegieite, with lesser amounts of nepheline and minor amounts of nosean. The fines consisted of the major phase carnegieite with lesser amounts of nepheline and TiO_2 (a trace component in the clay). Performance of the solid products with respect to solubility and retention of elements of interest under various leach test conditions is being addressed by ongoing work to be reported later by SRNL. Elemental analysis of the products indicate that aluminum and chromium, on a weight percent basis, partitioned somewhat preferentially to the bed product; calcium, phosphorous, and chlorine distributed evenly. Rhenium, sodium, and potassium appear to partition somewhat to the fines, but not as significantly as do silicon and sulfur. Cesium clearly partitions preferentially to the filter fines.

9) The overall operations and performance of the fluidized bed processing test system equipment was good. Several minor incidents occurred which required operator actions/interventions. These were, however, generally corrected rapidly and had no significant discernible impacts upon the mineralized steam reforming process. Several equipment issues may have had a secondary effect that helped trigger the final de-fluidization event. Although, the root cause was most likely over quenching the bed from process conditions that pushed the limits of the fluidized bed test system. The particular system/equipment incidents have been discussed in the results section and noted for potential system/equipment design modifications for improving future test operations. It is, however, also important to note several items: a) the modified nozzle and vessel bottom receivers operated very well to minimize and manage the reduced occurrence of nozzle accretions that had been a significant problem in the earlier mineralized testing on SBW, b) the associated pre-test atomization studies and cold flow tests, as reported in the appendices, were a key to selecting appropriate atomization conditions for test operations, c) the pre-test flow-model visualization tests provided valuable insight into the fluidized bed dynamics for selecting appropriate test conditions and data interpretation, and d) equipment changes to the hot filter, allowing for individual candle purging and as-needed filter product sampling/draining were successful in avoiding excess filter inventory buildup and candle thermal stress fracture conditions.

6. REFERENCES

Addison, C. C, 1964, and Logan, N., "Anhydrous Metal Nitrates," *Adv. Inorg. Chem. Radiochem.*, 6, 71.

Agarwal, J. C., Nov. 1962, Davis, Jr., W. L., and King, D. T.; *Chemical Engineering Progress*, Vol. 58, No. 11, p. 85.

Antal, M. J., 1979, et al., *A Study of the Steam Gasification of Organic Wastes*, Final Progress Report to the U.S. Environmental Protection Agency, Princeton University, Princeton, NJ.

ASTM, 2002, *Standard Test Method for Sampling and Fineness Test of Pulverized Coal*, D 197 – 87 (Reapproved 2002), ASTM International, West Conshohocken, PA.

Barrer, R. M., 1959, J. W. Baynham, F. W. Bultitude, and W. M. Meier, *Hydrothermal Chemistry of the Silicates. Part V23I, Low-Temperature Crystal Growth of Aluminosilicates, and of Some Gallium and Germanium Analogues***,** 195-208.

Bartos, H. R., 1956, and Margrave, J. L., *J. Phys. Chem.*, 160, 256.

Berry, L. G., 1959, and Mason, B., *Mineralogy Concepts, Descriptions, Determinations***,** W.H. Freeman & Co., San Francisco, CA, 630pp.

Boardman, R. D, 2004, B. H. O'Brien, N. R. Soelberg, S. O. Bates, C. P. St. Michel, R. A. Wood, and B. J. Ward, "High-Temperature MACT Calcination Test," INEEL/EXT-04-01625, February.

Bradley, R. F., 1972, Goodlett, C. B., *Denitration of Nitric Acid Solutions by Formic Acid*, DP-1299, Savannah River Laboratory, Aiken, SC.

Bray, L. A. 1963, *Denitration of Purex Wastes with Sugar,* HW-76973; Hanford Atomic Products Operation, Richland, WA.

Brookins, D. G, 1984, *Geochemical Aspects of Radioactive Waste Disposal***,** Springer-Verlag, New York, 347pp.

Brown, R. W., 1975, Lippiat, J. H., Price, D., Izod, D. C. A., *Intl. J. Mass Spect. Ion Phys.*, 16, 101.

Cheng, I. F., 1997, Muftikian, R., Fernando, Q., Korte, N., *Chemosphere*, 35, 2685.

Cox, J. L. , 1994, Hallen, R. T., Lilga, M. A., *Environ. Sci. Technol.*, 28, 423.

Dana, E. S., 1932, *A Textbook of Mineralogy*, John Wiley & Sons, Inc., New York, 851pp.

Deer, W. A., 1963, Howie, R. A., and Zussman, J., *Rock-Forming Minerals, Vol IV***,** John Wiley & Sons, Inc., New York, 435pp.

Dotson, J. M., 1975, Peters, T. E., U. S. Patent 3,862,296.

Elliott, M. A., 1981, Wiley, Ed, *Chemistry of Coal Utilization, 2nd Suppl. Vol.*, Interscience, New York, p. 1500.

Fitzgerald, T. J. and Crane, S. D., 1980, in *Proc. 6th Int. Conf. On Fluidized Bed Combustion*, Vol. 3, p. 815, Atlanta, GA.

Freeman, E. S., 1956, *J. Phys. Chem.*, 60, 1487.

Gunderloy Jr., F. C., 1968, Fujikawa, C.Y., Dayan, V.H., Grid, S., *Dilute Solution Reactions of the Nitrate Ion as Applied to Water Reclamation*, Technical Report No. TWRC-1; FWPCA: Cincinnati, OH.

Gunderloy Jr., F. C., 1970, Wagner, R. I., Dayan, V. H., *Development of a Chemical Denitrification Process*, Technical Report No. EPA 17010EEX/10/70; U.S. Environmental Protection Agency, Water Quality Office: Washington, DC.

Hayhurst, A. N., 1992, and Lawrence, A. D., *Prog. Energy Combust. Sci.*, 18, 529.

Horio, M. et al., 1986, in *Fluidization V*, K. Østergaard and A. Sørensen, Eds., p. 151, Engineering Foundation, New York, 1986; AIChE J., **32**, 1466.

Jantzen, C. M., 1982, Clarke, D. R., Morgan, P. E. D., and Harker, A. B., "Leaching of Polyphase Nuclear Waste Ceramics: Microstructural and Phase Characterization," *J. Am. Ceram. Soc.*, 65[6], 292-300.

Jantzen, C. M., 2002, *Engineering Study Of The Hanford Low Activity Waste (LAW) Steam Reforming Process (U)*, WSRC-TR-2002-00317, REV. 0, July 12.

Jantzen, C. M., 2003, *Disposition of Tank 48H Organics by Fluidized Bed Steam Reforming (FBSR)*, WSRC-TR-2003-00352, September.

Jantzen, C. M., 2004, J. C. Marra, and J. M. Pareizs, *Analysis of Raw Materials for Fluidized Bed Steam Reforming (FBSR)*, SRNL-ITB-2004-0004, June 30.

Kirk-Othmer, 1995, *Encyclopedia of Chemistry*, Vol. 16.

Klingenberg, R. 1986, and Felsche, J., "Interstitial Cristobalite-type Compounds, $(Na_2O)_{0.33}Na[AlSiO_4]$)," *J. Solid State Chemistry*, 61, 40-46.

Kramer, C. M., 1983, et al., *High Temperature Science*, 16, 257.

Kunii, D. 1991, and Levenspiel, O., *Fluidization Engineering*, 2nd Edition, Butterworth-Heinemann, Newton, MA.

Kuo, Kenneth Kuan-yun, *Principles of Combustion*, John Wiley & Sons, 1986, p. 372

Marshall, D. W., May 2003, N. R. Soelberg, and K. M. Shaber, *TWR Bench-Scale Steam Reforming Demonstration*, INEEL/EXT-03-00437.

Mattus, A. J., 1993, Lee, D. D., *The Nitrate to Ammonia and Ceramic (NAC) Process – A Newly Developed Low-Temperature Technology*, CONF-930873-18; Oak Ridge National Laboratory, Oak Ridge, TN.

McCarthy, G. J., 1976, and M. T. Davidson, "Ceramic Nuclear Waste Forms: I," *Am. Ceram. Soc. Bull.*, 54, 782-786 (1975) and "Ceramic Nuclear Waste Forms: II," *Am. Ceram. Soc. Am. Ceram. Soc. Bull.*, 55[2]190-194.

Meile, L. J., January 1984, and Johnson, A. J., *Waste Generation Reduction - Nitrates FY 1982 Status Report*, Rockwell International, RFP-3465, DOE/TIC-4500 (Rev. 72).

Morgan, P. E. D., 1981, Clarke, D. R., Jantzen, C. M., and Harker, A. B.**,** "High-Alumina Tailored Nuclear Waste Ceramics," *J. Am. Ceram. Soc.*, 64 [5] 249-58.

Murphy, A. P., 1991, *Nature*, 350, 223.

Nimlos, M., 1990, and T. Milne, *Preliminary Screening of Steam-reforming Efficacy of Rhodium Catalysts for Destroying Halon 1301 (CF_3Br)*, Letter Report to Sandia from SERI dated June 28, 1990.

Nimlos, M. R., 1992, and T. A. Milne, *Environ. Sci. Technol.*, 26, 545.

Rassat, S. D., 2003, L. A. Mahoney, R. L. Russell, S. A. Bryan, and R. L. Sell, *Cold Dissolved Saltcake Waste Development, Preparation, and Analysis*, PNNL-14194 Rev. 1, May.

Rusin, J. M., 1979, M. F. Browning, G. J. McCarthy**,** "Development of Multibarrier Nuclear Waste Forms," *Sci. Basis for Nucl. Waste Mgt. I*, G. J. McCarthy (Ed.), Plenum Press, New York, 169-180.

Ryan, J. L., 1995, *Redox Reactions and Foaming in Nuclear Waste Glass Melting*, PNNL-10510, August.

SAIC, 2004, *Steam Reformer Operating Instructions*, SAIC-SR-OI-01, Current revision.

Seymour, R. G., 1995, *Development of the High-Level Waste High-Temperature Melter Feed Preparation Flowsheet for Vitrification Process Testing,* WHC-SD-WM-SP-008, February.

Soelberg, N. R., 2003, D. W. Marshall, S. O. Bates, D. D. Siemer, *SRS Tank 48H Waste Steam Reforming Proof-of-Concept Test Results*, INEEL/EXT-03-01118, September.

Soelberg, N. R., 2004a, D. W. Marshall, D. D. Taylor, and S. O. Bates, *Phase 2 TWR Steam Reforming Tests for Sodium-Bearing Waste Treatment*, INEEL/EXT-04-01494, January 30.

Soelberg, N. R., 2004b, D. W. Marshall, S. O. Bates, and D. D. Taylor, *Phase 2 THOR^{sm} Steam Reforming Tests for Sodium-Bearing Waste Treatment*, INEEL/EXT-04-01493, January 30.

Appendix A

Hydraulic Similarity Tests

D. W. Marshall

Appendix A

HYDRAULIC SIMILARITY TESTS

Introduction To Hydraulic Similarity

At times it is desirable to model a fluidized bed system using smaller equipment or parameters that are more conducive to getting the data needed for making judgments about the system. It is important to select bed media and operating parameters such that the hydraulic behavior of the model is representative of the actual system when such physical models are used. The bed recirculation, convection cell geometry, and fluidization mode may not match that of the actual system if hydraulic similarity is not achieved.

Direct observations of the bed convection cells or fluidization mode cannot be made of the 6-inch fluidized-bed steam reformer (FBSR) when it is operating at temperature. It was desirable, therefore, to model the FBSR using a Plexiglas tube and suitable bed material so that the convection could be photographically documented during tests of the INEEL ring distributor and compared to the THOR^{SM} Treatment Technologies proprietary distributor. The objective was to monitor fluidization of bed material and flow patterns resulting from the gas injection points and the of distributor geometries rather than to evaluate distributor pressure drop. Efforts were made to select distributors, from the existing stock, that have similar pressure drops during the experiment.

Methodology

Hydraulic similarity can be satisfactorily achieved when scaling parameters are matched between the actual system and the physical model, which operates at less harsh conditions. Horio, et al., proposed the use of two scaling parameters based on the square root of the Froude numbers. Fitzgerald and Crane proposed the use of more restrictive scaling parameters that include the Reynolds number, solid-gas density ratio, Froude number, geometric similarity of the reactor and bed medium. These two sets of scaling parameters were tested by Roy and Davidson, who found that the simpler set proposed by Horio was best suited for particle Reynolds numbers less than 30 and the Fitzgerald & Crane parameters were better suited for particle Reynolds numbers over 30. A concise summary of physical models and these parameters has been provided by Kunii and Levenspiel.

The particle Reynolds number is less than 10 at FBSR operating conditions (see Table A-1), and the scaling parameters proposed by Horio, et al. are appropriately used. These are the Froude number for the minimum fluidization velocity and the difference of the square roots of the Froude numbers at the operating parameters and that at minimum fluidization velocity:

$$Fr_{mf} = \frac{u_{mf}^2}{g \cdot d_p} \qquad \text{Parameter (1)}$$

$$\sqrt{Fr} - \sqrt{Fr_{mf}} = \frac{u - u_{mf}}{\sqrt{g \cdot d_p}} \qquad \text{Parameter (2)}$$

Table A-1. Hydraulic similarity test operating conditions.

Reference Case		Physical Model		
Reactor diameter	6.065 in.	Reactor diameter		5.75 in.
Bed medium	alumina	Bed medium		silica sand
Particle density	3.95 g/cc	Particle density		2.63 g/cc
Particle size (HMPD)	245μm	Particle size (HMPD)		214 μm
Reactor temperature	720°C	Reactor temperature		~27°C
Min. fluidizing velocity (U_{mf})	0.038 m/s	Min. fluidizing velocity (U_{mf})		0.038 m/s
Particle Reynolds No. (Re_{mf})	0.05	Particle Reynolds No. (Re_{mf})		0.49
Velocity ratio U/U_{mf}	6	Velocity ratio U/U_{mf}		5.4
Bed pressure (0" elevation)	12.3 psia	Bed pressure (0" elevation)		13.4 psia
Bed differential pressure	45 in.WC	Bed differential pressure		30 in.WC
Fluidizing gas	steam	Fluidizing gas		air
Fluidizing gas rate	2.8 kg/hr	Fluidizing gas rate		13.9 kg/hr
Instrument purge flow	1.0 kg/hr			
Froude number at U_{mf} (Fr_{mf})	5.96e-4	Froude number at U_{mf} (Fr_{mf})	6.95e-4	Ratio = 1.17
Fluidized without feed - Reference		*Fluidized without feed - Model*		
SBW+clay feed rate (UTB or lower nozzle)	0 kg/hr	Air injection (lower or UTB nozzle)		24.0 kg/hr
SBW+clay slurry NAR	0			
SBW+clay water fraction	0.67	Simulated instrument purge (upper nozzle)		3.0 kg/hr
Particle Reynolds No. (Re_{top})	0.4	Particle Reynolds No. (Re_{top})		3.8
$\sqrt{Fr_{bottom}} - \sqrt{Fr_{mf}}$	0.122	$\sqrt{Fr_{bottom}} - \sqrt{Fr_{mf}}$	0.117	Ratio = .96
$\sqrt{Fr_{middle}} - \sqrt{Fr_{mf}}$	0.130	$\sqrt{Fr_{middle}} - \sqrt{Fr_{mf}}$	0.122	Ratio = .93
$\sqrt{Fr_{top}} - \sqrt{Fr_{mf}}$	0.144	$\sqrt{Fr_{top}} - \sqrt{Fr_{mf}}$	0.129	Ratio = 0.90
Lower or UTB feed nozzle – no spare		*Lower or UTB feed nozzle – no spare*		
SBW+clay feed rate (UTB or lower nozzle)	6 kg/hr	Air injection (lower or UTB nozzle)		24.0 kg/hr
SBW+clay slurry NAR	500			
SBW+clay water fraction	0.67	Simulated instrument purge (upper nozzle)		3.0 kg/hr
Particle Reynolds No. (Re_{top})	0.9	Particle Reynolds No. (Re_{top})		7.8
$\sqrt{Fr_{bottom}} - \sqrt{Fr_{mf}}$	0.122	$\sqrt{Fr_{bottom}} - \sqrt{Fr_{mf}}$	0.117	Ratio = 0.96
$\sqrt{Fr_{middle}} - \sqrt{Fr_{mf}}$	0.463	$\sqrt{Fr_{middle}} - \sqrt{Fr_{mf}}$	0.458	Ratio = 0.99
$\sqrt{Fr_{top}} - \sqrt{Fr_{mf}}$	0.527	$\sqrt{Fr_{top}} - \sqrt{Fr_{mf}}$	0.519	Ratio = 0.98
Lower or UTB feed nozzle – with idled spare		*Lower or UTB feed nozzle – with idled spare*		
SBW+clay feed rate (UTB or lower nozzle)	6 kg/hr	Air injection (lower or UTB nozzle)		24.0 kg/hr
SBW+clay slurry NAR	500			
SBW+clay water fraction	0.67	Simulated instrument purge (upper nozzle)		3.0 kg/hr
Spare nozzle purge	1.4 kg/hr	Spare nozzle purge		4.7 kg/hr
Particle Reynolds No. (Re_{top})	1.0	Particle Reynolds No. (Re_{top})		8.7
$\sqrt{Fr_{bottom}} - \sqrt{Fr_{mf}}$	0.122	$\sqrt{Fr_{bottom}} - \sqrt{Fr_{mf}}$	0.117	Ratio = 0.96
$\sqrt{Fr_{middle}} - \sqrt{Fr_{mf}}$	0.488	$\sqrt{Fr_{middle}} - \sqrt{Fr_{mf}}$	0.510	Ratio = 1.05
$\sqrt{Fr_{top}} - \sqrt{Fr_{mf}}$	0.581	$\sqrt{Fr_{top}} - \sqrt{Fr_{mf}}$	0.573	Ratio = 0.99

The first parameter, Fr_{mf}, is essentially uniform throughout the bed and was computed only once. The second parameter, however, varies depending on where atomizing gases, aqueous feed, and other gases are introduced or generated. For simplicity (and for the lack of reliable mixed-gas property data) the gases were assumed to behave as ideal gases, gas generation beyond water vaporization was neglected, and all gases were assumed to have the same physical properties of the fluidizing gas. These assumptions should not have introduced large errors into the calculations since water vapor is the dominant species in the FBSR and air is the only species in the physical model.

Options exist to inject feed at one or more of three levels; 1) through the uniaxial-tube Bernoulli-effect (UTB) nozzle that extends through the reactor receiver plate into the distributor region, 2) through a horizontal nozzle located about four inches above the distributor, and 3) through a horizontal nozzle located about 13 inches above the distributor. The small elevation difference between the UTB nozzle and the lower horizontal nozzle prompted another assumption to treat these points as being the same elevation. This divides the reactor into three distinct regions, which are:

1. Between the distributor and the lower feed nozzle elevations,

2. Between the lower and upper feed nozzle elevations, and

3. The surface of the fluidized bed.

The elevations are taken at the distributor (0”), just below the upper feed nozzle elevation (+12”), and at the mean elevation of the bed surface (+30”) for the hydraulic similarity calculations.

Test Conditions

The reference case conditions were selected to be representative of the conditions to be used during the mineralizing flowsheet demonstrations. The feed rate was not expected to exceed 6 kg/hr and the nozzle atomizing ratio was expected to remain relatively low to maximize residence time and minimize feed plume penetration through the bed. The bed media was assumed to be white alumina with an average particle size of 245µm (60-grit). Fluidizing gas velocity was assumed to be six times the minimum fluidizing velocity because this is needed with the virgin bed to maintain adequate pressure drop in the distributor.

The sum of instrument purges is assumed to be 1 kg/hr in the reactor section during actual tests. The flow is adjusted to satisfactorily match the scaling parameters and divided equally between the lower and upper gas injection (feed) points in the physical model to achieve hydraulic similarity.

Silica sand for the bed in the physical model was available at the SAIC STAR Center. The sand, as received, had a mass-mean particle diameter (MMPD) of 270µm and a harmonic-mean particle diameter (HMPD) of 216µm. For hydraulic similarity, it is desirable to have an HMPD of 0.203µm, which could have been achieved with the available sand if a 40-mesh sieve screen had been available to screen out the larger particles. A 35-mesh sieve was used, which reduced the HMPD to approximately 0.214µm, based on a previous sand sample. Because the sand HMPD was larger than desired, the Froude number at minimum fluidization could not be strictly matched with the reference case. The second matching parameter (difference in the square roots of the Froude numbers) matched reasonably well, despite the initial calculations being based on the ideal particle size. The larger particle size resulted in the fluidizing gas flow in the physical model being 5.4 times the minimum fluidizing velocity rather than 6 times the minimum in the reference model.

The experiment consisted of several tests intended to represent different modes of operation. These tests are designated in numerical order (e.g., 1, 2, 3, etc.). Several ad hoc tests were also conducted because the desired conditions were easily configured and achieved. The ad hoc tests are designated alphanumerically (1a, 1b, etc.). Table A-2 shows the conditions planned and tested. Two other tests were planned that would have simulated operation with feed entering two feed nozzles (upper and lower or lower and UTB), rather than just one, but limitations on the equipment prevented the investigators from achieving the desired flow rate of air.

Quarter-inch tubing was used to represent the feed nozzles located at the 4"and 13" datum lines and the UTB nozzle. Although gas velocities in the immediate vicinity of the nozzles differ from the actual gas flows, the matching parameters are meant to show representative behavior of the bulk emulsion phase

Table A-2. Summary of the physical model test conditions.

Test	Distributor	Air flow rates				
		Fluidizing	UTB	Lower nozzle	Upper nozzle	Total
1	THOR^{SM}	13.9 kg/hr 6.3 scfm	---	---	---	13.9 kg/hr 6.3 scfm
1a	THOR^{SM}	13.9 kg/hr 6.3 scfm	---	24.0 kg/hr 11.0 scfm	3.0 kg/hr 1.4 scfm	40.8 kg/hr 18.6 scfm
1b	THOR^{SM}	13.9 kg/hr 6.3 scfm	24.0 kg/hr 11.0 scfm	---	3.0 kg/hr 1.4 scfm	40.8 kg/hr 18.6 scfm
1c	THOR^{SM}	13.9 kg/hr 6.3 scfm	16.0 kg/hr 7.3 scfm	---	3.0 kg/hr 1.4 scfm	32.8 kg/hr 15.0 scfm
2	Ring	13.9 kg/hr 6.3 scfm	---	---	---	13.9 kg/hr 6.3 scfm
3	Ring	14.0 kg/hr 6.3 scfm	---	24.0 kg/hr 11.0 scfm	3.0 kg/hr 1.4 scfm	40.9 kg/hr 18.6 scfm
3a	Ring	13.9 kg/hr 6.3 scfm	---	16.1 kg/hr 7.3 scfm	3.0 kg/hr 1.4 scfm	32.9 kg/hr 15.0 scfm
4	Ring	14.0 kg/hr 6.3 scfm	24.0 kg/hr 11.0 scfm	---	3.0 kg/hr 1.4 scfm	40.9 kg/hr 18.6 scfm
4a	Ring	13.9 kg/hr 6.3 scfm	16.0 kg/hr 7.3 scfm	---	3.0 kg/hr 1.4 scfm	32.8 kg/hr 15.0 scfm
5	Ring	13.9 kg/hr 6.3 scfm	24.0 kg/hr 11.0 scfm	4.7 kg/hr 2.1 scfm	3.0 kg/hr 1.4 scfm	45.6 kg/hr 20.8 scfm
5a	Ring	13.9 kg/hr 6.3 scfm	15.7kg/hr 7.2 scfm	4.7 kg/hr 2.1 scfm	3.0 kg/hr 1.4 scfm	37.3 kg/hr 17.0 scfm
6	Ring	13.9 kg/hr 6.3 scfm	4.7 kg/hr 2.1 scfm	24.0 kg/hr 11.0 scfm	3.0 kg/hr 1.4 scfm	45.6 kg/hr 20.8 scfm

Test Observations

Each of the test conditions was recorded using a digital video camera so that the emulsion flow and elevation of bubble/slug formation could be documented. Datum lines were drawn on the Plexiglas tube to denote the 4" and 13" elevations (relative to the bottom flange face) corresponding to the elevations of the feed ports in the actual process.

Overall bed level dropped during the course of the testing because elutriated bed particles were swept away by the ventilation system. The bed level would not have dropped as much had the Plexiglas model been fitted with an expanded freeboard and a cyclone catch recycle, as the actual system. Approximately 20-25% of the bed mass had been lost by the conclusion of the tests.

Test 1 showed the fluidization of the sand using the THOR^{SM} distributor. Bubbles in the emulsion were observed near the bottom flange, in the vicinity of the distributor, but not along the flange or walls positioned at right angles to the distributor. This is evidence that the gas is not uniformly distributed in the immediate vicinity of the distributor in spite of efforts to space orifices such that the gas would be more evenly distributed. The jet plumes reached the exterior walls of the reactor only near the distributor ends. The emulsion was fluidized, however, over the entire observable cross section of the bed. The emulsion was observed to descend along the wall orthogonal to the distributor. Slugs were generally symmetrical and tended to flow up the center of the column. All slugging was observed above the lower feed nozzle elevation, beginning approximately 7" above the distributor. Slugs were mostly axial with an occasional "flat" slug near the top of the bed (bubble filled the full cross section of the reactor).

Some Berger Brothers activated carbon was added to the fluidized bed to trace bulk emulsion flow. The carbon remained near the surface of the bed and did not get carried down the sidewalls with the emulsion.

Test 1a was conducted with the THOR^{SM} distributor and the addition of gas through the upper feed nozzle to represent the addition of instrument purge gases and gas through the lower side feed port to represent slurry feed evaporation and atomization. Some bubbles were observed impinging on the reactor wall opposite of the feed nozzle, indicating that the bed was being penetrated by the nozzle jet. It should be noted that the quarter-inch tubing used to inject the gases is not representative of the feed nozzle in terms of gas quantity or velocity at the nozzle. Hydraulic similarity is achieved approximately eight inches above the injection point. Nonetheless, this observation is consistent with observed fouling and accretions on the wall opposite the feed nozzle from past reactor operation, especially when a light-weight product replaces the starting bed. Low density bed media allow for deeper penetration of the gas plumes. Some gross recirculation of the bed was induced by injection of the gas at the lower feed port, resulting in somewhat more upward flow of the emulsion along the opposite wall and down flow of the emulsion above the feed port and cyclone catch recycle injection. Flat slugs were frequently observed. The activated carbon mixed in the top portion of the bed, but was not observed below the upper side port.

Test 1b was conducted with the THOR^{SM} distributor and the addition of gases to represent instrument purges, feed, and feed atomization. The feed and atomizing gas surrogate air was injected through the UTB instead of the lower feed port. The addition of the gas through the UTB caused gross recirculation of the bed emulsion with down flow dominating on the side of the reactor behind the UTB injector, which is angled upward from the bottom such that it passes through the distributor zone. The gross recirculation (i.e., "gulf streaming") of the bed was more pronounced than in Test 1a when the feed was introduced through the lower side feed port. The UTB jet plume was observed against the opposing reactor wall. As slugs passed the upper feed nozzle (13") elevation, the bulk flow of the emulsion would reverse directions, as evidenced by the observable plume from the purge injection. Slugs tended to be less centered in the bed; forming more "wall slugs" than axial slugs. The bed surface was more violent

and elutriated particles were more prevalent in the freeboard. Activated carbon was mixed in because of the violent bed surface, but was not observed below the upper side port.

The gross circulation of the bed causes the emulsion phase to flow downward, toward the distributor, at the elevation where cyclone catch recycle is introduced. This places the fine carbon particles in the bottom of the bed, near the vicinity of the distributor (and oxygen). Furthermore, the circulation of the emulsion sweeps recycled product fines into the feed zone where they may be captured and help form seed particles. The velocity of the emulsion phase past the cyclone catch recycle injection point seems to be higher than when the lower side feed port is used.

Test 1c was an unplanned test condition selected purely for the visualization of the bed at a reduced feed rate. Hydraulic similarity conditions had not been computed nor intentionally set. The air injection rate in the UTB nozzle was decreased from 24 to 16 kg/hr. This action caused the impingement of the air jet plume to be more intermittent and smaller than at the higher feed rate. The bed surface was also less violent.

Test 2 was conducted with the ring distributor installed and the bed fluidized at approximately $5.4*U_{mf}$. Bubbles were observed around the perimeter of the reactor wall in the vicinity of the distributor. The distribution appears to be more uniform than the THOR^{SM} distributor, which only exhibited bubbling near the reactor walls where the distributor terminated. This result was not unexpected because the mean free path between the ring and the reactor wall is generally less than it is from the orifices of the THOR^{SM} distributor to the reactor wall except near the edge of the distributor. Slugs formed at about the same level as in Test 1, approximately 7" above the distributor. Slugs were predominately axial. Beyond a few inches above the distributor, the emulsion flow was indistinguishable from that induced by the THOR^{SM} distributor. Activated carbon was observed on the surface of the bed and appeared to mix in the top couple of inches of the bed.

Test 3 was conducted with conditions the same as during Test 1a, except that the ring distributor was used. Feed surrogate air was injected through the lower side port at 24 kg/hr and a surrogate instrument purge was added at 3 kg/hr through the upper side port. Some bubbles were observed impinging on the wall opposite of the lower side port, indicating full penetration of the bed by the jet plume. Gross bed recirculation patterns and slug formation was the same as in Test 1a. Carbon mixed in the top inches of the bed, but has not been observed descending the sides of the reactor with the emulsion phase.

Test 3a was conducted with reduced feed surrogate air (reduced from 24 to 16 kg/hr), but otherwise configured the same as Test 3. Feed jet plume penetration of the bed was reduced. More carbon was observed on the surface of the bed than in Test 3.

Test 4 was conducted with the same conditions as Test 3, except the feed surrogate air was directed through the UTB nozzle. The air jet plume impinged on the wall of the reactor and gross bed recirculation was more pronounced when using the UTB nozzle than a side mounted nozzle. The UTB discharged at an elevation just above the distributor and well below the point where bubble coalescence resulted in slugs.

Test 4a was conducted to visualize decreased feed while using the ring distributor. The air flow rates and injection points match that of Test 1c. Gross bed recirculation patterns appear to be the same except in the immediate region of the distributor. The ring distributor has a more uniform distribution of bubbles that are visible around much of the reactor perimeter, except where the down flow of the induced emulsion recirculation is most pronounced.

Test 5 was conducted to simulate a condition where the UTB nozzle was used for feed injection and the lower side port was fitted with an idled feed injector as a backup to the UTB. Air flow to the UTB was 24 kg/hr and to the lower nozzle injected 4.7 kg/hr. The combined gas flows caused a significant amount of bed to be ejected into the freeboard. Although the UTB and lower side ports are not coplanar, but have common radial vector components that may have increased the bed recirculation rate. The UTB plume impinged on the opposing reactor wall. No side nozzle bubbles were observed on the opposing wall, but this may have been obscured or captured by the UTB plume.

Test 6 was similar to Test 5 except that the feed surrogate air was injected through the side nozzle and the UTB was idled. The bed remained violently stirred, but elutriation was reduced because the bed surface was less violent than when the UTB was used.

Tests 7 and 8 were intended to simulate conditions where a clay slurry and liquid feed were fed through separate nozzles. The desired flows could not be achieved due to limitations in the air manifold used for the tests.

Conclusions

The THOR^{SM} and ring distributors adequately fluidize the bed. The emulsion phase was observed to be in motion at all points in the bed and around the bottom flange at the elevation of the distributor. The bubbles emanating from the THOR^{SM} distributor were visible near the edge of the supporting flange, but not along the reactor wall orthogonal to the distributor. The ring distributor bubbles were seen at the reactor wall around most of the reactor circumference. By all appearances, the ring distributor seems to distribute the gases more uniformly in the immediate vicinity of the distributor than the THOR^{SM} distributor. The movement of the emulsion phase appears to be independent of the distributor configuration at the elevation of the lower side port.

Carbon pieces mixed into the upper portion of the fluidized bed, but did not become distributed throughout the bed to a significant extent. None of the pieces were observed descending the reactor wall with the emulsion phase when about 500 cc of activated carbon added to the bed. This suggests that a small percentage of the carbon is distributed in the bed during normal operation. The quantity of carbon normally extracted from the process through bed sampling and bed draining activities suggests that a large inventory of carbon must normally exist in the bed.

The UTB nozzle induces greater bed recirculation because the nozzle was at an angle upward from the bottom with a ~20° radial component. This resulted in greater wall slugging occurring, which in turn caused the bed surface to be more violent and more particles to be elutriated from the bed.

References

T. J. Fitzgerald and S. D. Crane, in *Proc. 6th Int. Conf on Fluidized Bed Combustion*, vol.3, p. 815, Atlanta, GA, 1980.

M. Horio et al., in *Fluidization V*, K. Østergaard and A. Sørensen, eds., p. 151, Engineering Foundation, New York, 1986; *AIChE J.*, **32**, 1466 (1986).

D. Kunii and O. Levenspiel, *Fluidization Engineering*, 2nd Ed., Butterworth – Heinemann, 1991, pp 152 – 153.

R. Roy and J. F. Davidson, in *Fluidization VI*, J. R. Grace Et al., eds., p. 293, Engineering Foundation , New York, 1989.

Appendix B

Nozzle Atomization Test Results

Nicholas R. Soelberg

Appendix B

NOZZLE ATOMIZATION TEST RESULTS

Mineralizing clay was blended with the sodium-bearing waste (SBW) Hanford low activity waste (LAW) simulants to perform the fluidized bed steam reforming (FBSR) tests. Nozzle atomization performance is essential to maintaining long-term FBSR operation and achieving the desired FBSR products. Sufficient atomization is necessary to avoid excessively large droplets (poor local dispersal of slurry over the bed region/surface being sprayed) which may lead to localized overcooled granules and possible formation of larger agglomerations of bed particles that could cause defluidization of the bed and failure of the operation.

Conversely, increased atomization can produce a finer distribution of spray over the bed region, but if excessive, may lead to undesirable fine particles that elutriate from the bed. Elutriation of fine particles from the bed process is mitigated to some extent by cyclone capture and recycle of elutriated fines to the bed for further potential incorporation into bed product. Increased atomization gas also adds to the total gas flow effectively fluidizing the bed. The total fluidizing gas flow must be controlled within a desired range to avoid additional elutriation of small particles.

Avoiding persistent nozzle accretions is necessary to prevent the formation of solids attached to the nozzle tip that can impair nozzle atomization performance. Small nozzle accretions that form and break off of the nozzle might not impair nozzle atomization, but accretions that persist and grow on the nozzle can contribute to poor atomization and bed defluidizing agglomerations.

Several different nozzle sizes and designs were evaluated prior to, during, and after the FBSR tests leading up to the Hanford LAW FBSR test, in an effort to improve longer-term atomization performance and minimize the chance of defluidizing agglomerations during FBSR operation because of nozzle accretions or other forms of nozzle anomalies. These designs included (a) SprayCo nozzles of different sizes, with and without the SprayCo antibearding configuration, that were designed for atomizing feed through the FBSR side wall, and (b) uniaxial-tube Bernoulli-effect (UTB) nozzles of different sizes and configurations. The UTB nozzles are modeled after the nozzle design used in prior THOR^{sm} demonstration testing and are designed to atomize feed co-axially with the flow of the FBSR fluidizing gas.

As new nozzle designs were developed, the atomization performance of each nozzle design and size was tested by spraying feed slurries through the nozzles under selected atomizing conditions, and observing the atomizing results. Several different nozzle atomization tests were performed, on May 6, June 7, June 22, and July 30, all prior to the Hanford LAW FBSR test performed in August 2004.

Liquid atomization depends on, among other factors, the liquid viscosity. Viscosities of various radioactive waste simulants used in fluidized bed steam reforming (FBSR) testing can vary widely, especially when clay, a mineralizing additive, is slurried with the simulant. Viscosity measurements were made for slurries of the Hanford LAW simulant in conjunction with the nozzle atomization tests prior to the Hanford LAW FBSR test. The viscosity measurements were used to determine relative viscosity data for slurries with different clay concentrations, for evaluating the results of the nozzle atomization tests, and to provide assurance prior to the FBSR test that the selected feed slurry would not have feed-related problems due to viscosity.

May 6, 2004 Nozzle Atomization Tests

Earlier, more qualitative, investigatory nozzle atomization tests were performed on May 6 (prior to the May Shakedown Test) and June 7, 2004. The May 6 test was performed primarily to determine appropriate Troy clay – water slurry spray conditions for the May Shakedown Test. The 40 wt% clay-water slurry rapidly (within 1 minute of operation) plugged the SprayCo nozzle with a 0.060 inch ID liquid tube. The plugging could not be removed and prevented by normal nozzle cleaning activities such as rodding out the feed tube. This size nozzle was used in the Phase 2 THOR mineralizing test, when the feed was slurried with SnoBrite clay that had a smaller particle size (about 5 um mass mean diameter) than does the Troy clay (about 15 um mass mean diameter) (Jantzen, 2004). Apparently the larger particle size of the Troy clay affected the nozzle performance. Nozzles with 0.060 ID liquid tubes were considered too small for feeding simulant slurries in the upcoming FBSR tests, based on this result.

The 0.060-inch nozzle was replaced with a 0.100-in ID nozzle. While the 0.060 nozzle was an antibearding nozzle, the 0.100 nozzle is not available in the antibearding design. The 40 wt% slurry also plugged the 0.100 nozzle, so the 40 wt% slurry was modified with added water to lower the concentration to 33.3 wt%. This slurry atomized without plugging with the 0.100 nozzle and an average NAR of at least 1,000. Pulsing of the peristaltic pump caused the liquid flow to oscillate, causing the NAR to oscillate as the atomizing gas flow was controlled at a constant flow rate. The actual instantaneous NAR varied above and below 1,000 with the liquid oscillation. This may have caused the NAR to be higher than necessary, to ensure that atomization was maintained as the liquid flow rate pulsed to a higher than average flow rate.

At the end of this test, the feed nozzle was switched back to the 0.060 nozzle to determine if the 33.3 wt% slurry could be fed through this nozzle. This nozzle again plugged rapidly and repeatedly, so the SprayCo nozzle with a 0.100 inch ID liquid tube was selected for feeding the clay-water slurry in the May Shakedown Test.

The atomizing gas back-pressure, used to indicate when the atomizing gas velocity at the nozzle tip reaches sonic velocity, was not measured during these tests.

June 7, 2004 Nozzle Atomization Tests

Additional, qualitative nozzle atomization tests were performed on June 7, after the May Shakedown Test, to determine what sizes of SprayCo and UTB nozzles, and atomizing gas flow rates, were appropriate for Troy clay slurried in SBW lite simulant and OptiKast clay slurried in Hanford LAW lite simulant. The "lite" simulants were prepared using the exact proportions of the major chemical constituents of these simulants, leaving out minor (especially hazardous) constituents such as lead, nickel, mercury, and cesium. These minor constituents were not expected to significantly affect nozzle atomization. Excluding the minor hazardous or costly constituents facilitated safety and lowered cost during the nozzle atomization tests.

A pulse dampener installed after the May Shakedown Test significantly reduced pulsing caused by the peristaltic pump, potentially improving feed atomization at lower NARs.

Two different nozzles were tested:

- A standard SprayCo nozzle with a 0.100 inch ID and 0.150 inch OD liquid tube, and a 0.180 inch ID air cap

- A UTB nozzle with a 0.1175 inch ID, 0.1875 inch OD liquid tube, and a 0.2145 inch ID, 0.3125 inch OD atomizing gas tube

The tests were performing using air as the atomizing gas, and using Hanford LAW lite simulant, slurried with 784 g/L of the simulant. The degree of atomization and atomization pattern was observed subjectively at different slurry and atomizing gas flow rates. At slurry flow rates between 4 – 7.5 kg/hr, the slurry was not fully atomized, without visible "spitting" and non-uniform spray patterns, until the NAR was at least 450 NAR and the atomizing gas rate was at least 2.4 kg/hr atomizing gas flow rate. Lower NARs and atomizing gas flow rates could subject the bed to larger droplets that over-wet bed particles.

The air gap of the UTB nozzle gradually became occluded, probably because of a small amount of droplet recirculation that attached to the tips of liquid and atomizing gas tubes. This finding indicated that the UTB, if used, should be beveled to sharpen the edges of the nozzle tubes to reduce the surface area to which feed slurry droplets could adhere. After this nozzle atomization test, the UTB design was modified to bevel the tube tips. The liquid tube was beveled on the inside, and the air tube was beveled on the outside. These sharp edges should minimize the amount of surface on which liquid can attach, while maintaining the velocity and momentum of the atomizing gas at the nozzle tip.

The atomizing gas back-pressure, used to indicate when the atomizing gas velocity at the nozzle tip reaches sonic velocity, was not measured during these tests.

June 22, 2004 Nozzle Atomization Tests

Simulant slurry atomization tests were performed on June 22, 2004. These tests were more quantitative and less subjective than the prior nozzle atomization tests. These tests were performed to:

- Visualize the atomized spray of simulant slurry from feed nozzles under selected operating conditions
- Determine if the UTB waste injection nozzle atomizes the slurry similarly to the Sprayco nozzle when operated under similar conditions
- Measure the atomized spray droplet particle size
- Provide data needed to select the feed nozzle operating conditions (nozzle size and configuration, simulant slurry feed rate, atomizing gas flow rate, and NAR) for the FBSR experimental demonstrations.

Experimental Setup

A simplified open spray booth was set up in the FBSR enclosure at the SAIC STAR Center. The spray booth is shown in Figure B-1. Each of two spray nozzles that were tested (the UTB nozzle fabricated by SAIC and a commercial SprayCo nozzle) were mounted on a temporary stand so that the atomized spray from the nozzle can be directed into a ventilated duct. The spray was drawn into the ventilation duct to prevent excessive and hazardous mist from forming in the enclosure. An open space of about 1-2 feet between the nozzle tip and the inlet to the ventilation duct enabled visual observation of the spray, photography, and droplet sampling.

Figure B-1. The spray test setup in the FBSR enclosure, with a UTB nozzle mounted to spray into the ventilation hood.

The nozzle sizes were determined based on spray tests that were done in May. During those tests, nozzle sizes that were too small rapidly plugged with slurry. The minimum nozzle sizes were determined from these tests.

The Sprayco nozzle had a 0.100 inch diameter liquid nozzle, a 0.150 outer dimension, and a 0.180 inch air cap, the same dimensions as the SprayCo nozzle used in prior tests. These dimensions determined a thickness of 0.015 inches for the annular atomizing gas nozzle. This size was not available in the "antibearding" design; the standard available nozzle components were used.

The UTB and Sprayco nozzles were tested using SBW simulant slurried with Troy clay and Hanford LAW simulant slurried with OptiKast clay. The OptiKast clay had a smaller average particle size (about 4 um MMPD, similar to that of the Phase 2 SnoBrite clay, which was about 5 um MMPD) in comparison to the Troy clay, which was about 15 um MMPD. Both simulants were prepared for the spray tests to exclude the minor constituents that were either hazardous or thought to not contribute significantly to the slurry rheology or atomization characteristics. Slurry viscosity tests showed that viscosities of the "SBW Lite" simulant, with and without clay, were similar to the viscosities of the actual SBW simulant with and without clay.

The atomization tests were performed using the lite simulants blended with a representative amount of clay. The SBW simulant was blended with 291 g Troy clay (as received) per liter of SBW simulant. The Hanford LAW simulant was blended with 784 g OptiKast (as received) per liter of Hanford LAW simulant.

Diagnostics

Two different techniques were used to document the tests and attempt to determine the particle size range of the atomized droplets for each nozzle under different nozzle operating conditions. High-speed photography provides photograph records of each spray condition. The photography was done using a film camera, 400 ASA film, and a 1/40,000th second flash. The camera was aimed at a 90^{o} angle to the spray, at a distance of 1-2 ft from the spray. The flash was directed at a 90^{o} angle to spray, and also at 90^{o} to the camera. A black background behind the spray enabled the white slurry droplets to stand out from the background in the photos.

Samples of the atomized droplets were collected on glass microscope slides for subsequent microscope and particle size analysis. The slides were first numbered and coated with a thin film of oil. The oil caused the water-based droplets to bead up separately rather than run together on the glass. Droplet samples were collected by swiping the oil-coated slides through the spray pattern. Optical microscope analysis, including collection of digital photos, was performed on the slide samples. The digital photos were analyzed to determine the droplet particle size distribution using Image Pro Plus computer software for counting and sizing particles.

Atomized Spray Patterns

The Hanford LAW slurry spray test results with the SprayCo nozzle are shown in Table B-1. The SprayCo nozzle was tested at two different flow rates at NARs ranging from 100 to 750.

Table B-1. Hanford LAW slurry spray test summary.

784 g OptiKast clay per L Hanford LAW simulant										
Nozzle	Simulant slurry rate, kg/hr	Atomizing air rate, kg/hr	Atomizing air rate, scfm	Atomizing gas velocity, m/s	NAR	Photo film roll	Photo frame number	Slide number	Measured droplet MMPD from slides, mm	Observations
Sprayco	7	3.4	1.71	163	600	2	33	14	---	Unsteady feedrate
Sprayco	7	2.6	1.31	125	450	3	1-10	15	0.148	Unsteady feedrate
Sprayco	3.5	2.1	1.05	100	750	2	28-32	12, 13	0.190	
Sprayco	3.5	1.67	0.84	80	600	2	23	11	0.374	
Sprayco	3.5	1.25	0.63	60	450	2	22	10	0.764	
Sprayco	3.5	0.83	0.42	40	300	2	13	9	1.288	
Sprayco	3.5	0.42	0.21	20	150	2	12	---	---	Dribble from tip

1. The atomizing gas backpressure was not measured. The atomizing gas velocity at the nozzle was calculated assuming that the nozzle pressure was at 14.7 psig, standard pressure, although the actual gas pressure in the nozzle was between the ambient pressure (about 12.3 psia) and the nozzle backpressure, which could have been several psig or more. Based on these velocities, the atomizing gas velocity was not sonic for all of the atomizing tests.

2. The area of the air gap for the SprayCo nozzle is 0.0077 inches.

3. The standard temperature is 68^{o}F.

The sequence of high speed photos for each test condition are shown in Figures B-2 through B-4. The degree of atomization was high for the SprayCo nozzle with a Hanford LAW slurry feed rate of 7 kg/hr and NAR at 600. The energy of atomization decreased as the NAR and atomizing gas flow rate decreased. The slurry was visibly less atomized at NARs of 450 and 300 than at higher NARs, with a wider total spray pattern of 70-90^{o}. The spray was clearly less atomized at 300 NAR, affected by gravity, and was considered to be unsatisfactory for FBSR operation. A NAR of 150 provided no atomization.

Droplet Particle Size Distribution Measurements

The oil causes the droplets collected on the slides to bead up rather than run together. However, after sample collection, the larger droplets tended to flatten onto the glass, making a disc on the glass that was larger than the original spherical droplet. This tendency was more visible with the larger droplets. If the smaller droplets had the same tendency, it was not noticeable to the naked eye during sample collection. Because of this tendency, the droplet size measurements for at least the larger droplets (and maybe the smaller droplets too) were larger than the actual spherical droplets. The droplet size measurements may be up to 10-50% larger than the true droplet sizes. The measured sizes are not adjusted for this observed bias.

Figures B-5 and B-6 show example photographs of droplets collected on microscope slides.

Figure B-7 summarizes the average droplet particle sizes. The comparison of the measured MMPDs show that the MMPDs are significantly affected not only by the NAR but also by the slurry feed rate and the atomizing gas flow rate.

Figure B-8 shows a better correlation of droplet size compared to atomizing gas flow rate. The correlation is co-linear over the measurement range. This correlation suggests that the atomizing gas flow rate affects the droplet size more than nozzle type, slurry feed rate, or NAR.

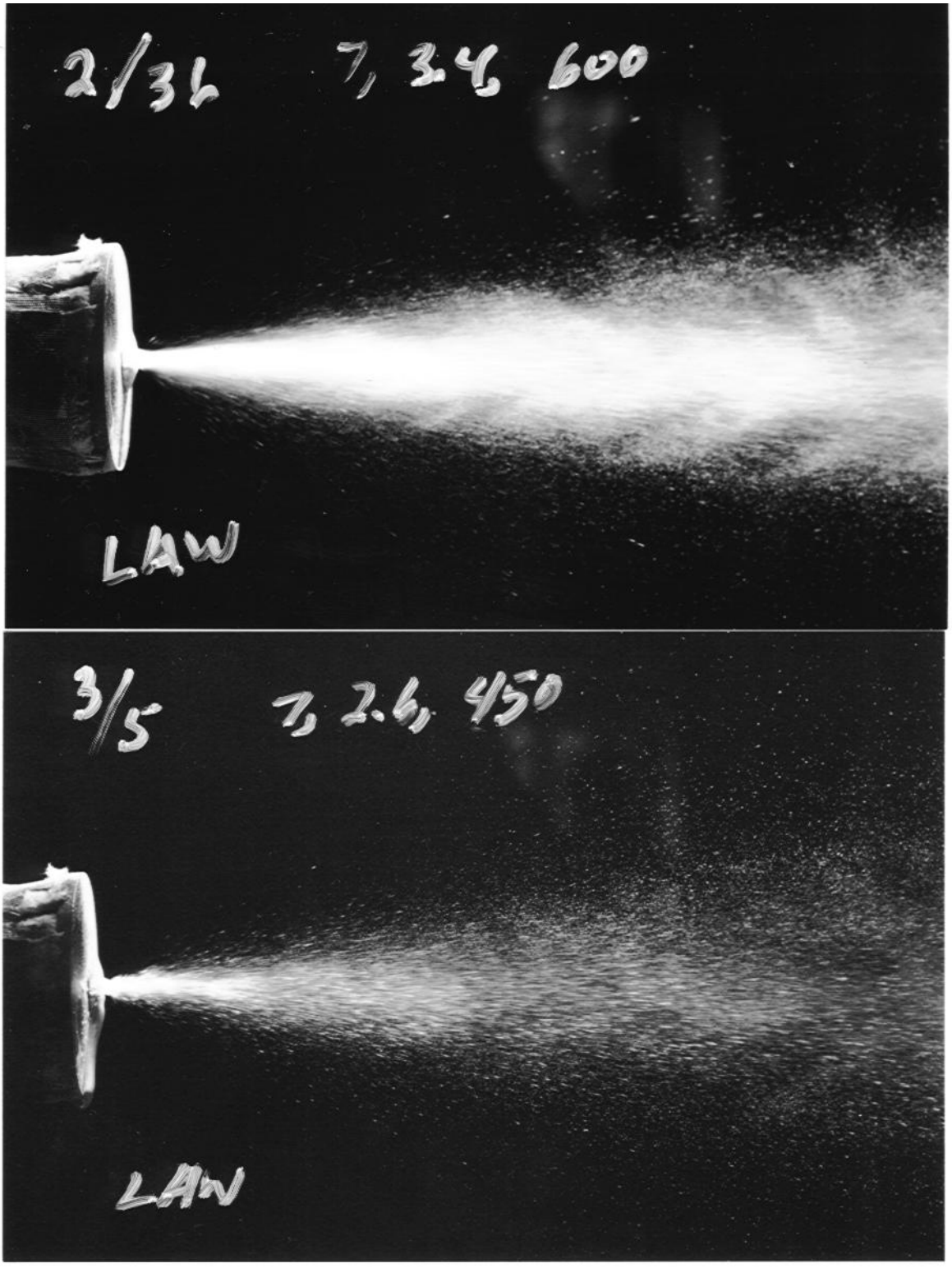

Figure B-2. NAR decreasing from 600 to 450 for the Sprayco nozzle at a Hanford LAW slurry feed rate of 7 kg/hr.

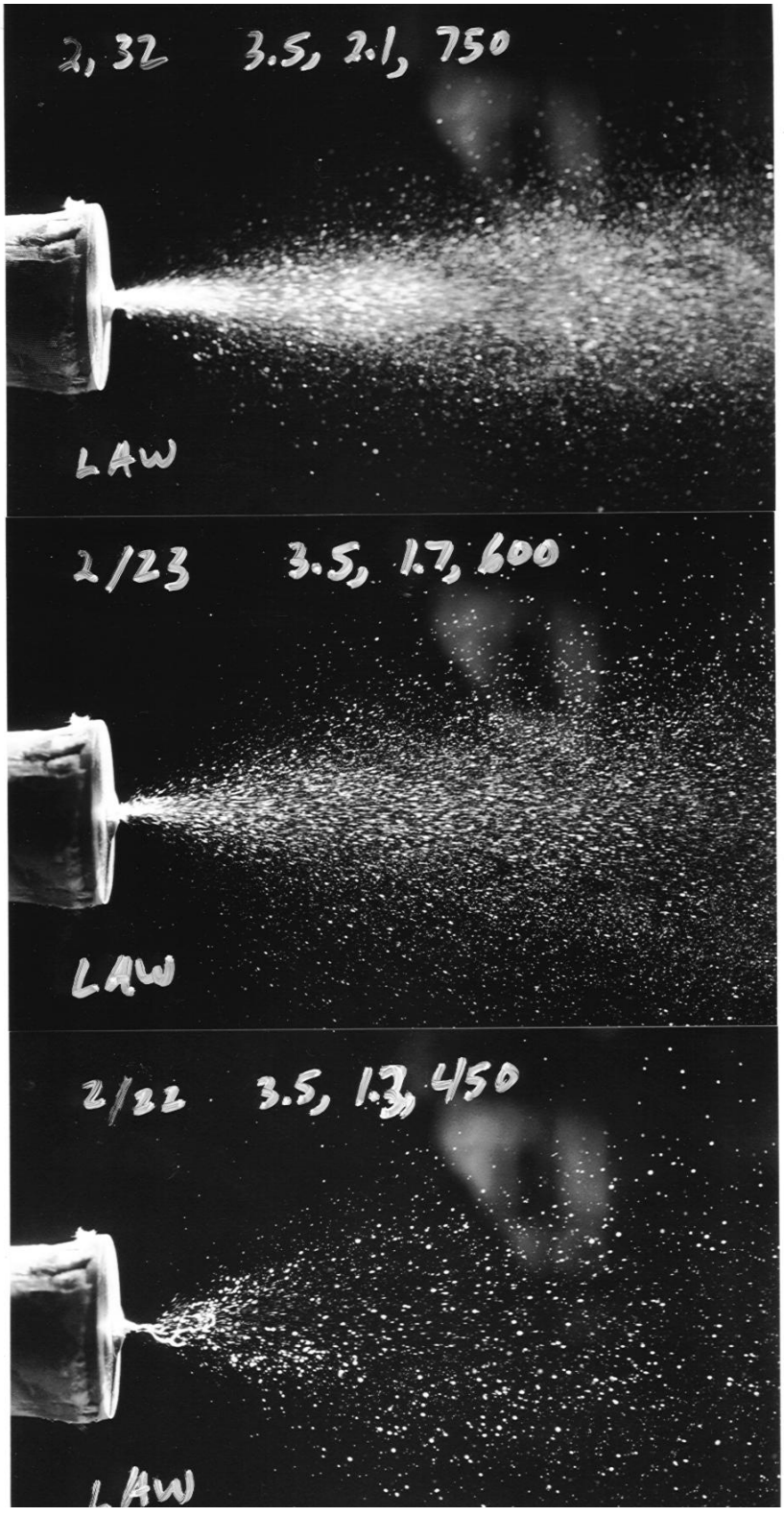

Figure B-3. NAR decreasing from 750 to 450 for the Sprayco nozzle at a Hanford LAW slurry feed rate of 3.5 kg/hr.

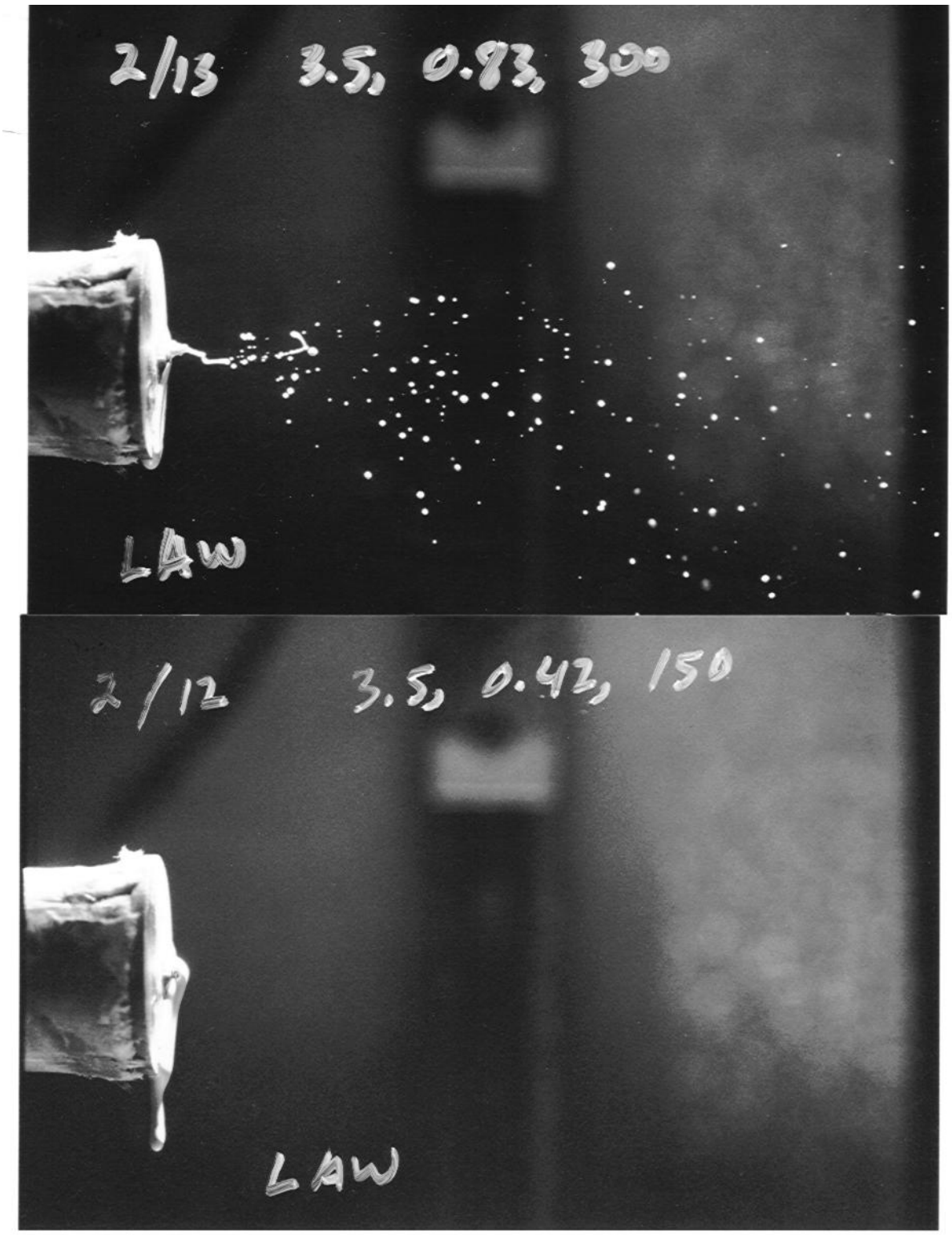

Figure B-4. NAR decreasing from 300 to 150 for the Sprayco nozzle at a Hanford LAW slurry feed rate of 3.5 kg/hr.

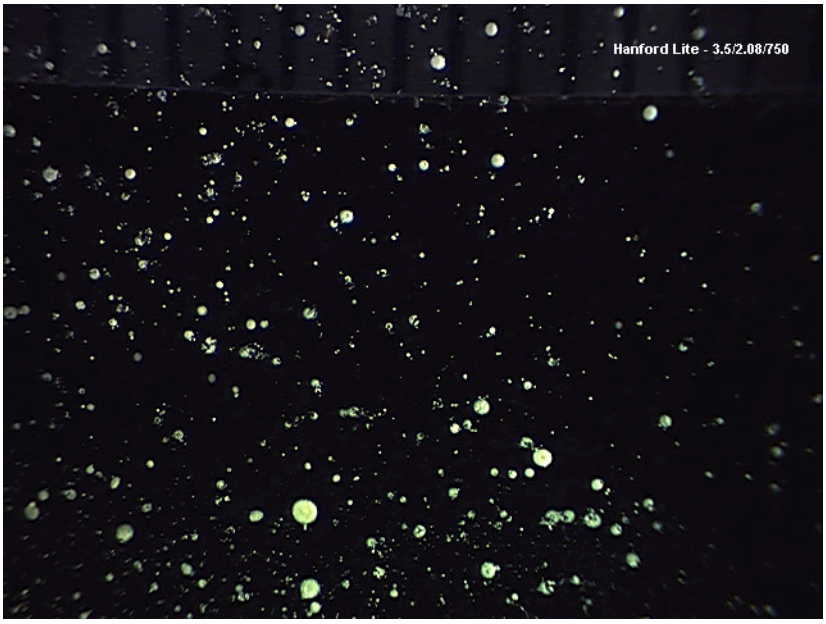

Figure B-5. Atomized spray droplets for the Sprayco nozzle, with a Hanford LAW slurry feed rate of 3.5 kg/hr, an atomizing gas flow rate of 2.1 kg/hr, and a NAR of 750.

At the top of the photo is a faint millimeter scale. The larger droplets are 0.3 – 0.4 mm in size.

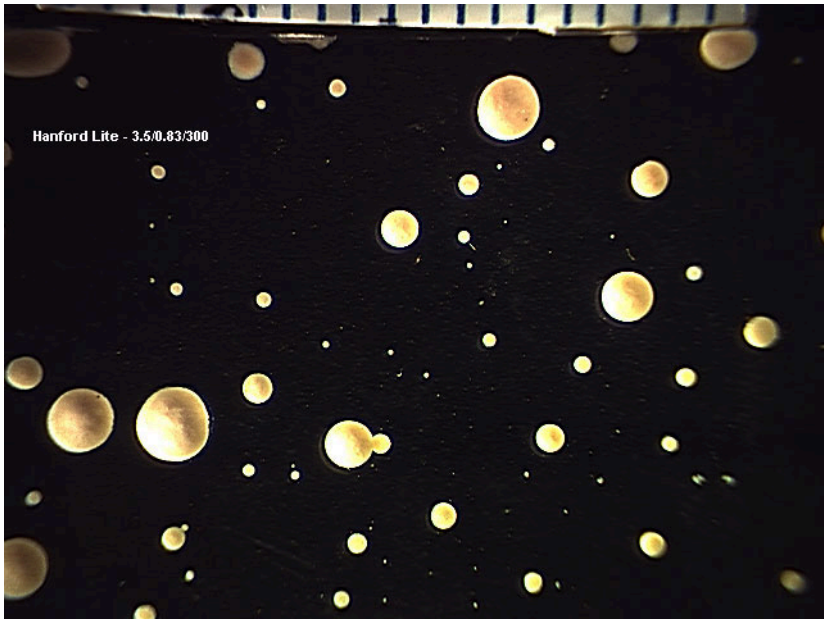

Figure B-6. Atomized spray droplets for the Sprayco nozzle with a Hanford LAW slurry feed rate of 3.5 kg/hr, an atomizing gas flow rate of 0.83 kg/hr, and a NAR of 300.

At the top of the photo is a millimeter scale. This figure is the same magnification as Figure 5-1. The larger droplets are 1 – 2 mm in size. The discoloration inside the larger droplets is due to water drying during the few hours after the slide was collected and when the microscope photo was taken.

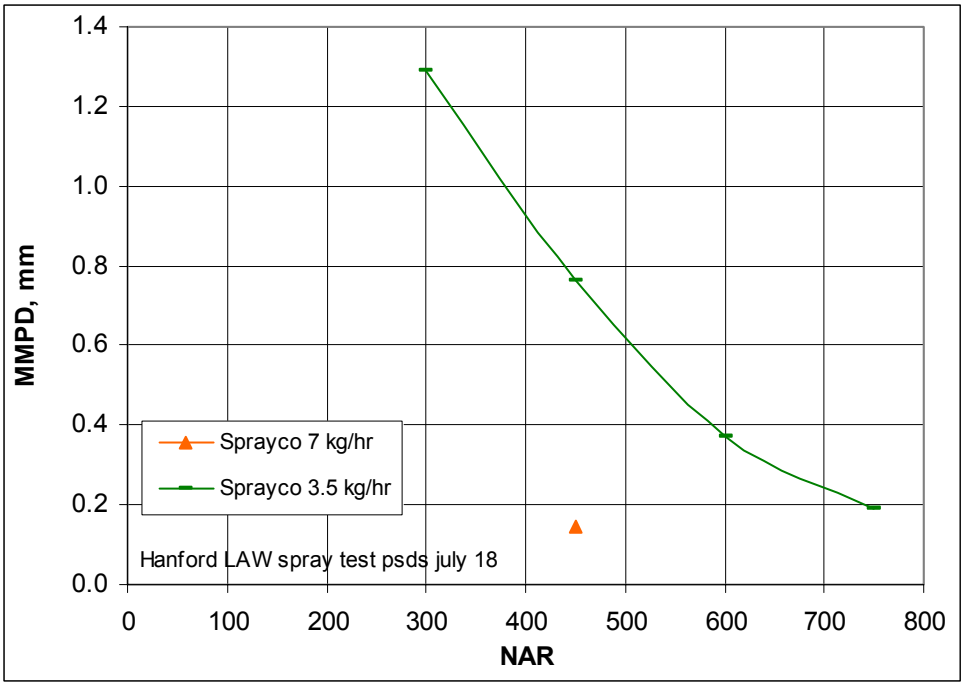

Figure B-7. Average atomized droplet size compared to NAR for the Hanford LAW simulant slurry.

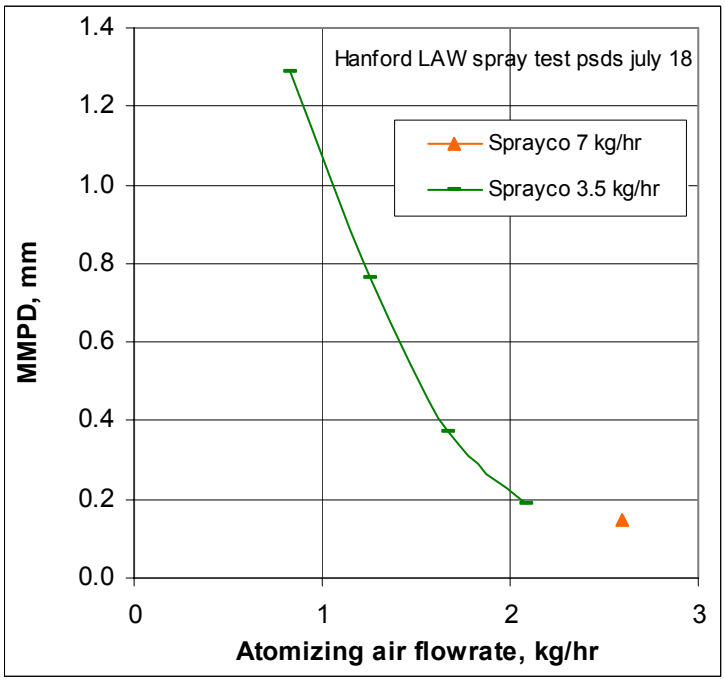

Figure B-8. Average atomized droplet size compared to atomizing gas flow rate for the Hanford LAW simulant slurry.

The smallest average droplet sizes ranged between 0.1 to 0.2 mm, the same order of magnitude as the starting bed media. The lowest average particle sizes were achieved with an atomizing gas flow rate of at least 2.5 kg/hr. The average droplet sizes began to rapidly increase for atomizing gas flow rates below 2.5 kg/hr. Extrapolation of the measured data suggests that the average droplet size continues to decrease with increasing atomizing gas flow rate. The average droplet size would be about 0.1 mm for an atomizing gas flow rate of 4 kg/hr.

The correlation between NAR and average particle size was less clear, because of the impact of the total atomizing gas flow rate on the droplet particle size. For example, the average droplet size for a NAR of 450 ranged from 0.148 mm to almost 0.8 mm for different nozzles, slurry feed rates, and atomizing gas feed rates.

The cumulative particle size distribution measurements for the SprayCo nozzle and Hanford LAW slurry are shown in Figure B-9. Even for the most efficient atomizing conditions that were tested (when the atomizing gas rate exceeded 2.5 kg/hr), the largest droplets ranged up to 0.2 – 0.6 mm depending on the nozzle type, slurry feed rate, and atomizing gas rate. Atomizing gas flow rates of 4 kg/hr or higher are recommended if large particles are not desired because they are significantly larger than the average fluidized bed particle size.

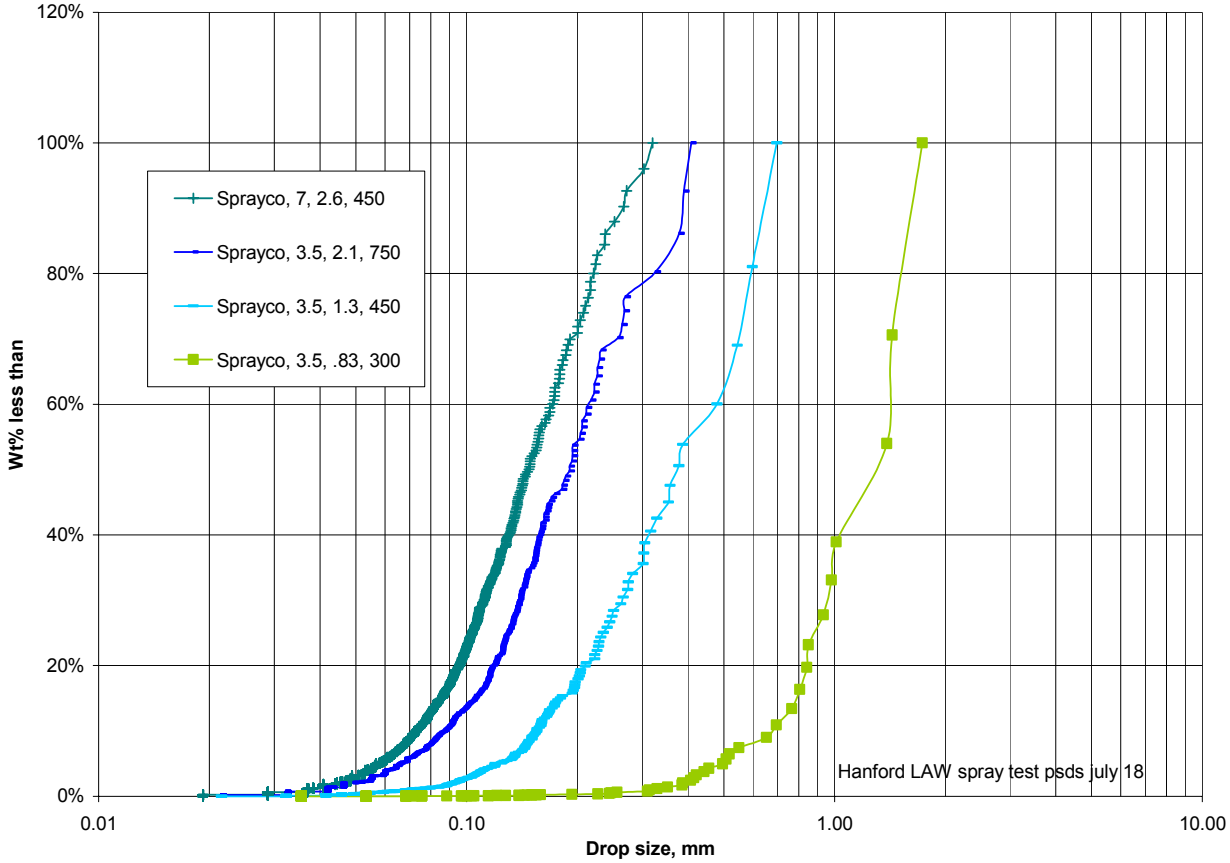

Figure B-9. Measured cumulative particle size distributions for the ranges of nozzle operating conditions of the Hanford LAW slurry spray tests.

July 30, 2004 Nozzle Atomization Tests

Following the May and June slurry atomization tests, and the May and June shakedown tests and the July SBW test, the newly designed SprayCo nozzle with the 0.100 inch ID liquid tube, modified with the heat/mass shield and the extended liquid tube (called the Marshall/Eldredge nozzle), was selected for the Hanford LAW FBSR test. The atomization performance of this newly modified nozzle was tested on July 30, prior to the Hanford LAW FBSR test, to verify if the atomization performance was still comparable to the standard, same-sized SprayCo nozzle. Qualitative real time visual comparisons were made, which indicated that the atomized spray patterns and behavior of the new nozzle effectively matched those observed for the SprayCo nozzle. No aberrant behavior was noted. No attempt was made to obtain quantitative spray droplet size data, as had been done in the earlier SprayCo test, and project schedule and cost constraints did not allow for further work in this area. A limited qualitative photographic record of the tests was made.

Slurry Viscosity Measurements

The viscosity measurements were made using a Brookfield Model LVDV-1+ viscometer. This viscometer measures viscosity at different shear rates by measuring the torque on a rotating spindle immersed in the sample fluid. Different spindles were used to provide viscosity results at spindle torques within 10-100% of the instrument full-scale torque (674 dyne-cm), for a range of spindle revolutions per minute (between 0.3-100 rpm) allowed by the instrument. The best spindles for the Hanford simulant slurries had a disk that rotated in the sample fluid. The use of a disk spindle rather than a cylindrical spindle prevented calculations that relate the measured viscosity (in centipoise, cp) to a specific shear rate (in seconds-1).

Viscosity measurements prior to the FBSR test were made using a “lite” version of the Hanford LAW simulant. The “lite” simulant was prepared using the exact proportions of the major chemical constituents of these simulants, leaving out minor (especially hazardous) constituents such as lead, nickel, and mercury. These minor constituents were not expected to significantly affect the simulant viscosity. Slurries of the lite versions were blended with various concentrations of OptiKasT clay, determined to provide a range of viscosity results that would bracket the clay selection and concentration for the FBSR tests. The viscosity of a sample of the actual Hanford LAW and clay slurry used in the FBSR test was subsequently measured for comparison to the pretest measurements.

Figure B-10 shows results of the Hanford LAW lite slurry viscosity measurements done prior to the Hanford LAW FBSR test, compared to the viscosity of the actual slurry used in the Hanford LAW FBSR test, measured under identical conditions. As expected, these slurries were much more viscous than water (which has a nominal viscosity of 1 cp), the Hanford LAW simulant, and the Hanford LAW lite simulants without clay. The viscosities of water and the Hanford LAW simulants (without clay) were too low for accurate measurement using the test apparatus, but the measurements showed that the viscosities of the Hanford LAW and Hanford LAW lite simulants were within about a factor of 2 of water viscosity under the viscosity test conditions.

The slurry viscosities ranged between 100 – 10,000 times higher than the Hanford LAW simulant without any clay. Slurries with higher clay concentrations exhibited higher viscosities at the same shear rate, although the shear rate could not be determined from the test apparatus. The slurries were shear-thinning at all but the very lowest shear rates and higher clay concentrations. This finding, in combination with results of the nozzle atomization tests, provided confidence prior to the FBSR test that the feed slurry would not cause feed atomization problems because of high viscosities, since shear rates during slurry atomization are known to be very high (Alderman, N. J. and N. I. Heywood, “Improving

Slurry Viscosity and Flow Curve Measurements," Chemical Engineering Progress, April 2004). The range of shear rates during pumping, mixing, and stirring processes is typically 10 – 1,000 s^{-1}, while shear rates during spraying and atomization typically range between 10^5 – 10^6 s^{-1}. Shear rates in the slurry sample during the viscosity tests were not greater than 10 – 1,000 s^{-1}, considering the degree of fluid agitation during the viscosity tests compared to typical fluid agitation during pumping, mixing, and stirring processes.

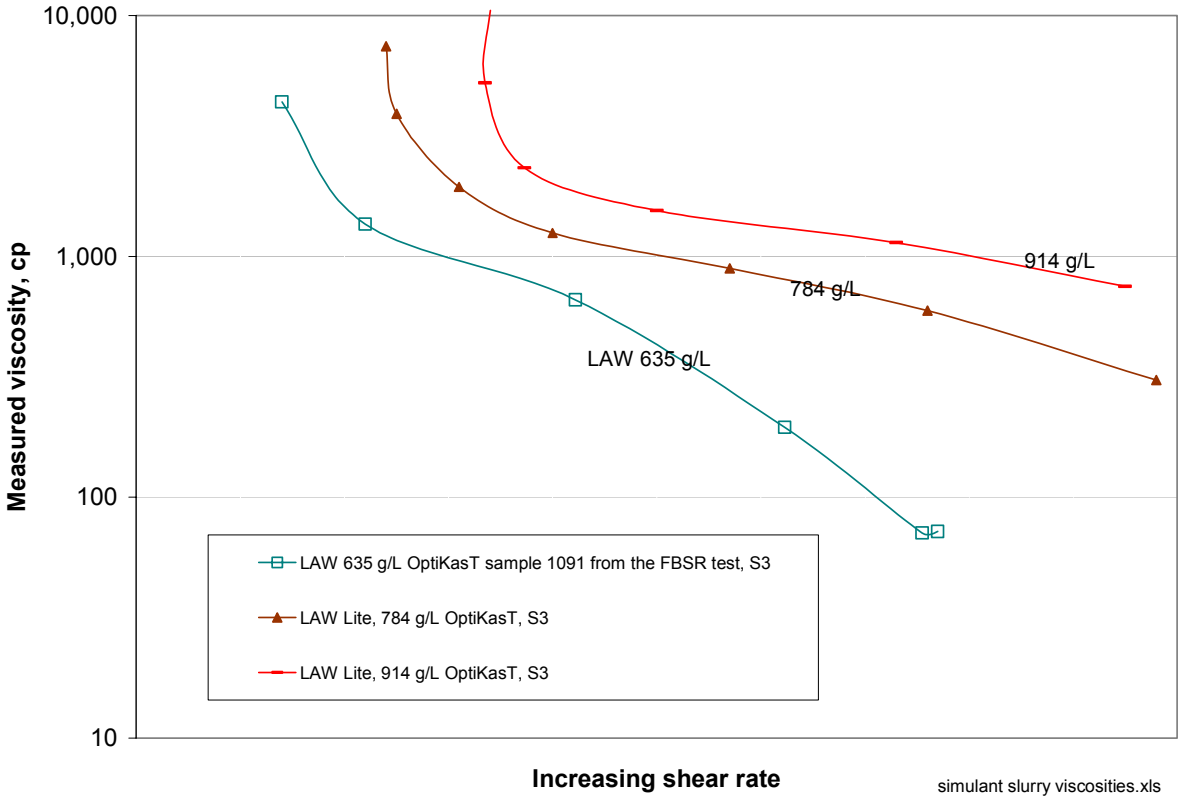

Figure B-10. Measured viscosities for Hanford LAW simulant slurries and FBSR feeds.

Appendix C

Carbon Reductant Selection

Nicholas R. Soelberg

Appendix C

CARBON REDUCTANT SELECTION

An evaluation of different potential carbon reductants was performed during the third quarter of FY2004, to select the carbon reductant(s) to be used in the fluidized bed steam reforming tests. Several different candidate carbons were evaluated. This evaluation was performed using the results of laboratory anayses performed at Savannah River National Laboratory[1,2], and results of the evaluation are summarized below.

Carbon Reductant Ranking Criteria

The candidate carbons were evaluated and ranked according to the following criteria:

- *Mass loss during a thermal gravimetric analysis (TGA) oxidation stage*: The higher the mass loss, the more reductant is available per mass of additive. The difference between this mass loss and 100% is the total moisture and ash, both undesired in the carbon additive. The moisture or ash content alone were not considered separate ranking criteria, since they are included in this criterion. The high moisture content of the BS-NB carbon (C1) causes a low ranking for this carbon for this criterion.

- *Temperature at start of oxidation during TGA*: This criterion indicates initial carbon reactivity.

- *Slope of mass loss during oxidation*: This criterion indicates how rapidly the oxidation can occur. Since the temperature at the end of oxidation is included in the slope calculation, it is not listed as a separate criterion.

- *Carbon particle size distribution*: Larger particles are desirable, as long as they can (a) be fed in the carbon reductant feed system, and (b) stay fluidized or "floated" on the smaller bed particles, because more mass will be utilized in the bed before the size is so small that it passes on through the cyclone. Large amounts of fines are undesirable, because these would tend to be elutriated out of the fluidized bed before the particles have had sufficient residence time for efficient reaction completeness.

Other criteria were considered but not included in this analysis:

- *Particle toughness*: Hardness of particles could be good (indicating toughness) or bad (indicating brittleness). Tests considered were Ball-Pan hardness (ASTM D 3802) and the Hardgrove Grindability Index test (ASTM D-409).

- *Particle density*: A lower particle density indicates easier fluidization of the typically larger particles. This is desirable because it minimizes the amount of the carbon particles removed with bed product.

---

[1] Jantzen, C. M., 2004, J. C. Marra, and J. M. Pareizs, *Analysis of Raw Materials for Fluidized Bed Steam Reforming (FBSR)*, SRNL-ITB-2004-0004, June 30.

[2] Marra, Jim, "Carbon Source Data," personnal communication to A. L. Olson, March 16, 2004.

- *Specific surface area/porosity*: More surface area is desirable, and is probably related to the slope of mass loss during TGA oxidation.

Particle toughness was excluded from the analysis due to lack of readily available data, even though particle toughness (resistance to attrition in the fluidized bed) was desired. Particle density could have been readily available through simple laboratory analysis, but was discarded as a criterion because it was not considered to be a very significant discriminator. Specific surface area/porosity was excluded as a separate criterion because (a) additional laboratory analyses would have been necessary to provide these data, and (b) the slope of mass loss during oxidation, which was included in the evaluation, was considered to be an adequate, representative surrogate for this criterion.

Carbon Thermal Gravimetric Analysis

Results of TGA analyses performed by SRNL are tabulated in Table C-1. Data for several key criteria related to carbon reactivity are provided by the TGA results. Tabulated data taken from the TGA charts include (a) the mass loss at temperatures up to about 100°C, due largely to sorbed H_2O and possibly other more volatile sorbed species, (b) mass loss during the oxidation stage at temperatures ranging from about 250-850°C, (c) the total mass loss (100% minus the total mass loss indicates the residual ash content), (d) the starting and ending temperatures for the oxidation stage, and (e) the slope of mass loss during oxidation. All of this data was from TGAs performed in an air atmosphere. Since the FBSR design uses steam as the fluidizing gas and the FSBR is operated in an O_2-deficient atmosphere, the air-TGA results may not entirely represent FBSR conditions. TGAs performed in a steam atmosphere may have better represented the carbon reactivities and performance in an FBSR environment. Efforts to modify the commercially available TGA equipment to operate in a steam atmosphere were not successful within available time and cost constraints, and so was not performed.

The moisture loss ranged below 10 wt%, consistent with vendor product data, except for the BS-NB sample, which had almost 20 wt% moisture loss. Perhaps this amount of moisture loss was from a non-representative sample. Mass loss during oxidation ranged above 90% for the wood-based carbons (except for the BS-NB sample, affected by the high moisture loss). The coke and anthracite-based carbons exhibited lower mass loss, indicating less useable reactive mass for denitrating the FBSR feeds. The wood-based carbons also exhibited lower temperatures at which oxidation mass loss started, lower oxidation end temperatures, and faster oxidation rates as indicated by the slope of the mass loss during oxidation.

Carbon Particle Size Distribution

Carbon particle size distribution data from the sieve tray measurements at SRNL are shown in Figures C-1 and C-2. The original data was converted to particle size distribution in terms of cumulative wt% less than each size cut, a graph of typically Gaussian differential particle distributions, and a single mass mean diameter (MMD) for each carbon. Three of the carbons (C5, C6, and C3) had significant mass fractions greater than the largest screen (4 mesh, 4.75 mm) used in the sieve analyses, so the actual MMD for these carbons is subject to some error. The sieve analyses for these carbons only captures the smaller half of the typical Gaussian particle size distributions.

The MMD calculation required that the average particle size of the >4 mesh mass be estimated. A maximum particle size for any carbon of 10 mm, and an average particle size of the >4 mesh mass of 7.4 mm was assumed. Even if appreciable error is introduced by the >4 mesh assumptions, the relative ranking of carbons is not changed, so further particle size analyses of the C5, C6, and C3 carbons was not warranted.

Table C-1. Results of carbon reductant TGA analyses in an air atmosphere.

Sample	ID	Type/size	Manufacturer	TGA mass loss, wt% (air atmosphere)			TGA temperature data (air atmosphere)			Particle size, MMD, mm
				25 < T < 200 to 500 C (attributed to mainly sorbed H2O, etc)	During oxidation stage, between 250-500 C and 430-700C	Total (100-ash)	T at start of oxidation, C	T at end of oxidation, C	Slope of oxidation step, %mass loss/°C	
C1	BS-NB	Wood base, 4x12 mesh	Barneby-Sutcliffe, Columbus, OH	19.7	76.8	96.5	350	490	0.55	3.3
C2	GC-CBM	Coal base, low density, 6x12 mesh	General Carbon, Paterson, NJ	3	94.6	97.6	480	690	0.45	3.6
C3	BS-WBC	Wood base, ~minus 0.5 inch	Barneby-Sutcliffe	3.6	94.9	98.5	250	430	0.53	5.3
C4	GC-CRB	Wood base, 4x6 mesh	General Carbon	4.7	91.8	96.5	470	660	0.48	4.3
C5	BB-NWC	Wood base, ~minus 0.7 inch	Berger Brothers, Chicago, IL	2.1	94.5	97.7	300	450	0.63	6.7
C6	MC-DRC	Coke, "dry rice size"	Mid-Continent Coal and Coke, Clairton, PA	0.82	86.7	87.5	460	650	0.46	7.2
C7	AI-776	Anthracite coal, ~minus 0.2 inch	Anthracite Industries, Sunbury, PA	5.1	88.2	93.3	530	730	0.44	1.7
C8	BS-AD	Wood base, 4x8 mesh	Barneby-Sutcliffe	6.9	91.2	98.1	400	560	0.57	3.6
C9	BS-VS	Anthracite coal, ~minus 0.4 inch	Barneby-Sutcliffe	4.5	77.9	82.4	530	850	0.24	4.8

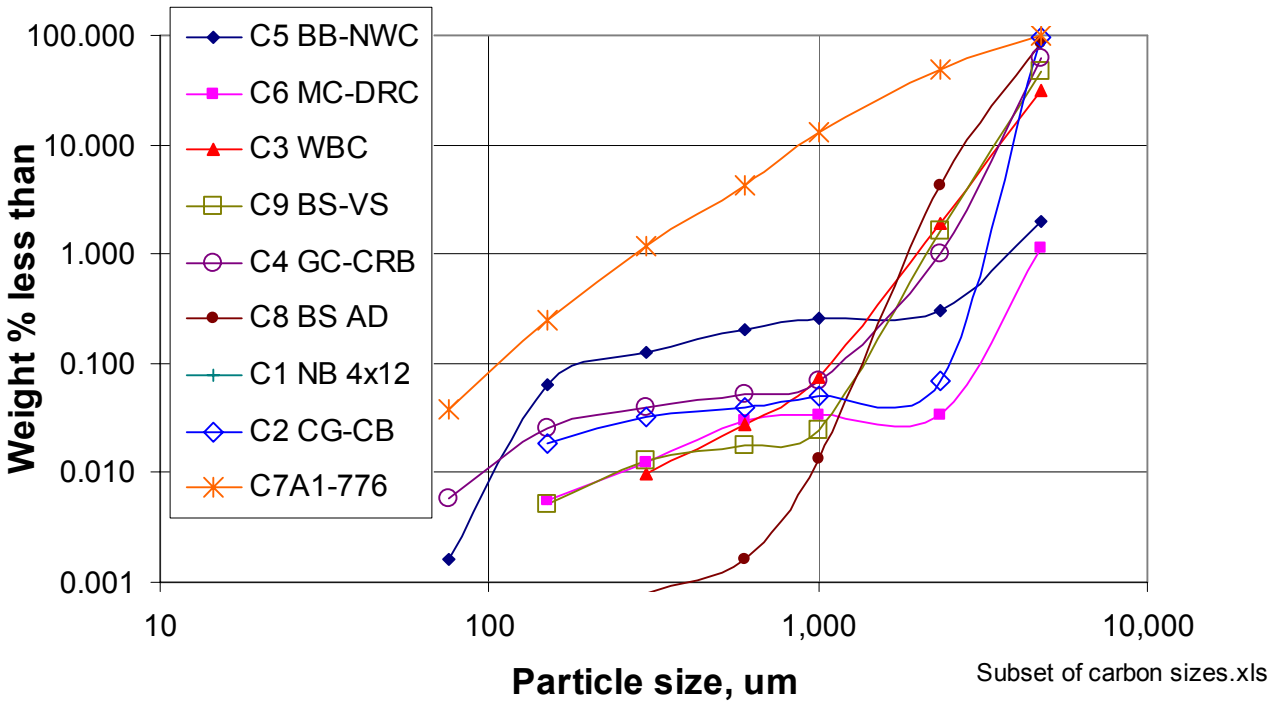

Figure C-1. Cumulative carbon reductant particle size distributions.

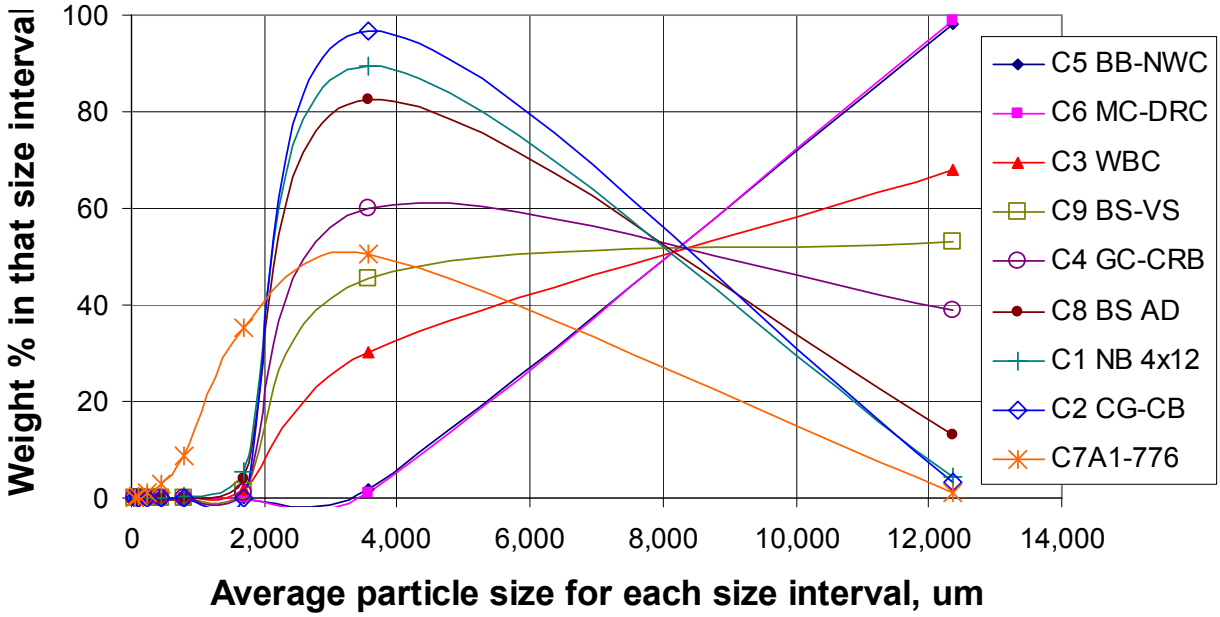

Figure C-2. Differential carbon reductant particle size distributions.

The MMDs for the 9 carbons ranged between 1.7 mm to 7.2 mm. How particle size impacts the performance of a carbon additive in a fluidized bed steam reformer (FSBR) is not entirely clear, but for this evaluation, independent of other criteria (such as specific surface area, ability to feed, and ability to fluidize), the larger particle size was considered desirable. More of the mass of larger particles would tend to stay in the bed and be reacted before the particle attrits or is reacted to a size small enough to be elutriated from the bed and cyclone. However, it is not desirable that the carbon particles are so large that (a) they cannot be fed through the carbon reductant feed system, or (b) they are so large that they cannot remain fluidized and are appreciably removed from the bed during sampling or harvesting of product.

Even particles significantly larger than the size that would be fluidized by the fluidizing gas tend to be buoyed up by, or float on, the mass of fluidized particles. Visual observations in the room-temperature 6-inch fluidized bed model at the SAIC STAR Center indicate that many of the carbon particles in the 2-4 mm size range tend to float near the top of the fluidized portion of alumina bed particles.

The carbon particle density and shape, in combination with the particle size, indicates the ability to be appropriately fluidized. However, these data were not readily available and were excluded from this analysis. Perhaps the ideal carbon would have a relatively large particle size, able to provide more of its mass in steam reforming reactions before the particle elutriates from the bed, an irregular shape, and a lower particle density, allowing the particle to be more easily fluidized in the bed and not drained from the bed.

Carbon Reductant Rankings And Selection

Results of this evaluation are summarized in Table C-2. The lowest numerical total ranking indicates the best carbons based on the criteria. All of the ranking criteria were equally weighted.

The top two carbons stand out from the rest based on their numerical rankings.

1.	C5	BB-NWC	Wood base, ~minus 0.7"	Berger Brothers, Chicago, Illinois (Score of 8)
2.	C3	BS-WBC	Wood base, ~minus 0.5"	Barneby-Sutcliffe. (Score of 9, almost same as C5)

The C5 carbon was selected for the FBSR tests, because it ranked highest and was available at a significantly lower cost. The C5 carbon (also referred to as “P3” carbon by Berger Brothers) was procured and tested in the reductant feeder, and found to restrict the feeder. A smaller particle-size range C5-type carbon (referred to as “P6”) was procured for feeder testing. This carbon could be reliably fed and so was procured for FBSR testing.

There were several carbons in the next tier, although their scores were all similar:

3.	C8	BS-AD	Wood base, 4x8	Barneby-Sutcliffe. (Score of 17)
4.	C6	MC-DRC	Coke, "dry rice size"	Mid-Cont. Coal and Coke, Clairton, PA. (Score 19)
5.	C4	GC-CRB	Wood base, 4x6	General Carbon. (Score of 20)
6.	C2	GC-CBM	Coal base, low density, 6x12	General Carbon, Paterson, NJ. (Score of 22)
7.	C1	BS-NB	Wood base, 4x12	Barneby-Sutcliffe, Columbus, OH. (Score of 23)

The BS-NB carbon, ranked 7th, was the carbon most highly recommended by THOR^{SM} Treatment Technologies for prior tests. Four other wood-based carbons, one coke-based carbon, and one coal-based carbon may perform as well as the BS-NB carbon according to this ranking. The BS-NB carbon was ranked lower because of the unexpectedly high moisture content. Another moisture analysis performed on the BS-NB carbon might confirm if the high moisture content indicated by the first analysis was correct.

The C6 coke-based carbon was included in the second-tier group because it ranked first (largest) for particle size, although it did not rank high in other criteria. The C2 coal-based carbon was included in the second-tier group because it had a high mass loss during TGA oxidation, although it did not rank high in other criteria. All the other high-ranked and medium-ranked carbons are wood-based. Based on the TGA analyses, wood-based carbons seem to be more reactive than the coke and coal-based carbons, confirming TTT's recommendations that the wood-based carbons are more reactive.

The two anthracite-based carbons ranked lowest, mainly because they were less reactive than the other carbons based on the TGA analyses.

The rankings could change if data were included for the particle toughness, particle density, ash composition, and steam TGA criteria.

Table C-2. Numerical rankings of carbon reductants.

Sample	ID	Type/size	Manufacturer	Mass loss during TGA oxidation stage, between 250-500°C and 430-700°C	Temp. at start of oxidation, °C	Slope of oxidation step, %mass loss/°C	Particle size, MMD, mm	Totals	Overall Rank
C1	BS-NB	Wood base, 4x12 mesh	Barneby-Sutcliffe, Columbus, OH	9	3	3	8	23	7
C2	GC-CBM	Coal base, low density, 6x12 mesh	General Carbon, Paterson, NJ	2	7	7	6	22	6
C3	BS-WBC	Wood base, ~minus 0.5 inch	Barneby-Sutcliffe	1	1	4	3	9	2
C4	GC-CRB	Wood base, 4x6 mesh	General Carbon	4	6	5	5	20	5
C5	BB-NWC	Wood base, ~minus 0.7 inch	Berger Brothers, Chicago, IL	3	2	1	2	8	1
C6	MC-DRC	Coke, "dry rice size"	Mid-Continent Coal and Coke, Clairton, PA	7	5	6	1	19	4
C7	AI-776	Anthracite coal, ~minus 0.2 inch	Anthracite Industries, Sunbury, PA	6	8	8	9	31	9
C8	BS-AD	Wood base, 4x8 mesh	Barneby-Sutcliffe	5	4	2	6	17	3
C9	BS-VS	Anthracite coal, ~minus 0.4 inch	Barneby-Sutcliffe	8	8	9	4	29	8

[carbon tga results.xls]ranking